# Image and non-imaging analysis

**Dom Pesce**
Center for Astrophysics | Harvard & Smithsonian

*18th NRAO Synthesis Imaging Workshop*
*May 25, 2022*

# What can you do with images?

# What can you do with images?

Just about anything!

# What do people *typically* do with images?

# What do people *typically* do with images?

Classic radio astronomy analyses include various styles of component-wise decomposition of the image into point sources, Gaussians, wavelets, etc.

- many examples exist in the literature
  - source catalog construction from various large-area sky surveys; e.g., Taylor et al. (1996), Condon et al. (1998), Mooley et al. (2016)
  - image decomposition into subcomponents; e.g., Miyoshi et al. (1995), Mertens et al. (2016)

# What do people *typically* do with images?

Classic radio astronomy analyses include various styles of component-wise decomposition of the image into point sources, Gaussians, wavelets, etc.

- many examples exist in the literature
  - source catalog construction from various large-area sky surveys; e.g., Taylor et al. (1996), Condon et al. (1998), Mooley et al. (2016)
  - image decomposition into subcomponents; e.g., Miyoshi et al. (1995), Mertens et al. (2016)

Other structures in radio images are often measured/characterized using custom-built feature extraction tools

- e.g., jet position angles and other properties; e.g., Valtonen & Wiik (2012), Walker et al. (2018)

# What do people *typically* do with images?

Classic radio astronomy analyses include various styles of component-wise decomposition of the image into point sources, Gaussians, wavelets, etc.

- many examples exist in the literature
  - source catalog construction from various large-area sky surveys; e.g., Taylor et al. (1996), Condon et al. (1998), Mooley et al. (2016)
  - image decomposition into subcomponents; e.g., Miyoshi et al. (1995), Mertens et al. (2016)

Other structures in radio images are often measured/characterized using custom-built feature extraction tools

- e.g., jet position angles and other properties; e.g., Valtonen & Wiik (2012), Walker et al. (2018)

The relatively recent explosion of image analysis tools from the machine learning / computer vision communities have permeated into radio astronomical image analyses

- e.g., neural network-based feature extraction; e.g., van der Gucht et al. (2020), Lin et al. (2020), Connor et al. (2022)

# Examples of image-domain analyses

# Examples of image-domain analyses

Matthews et al. (2010) fit two-dimensional Gaussians to thousands of SiO masers observed in Orion Source I

- position measurements over time yield proper motions

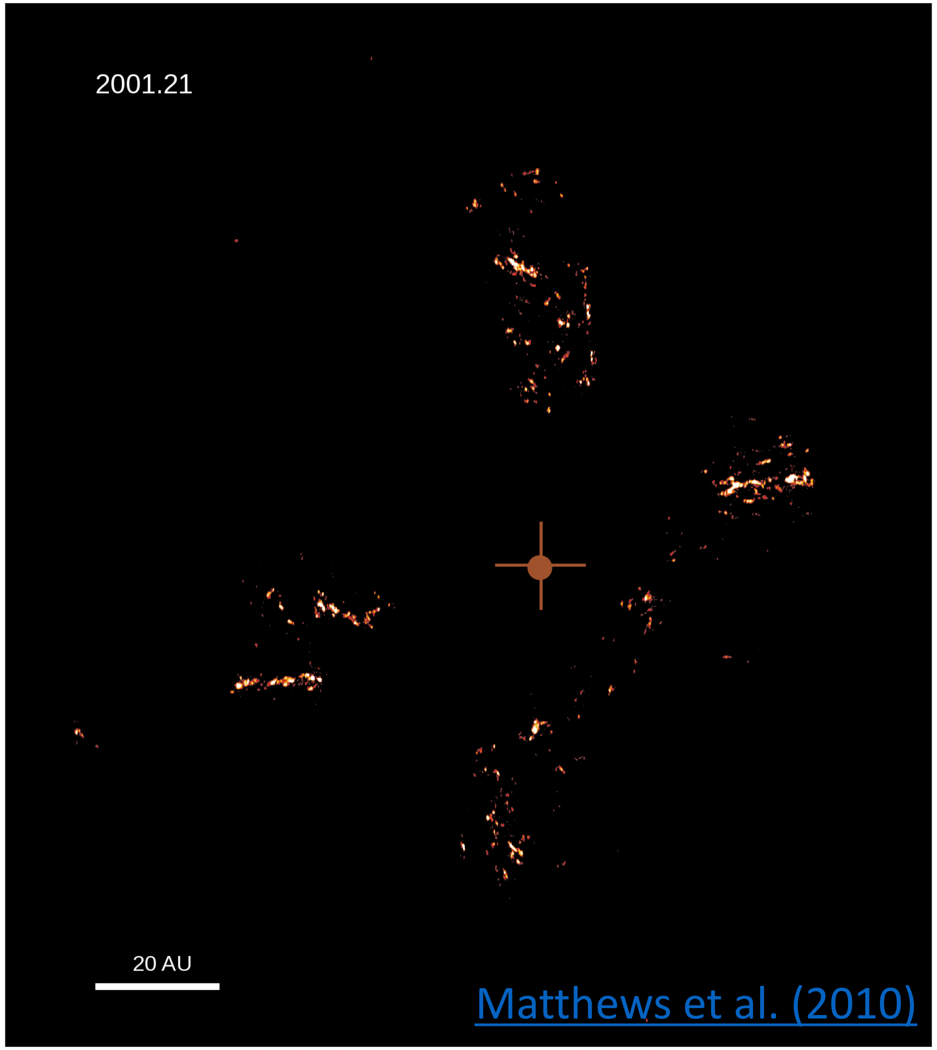


Matthews et al. (2010)

# Examples of image-domain analyses

Matthews et al. (2010) fit two-dimensional Gaussians to thousands of SiO masers observed in Orion Source I

- position measurements over time yield proper motions

Event Horizon Telescope Collaboration (2019) used image-domain techniques to measure various properties of the rings of emission seen toward the M87* black hole

- e.g., ring diameter, thickness, orientation

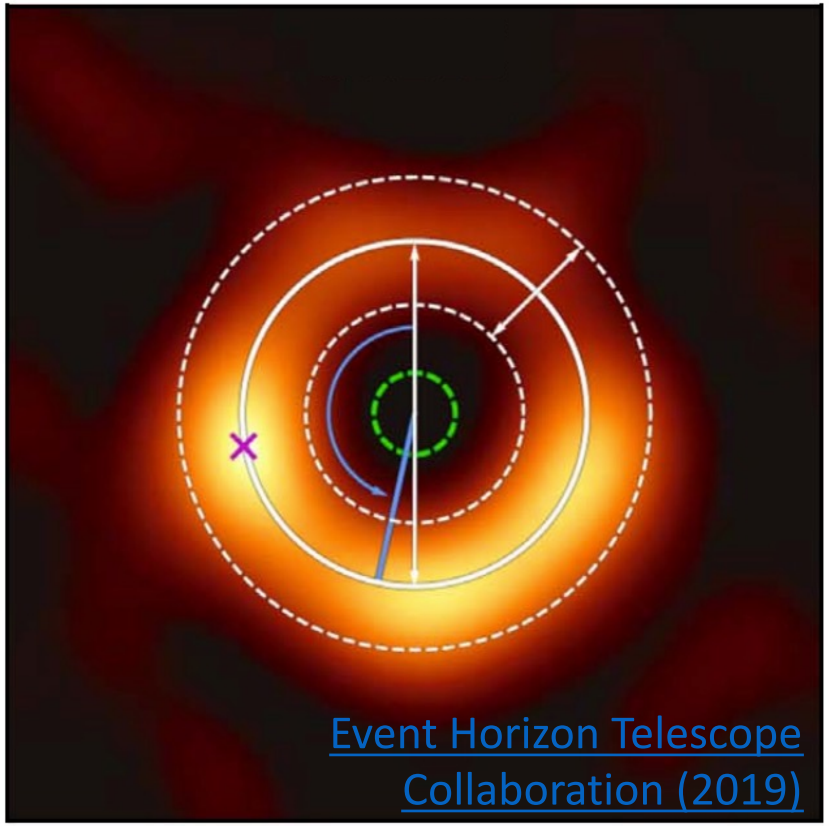

Event Horizon Telescope Collaboration (2019)

# Examples of image-domain analyses

Matthews et al. (2010) fit two-dimensional Gaussians to thousands of SiO masers observed in Orion Source I

- position measurements over time yield proper motions

Event Horizon Telescope Collaboration (2019) used image-domain techniques to measure various properties of the rings of emission seen toward the M87* black hole

- e.g., ring diameter, thickness, orientation

ALMA Partnership, Brogan et al. (2015) fit ellipses to the rings in the ALMA image of HL Tau

- measure the disk position angle and inclination
- used to deproject the disk and measure the relative brightnesses of different rings

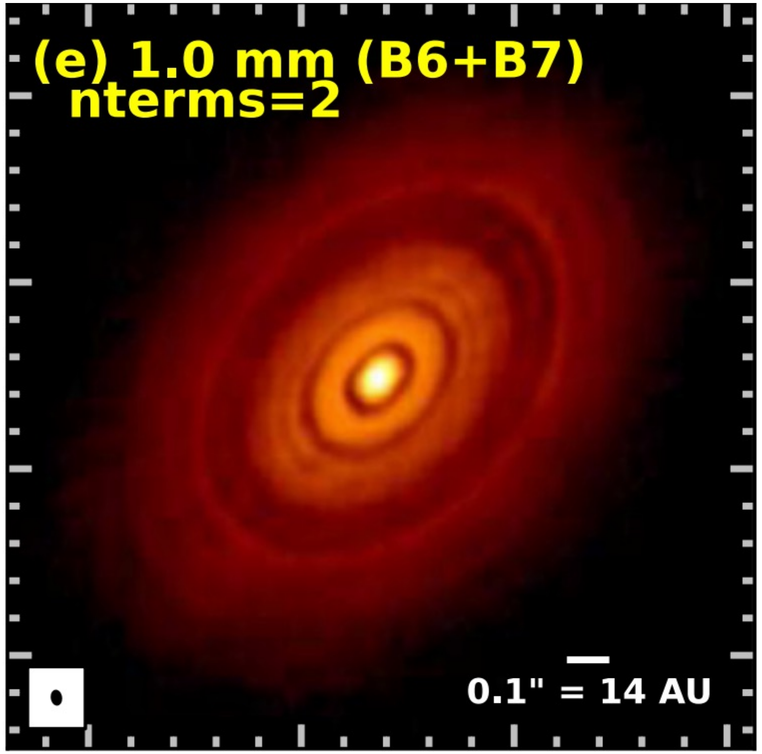


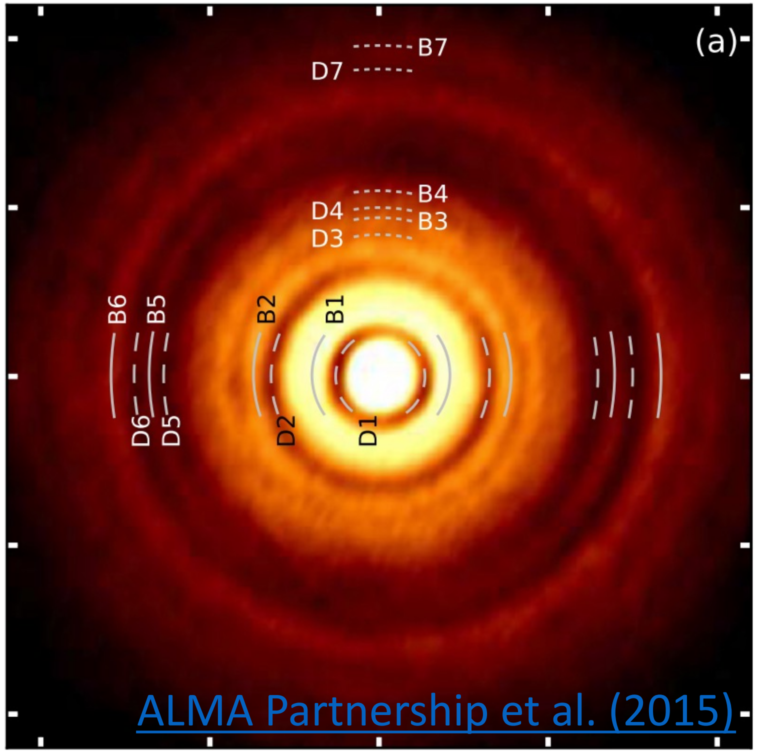


ALMA Partnership et al. (2015)

# Gaussian fitting demo: maser spots

# Gaussian fitting demo: maser spots

We'll consider an example dataset from ALMA observations of the water megamaser system in the Circinus AGN

- individual maser "spots" are unresolved

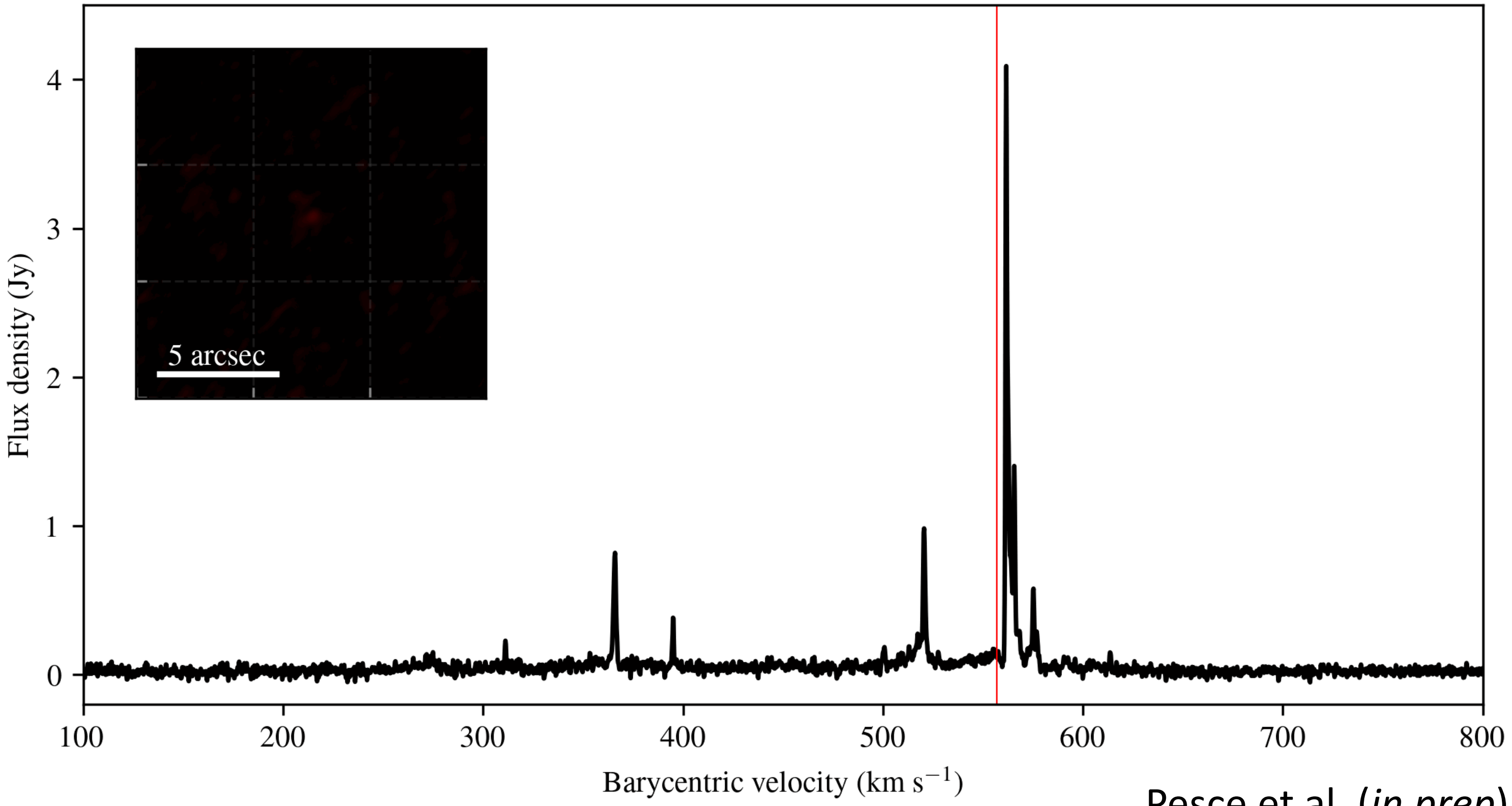


Pesce et al. (*in prep*)

# Gaussian fitting demo: maser spots

We'll consider an example dataset from ALMA observations of the water megamaser system in the Circinus AGN

- individual maser "spots" are unresolved

The location of a maser spot within a single frequency channel can be determined by fitting a Gaussian to the image

- e.g., using the task `jmfit` in AIPS or the task `imfit` in CASA
- or your own code!

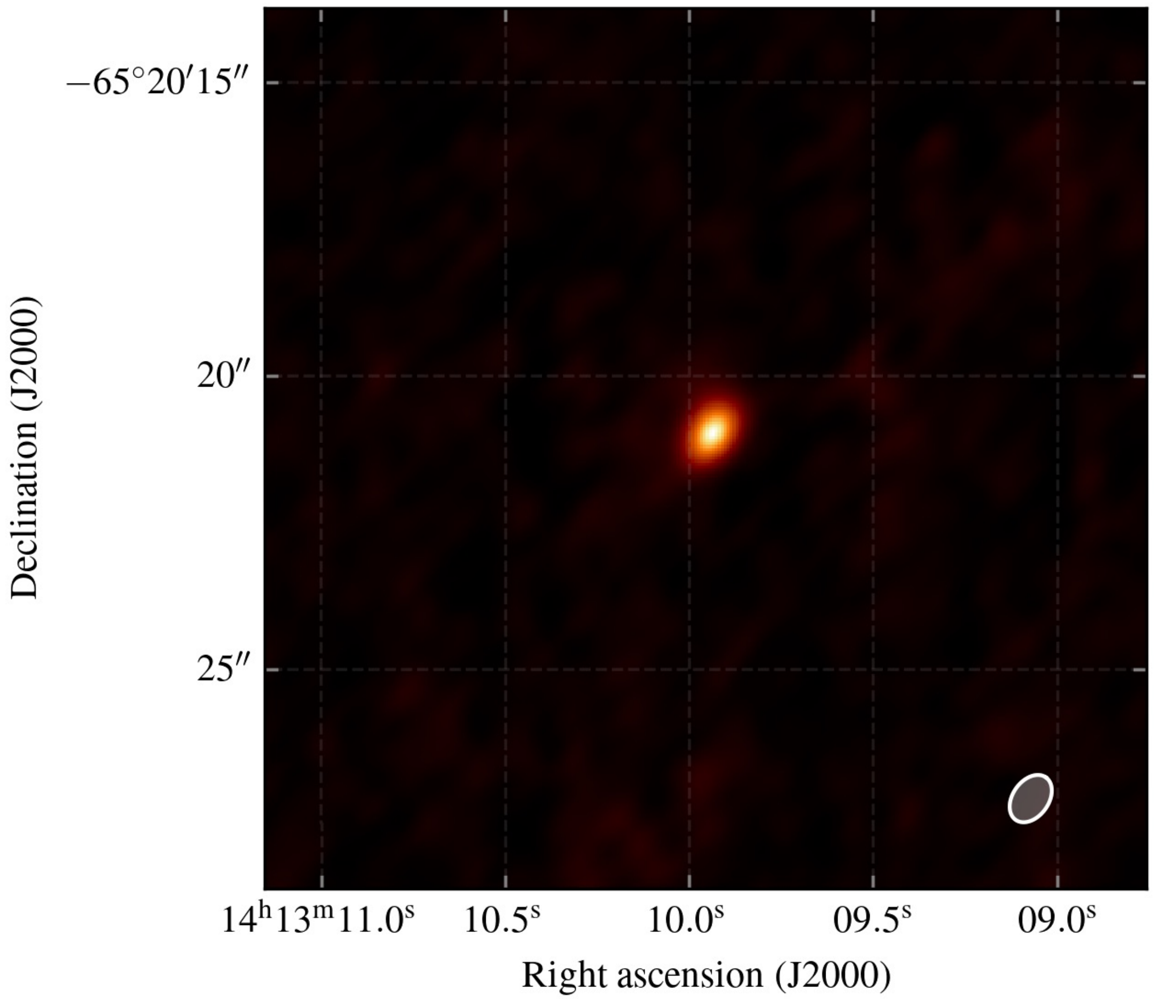


Pesce et al. (*in prep*)

# Gaussian fitting demo: maser spots

We'll consider an example dataset from ALMA observations of the water megamaser system in the Circinus AGN

- individual maser "spots" are unresolved

The location of a maser spot within a single frequency channel can be determined by fitting a Gaussian to the image

- e.g., using the task `jmfit` in AIPS or the task `imfit` in CASA
- or your own code!

In this case, a fit provides:

- (x,y) position
- (major, minor) axis widths
- peak brightness
- position angle

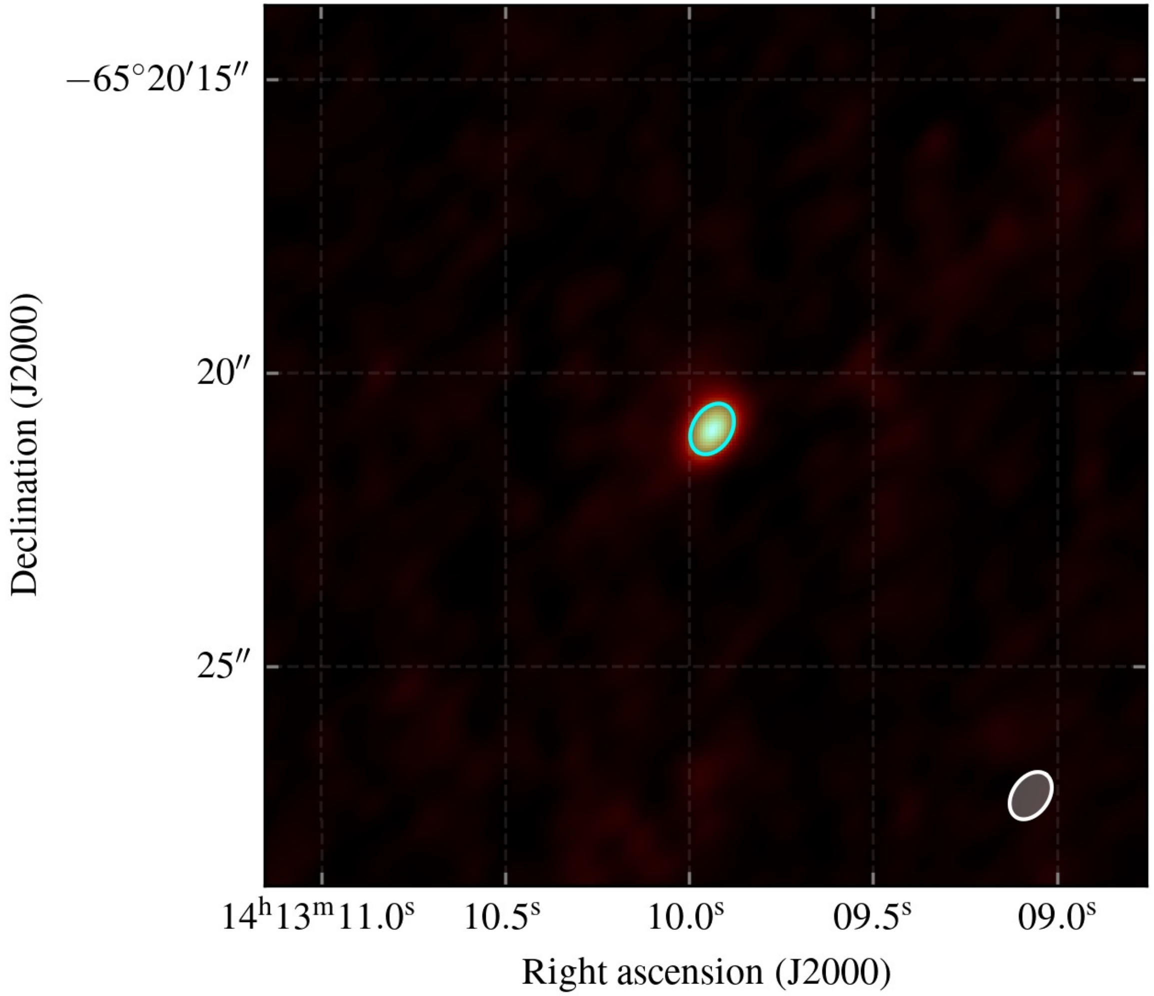


Pesce et al. (*in prep*)

# Gaussian fitting demo: maser spots

Let's look at the (x,y) locations of just the highest signal-to-noise ratio maser spots

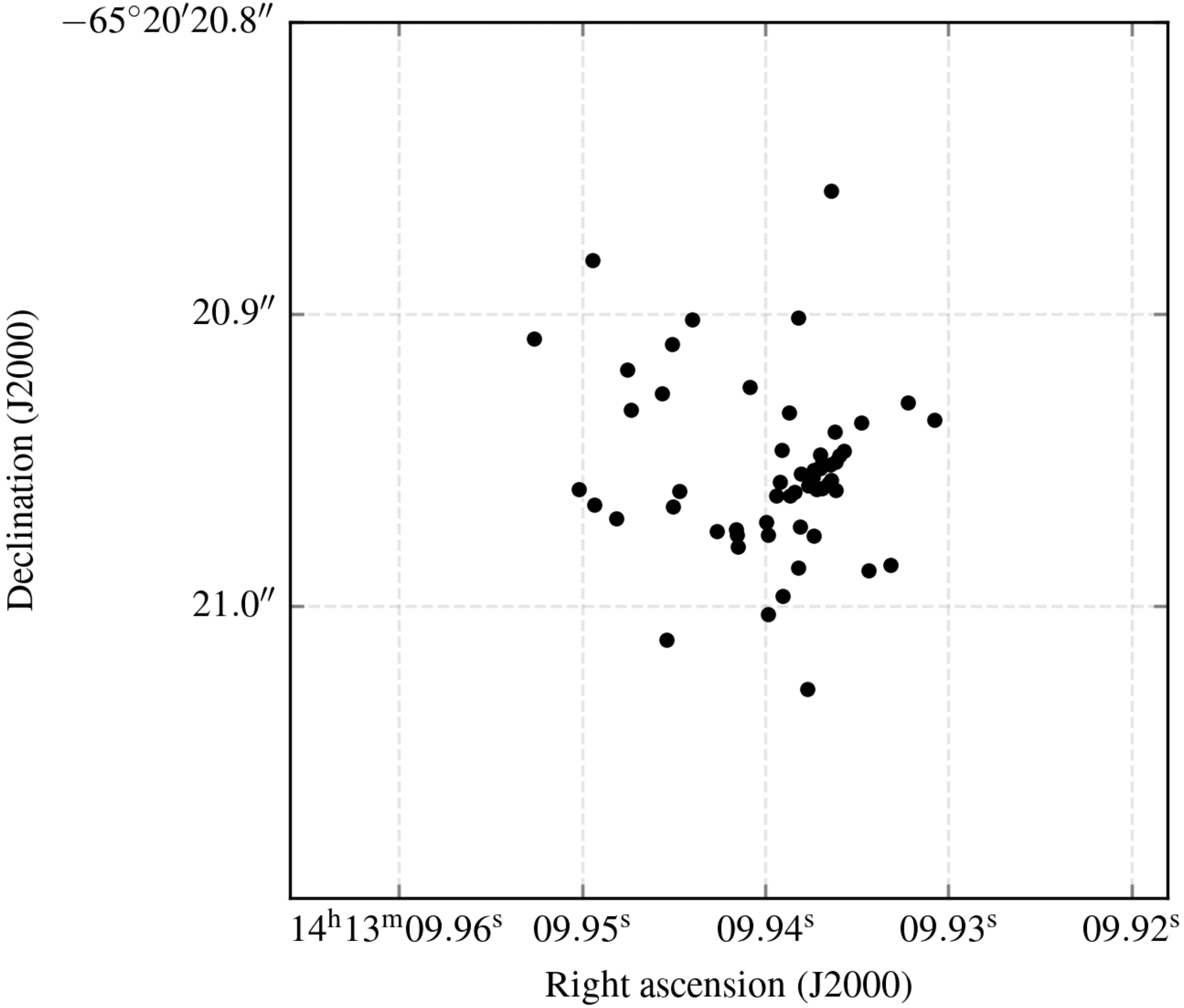


Pesce et al. (*in prep*)

# Gaussian fitting demo: maser spots

Let's look at the (x,y) locations of just the highest signal-to-noise ratio maser spots

- note that on the plotted scale, the beam is larger than the plot (!)

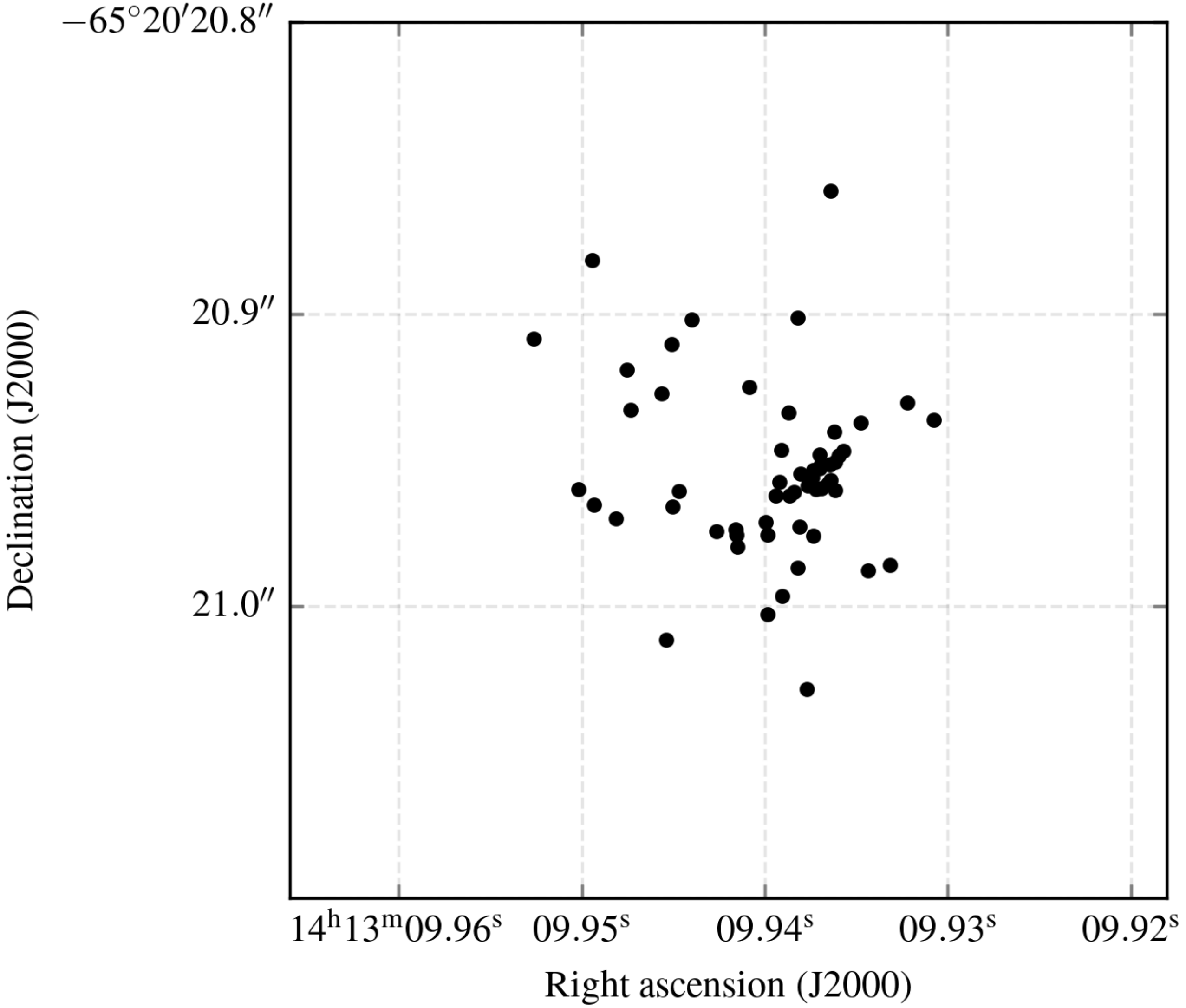


Pesce et al. (*in prep*)

# Gaussian fitting demo: maser spots

Let's look at the (x,y) locations of just the highest signal-to-noise ratio maser spots

- note that on the plotted scale, the beam is larger than the plot (!)

Coloring the maser spots by their relative velocity, we can see some evidence for rotation or inflow/outflow in this system

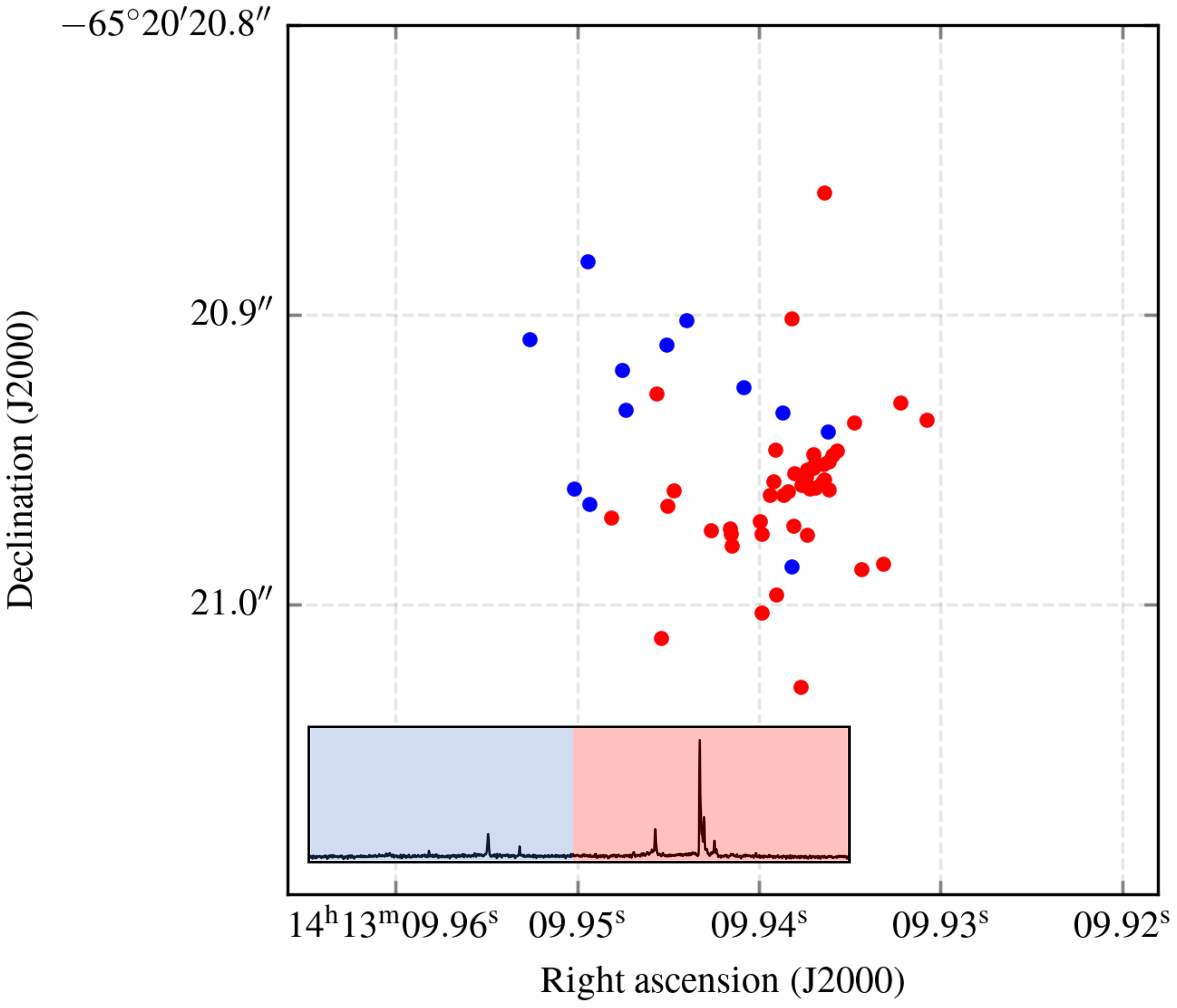


Pesce et al. (*in prep*)

# Gaussian fitting demo: maser spots

What about uncertainties?

# Gaussian fitting demo: maser spots

What about uncertainties?

The uncertainties $\sigma_x$ in position measurements are classically determined using an expression like

$$\sigma_x = k\left(\frac{\Delta_x}{\rho}\right)$$

where $\Delta_x$ is a measure of the width, $\rho$ is the signal-to-noise ratio (defined as the peak amplitude to the per-pixel RMS), and $k$ is a proportionality constant whose value depends on the specific function being fit

- for a 2D Gaussian with $\Delta_x$ set to the Gaussian FWHM, $k \approx 0.601$ (Condon 1997)

# Gaussian fitting demo: maser spots

What about uncertainties?

The uncertainties $\sigma_x$ in position measurements are classically determined using an expression like

$$\sigma_x = k\left(\frac{\Delta_x}{\rho}\right)$$

where $\Delta_x$ is a measure of the width, $\rho$ is the signal-to-noise ratio (defined as the peak amplitude to the per-pixel RMS), and $k$ is a proportionality constant whose value depends on the specific function being fit

- for a 2D Gaussian with $\Delta_x$ set to the Gaussian FWHM, $k \approx 0.601$ (Condon 1997)

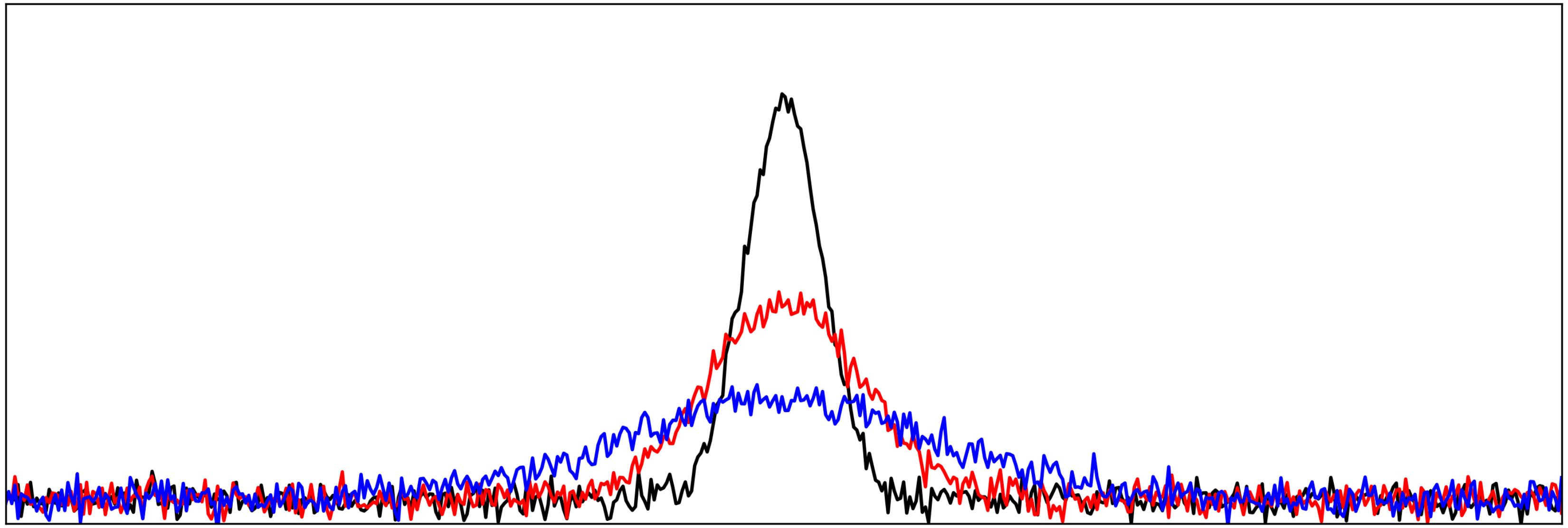

# Gaussian fitting demo: maser spots

What about uncertainties?

The uncertainties $\sigma_x$ in position measurements are classically determined using an expression like

$$\sigma_x = k\left(\frac{\Delta_x}{\rho}\right)$$

where $\Delta_x$ is a measure of the width, $\rho$ is the signal-to-noise ratio (defined as the peak amplitude to the per-pixel RMS), and $k$ is a proportionality constant whose value depends on the specific function being fit

- for a 2D Gaussian with $\Delta_x$ set to the Gaussian FWHM, $k \approx 0.601$ (Condon 1997)

However, this expression (and those like it) assumes:

- that the uncertainty in each pixel value is independent
- that the uncertainty in each pixel value is normally-distributed
- that the number of pixels across the width of the 2D Gaussian is large
- that the signal-to-noise ratio is "high" (i.e., this represents a linearized error estimate)

In practice, most of these conditions are rarely met

# Why might you want to carry out analyses on non-image data products?

# Why might you want to carry out analyses on non-image data products?

The first “analysis” one often wants to do is to simply inspect the data

- characteristics of the image structure can sometimes be seen directly in the visibilities
- can help to determine a good initial model for self-calibration

# Why might you want to carry out analyses on non-image data products?

The first “analysis” one often wants to do is to simply inspect the data

- characteristics of the image structure can sometimes be seen directly in the visibilities
- can help to determine a good initial model for self-calibration

Data may be sparse or even missing (e.g., no phases), or calibration issues may be severe

- in these cases, direct inversion (i.e., deconvolution) may not even be possible
- e.g., high-frequency VLBI (GMVA, KVN, EHT)

# Why might you want to carry out analyses on non-image data products?

The first “analysis” one often wants to do is to simply inspect the data

- characteristics of the image structure can sometimes be seen directly in the visibilities
- can help to determine a good initial model for self-calibration

Data may be sparse or even missing (e.g., no phases), or calibration issues may be severe

- in these cases, direct inversion (i.e., deconvolution) may not even be possible
- e.g., high-frequency VLBI (GMVA, KVN, EHT)

The measurements are natively made in the visibility space

- the measurement uncertainties are well-understood in the visibility space
    - images are not unique!  there is no such thing as “the image” corresponding to a dataset
    - for uncertainty quantification, working in the (u,v) space is often simpler
- residual calibration issues live most naturally in the visibility space

# Why might you want to carry out analyses on non-image data products?

The first “analysis” one often wants to do is to simply inspect the data

- characteristics of the image structure can sometimes be seen directly in the visibilities
- can help to determine a good initial model for self-calibration

Data may be sparse or even missing (e.g., no phases), or calibration issues may be severe

- in these cases, direct inversion (i.e., deconvolution) may not even be possible
- e.g., high-frequency VLBI (GMVA, KVN, EHT)

The measurements are natively made in the visibility space

- the measurement uncertainties are well-understood in the visibility space
    - images are not unique! there is no such thing as “the image” corresponding to a dataset
    - for uncertainty quantification, working in the (u,v) space is often simpler
- residual calibration issues live most naturally in the visibility space

*Imaging itself is an analysis that uses a non-image data product!*

# Data inspection example

Data credit: MOJAVE team (Lister et al. 2018)

# Data inspection example

We'll consider an example "a priori unknown" dataset, taken by the MOJAVE team (Lister et al. 2018)

- target source is the quasar NRAO 190
- observations were carried out in December 2019, using the VLBA at 15 GHz

What can we learn about the source just by inspecting the calibrated visibility data?

Data credit: MOJAVE team (Lister et al. 2018)

# Data inspection example

We'll consider an example "a priori unknown" dataset, taken by the MOJAVE team (Lister et al. 2018)

- target source is the quasar NRAO 190
- observations were carried out in December 2019, using the VLBA at 15 GHz

What can we learn about the source just by inspecting the calibrated visibility data?

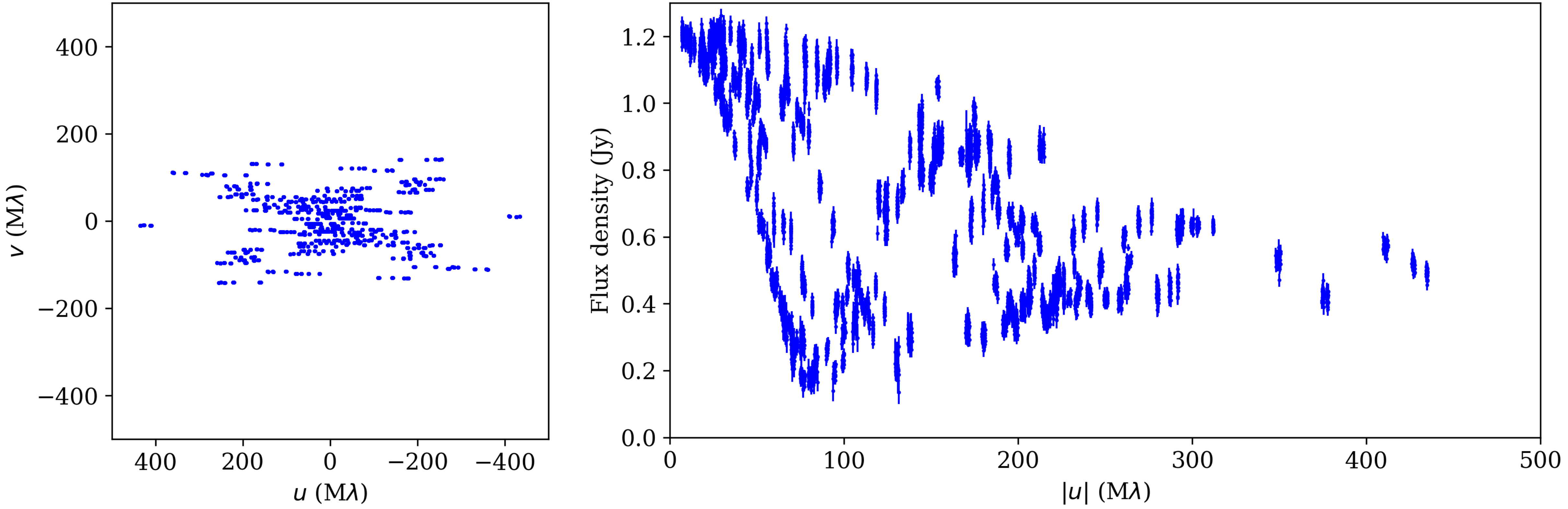

Data credit: MOJAVE team (Lister et al. 2018)

# Data inspection example

Info gathered:

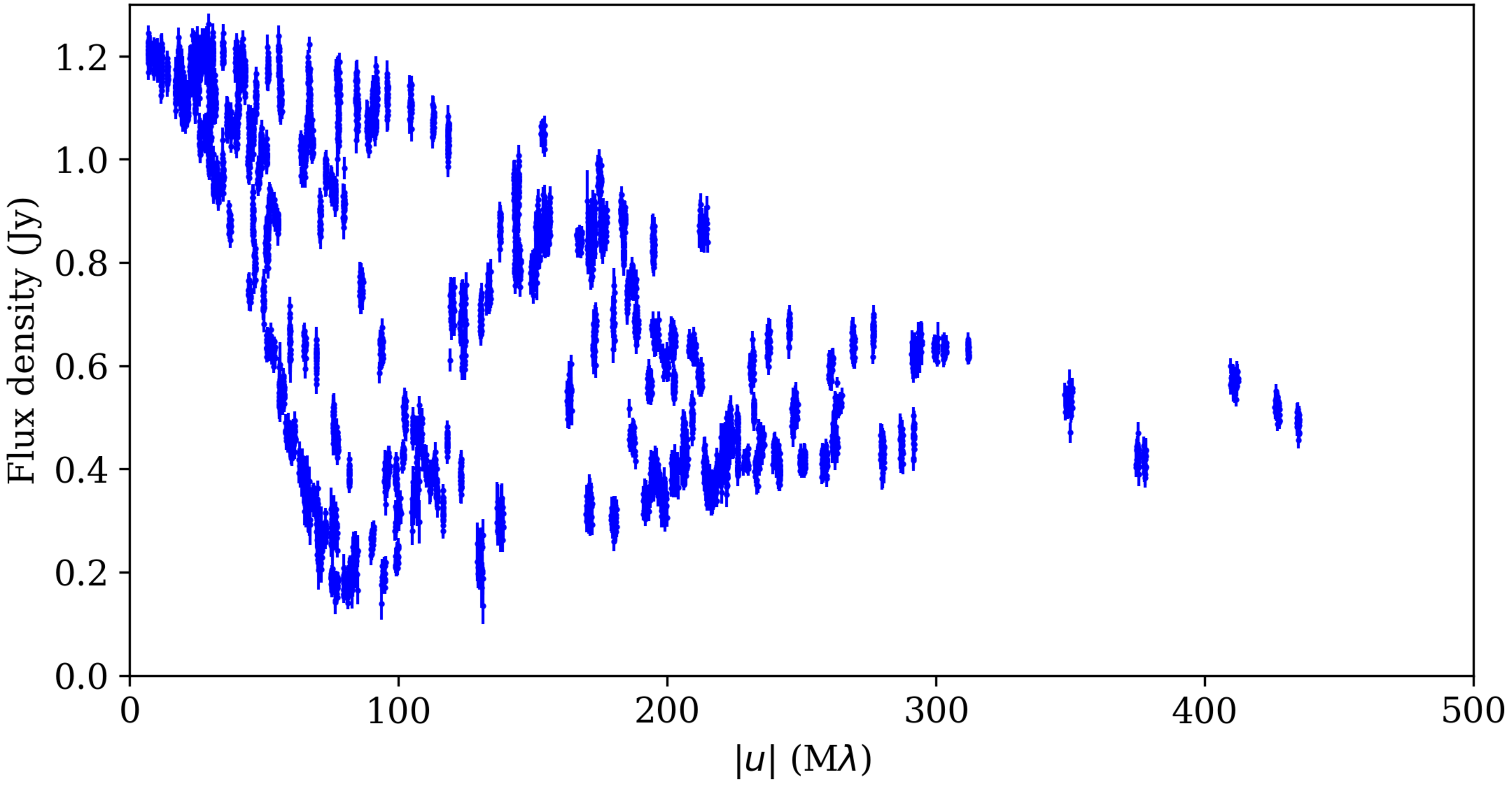

Data credit: MOJAVE team (Lister et al. 2018)

# Data inspection example

Info gathered:

The visibility amplitudes on the shortest baselines converge to ~1.2 Jy

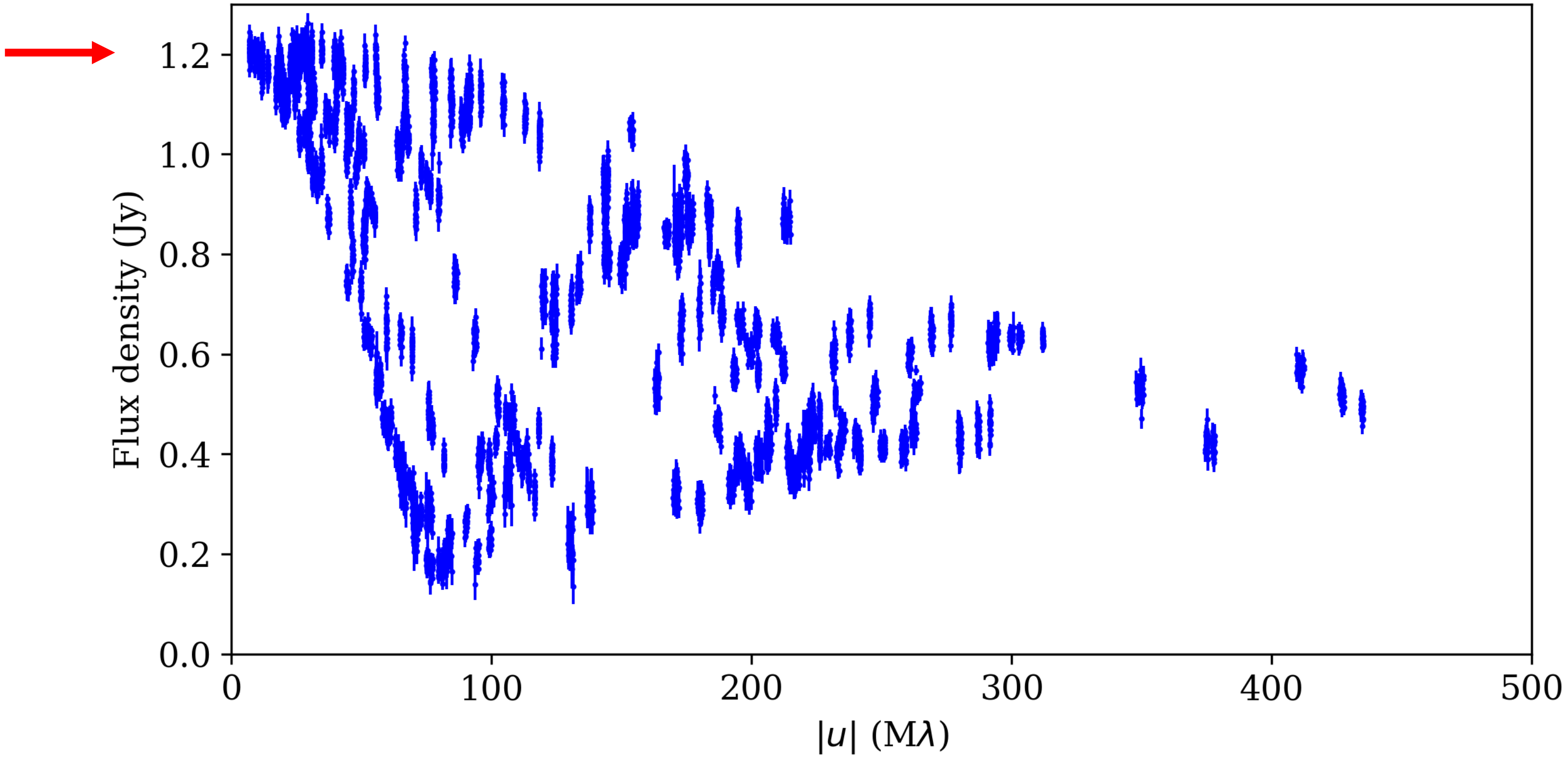

Data credit: MOJAVE team (Lister et al. 2018)

# Data inspection example

Info gathered:

The visibility amplitudes on the shortest baselines converge to ~1.2 Jy

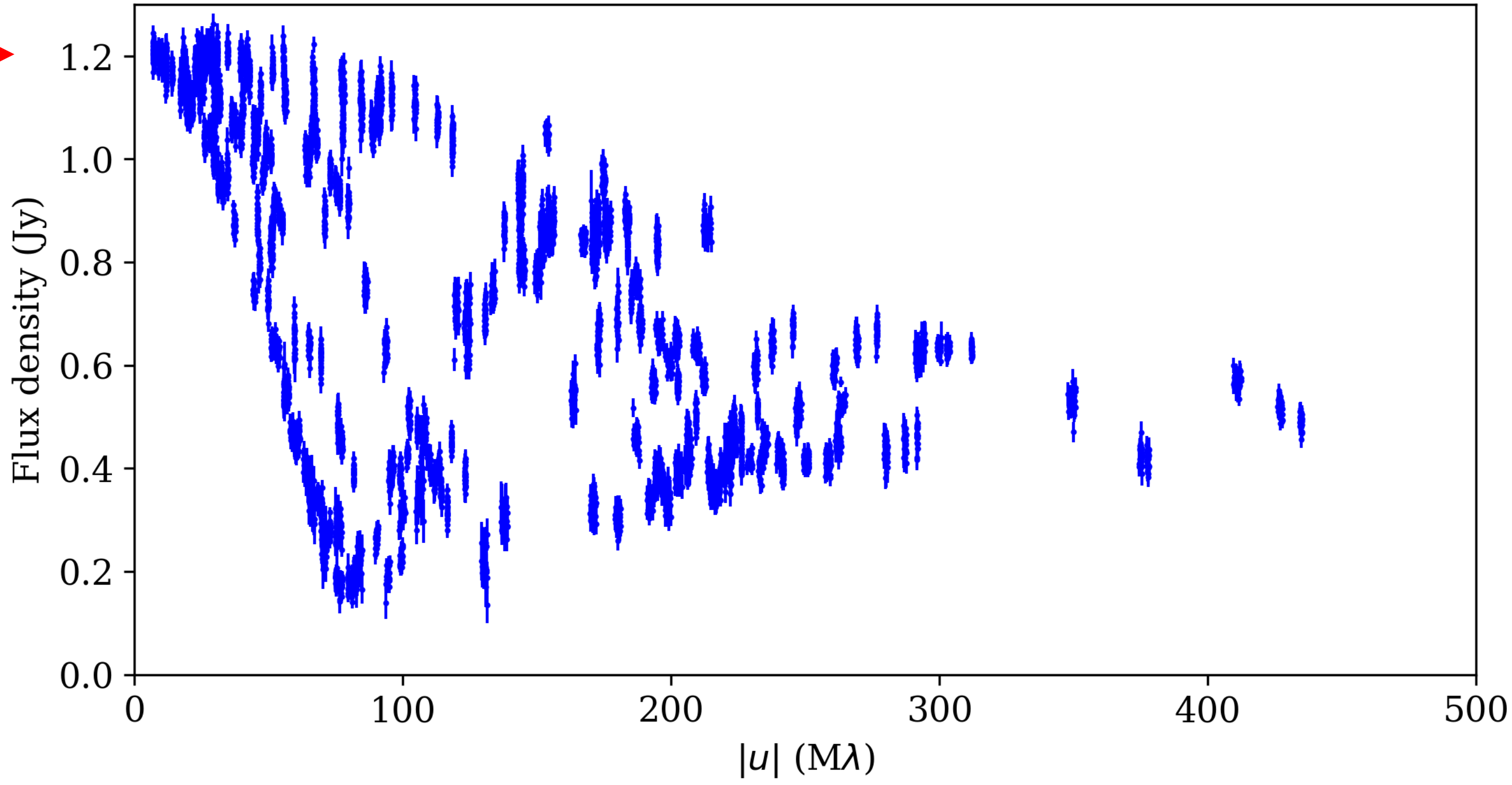


Recall:

$$V(u,v) = \iint I(x,y) e^{-2\pi i(ux+vy)} dx dy$$

$$V(0,0) = \iint I(x,y) dx dy$$

Data credit: MOJAVE team (Lister et al. 2018)

# Data inspection example

Info gathered:

- the total (i.e., spatially-integrated) flux density in the image should be ~1.2 Jy

The visibility amplitudes on the shortest baselines converge to ~1.2 Jy

Recall:

$$V(u,v) = \iint I(x,y) e^{-2\pi i(ux+vy)} dx dy$$

$$V(0,0) = \iint I(x,y) dx dy$$

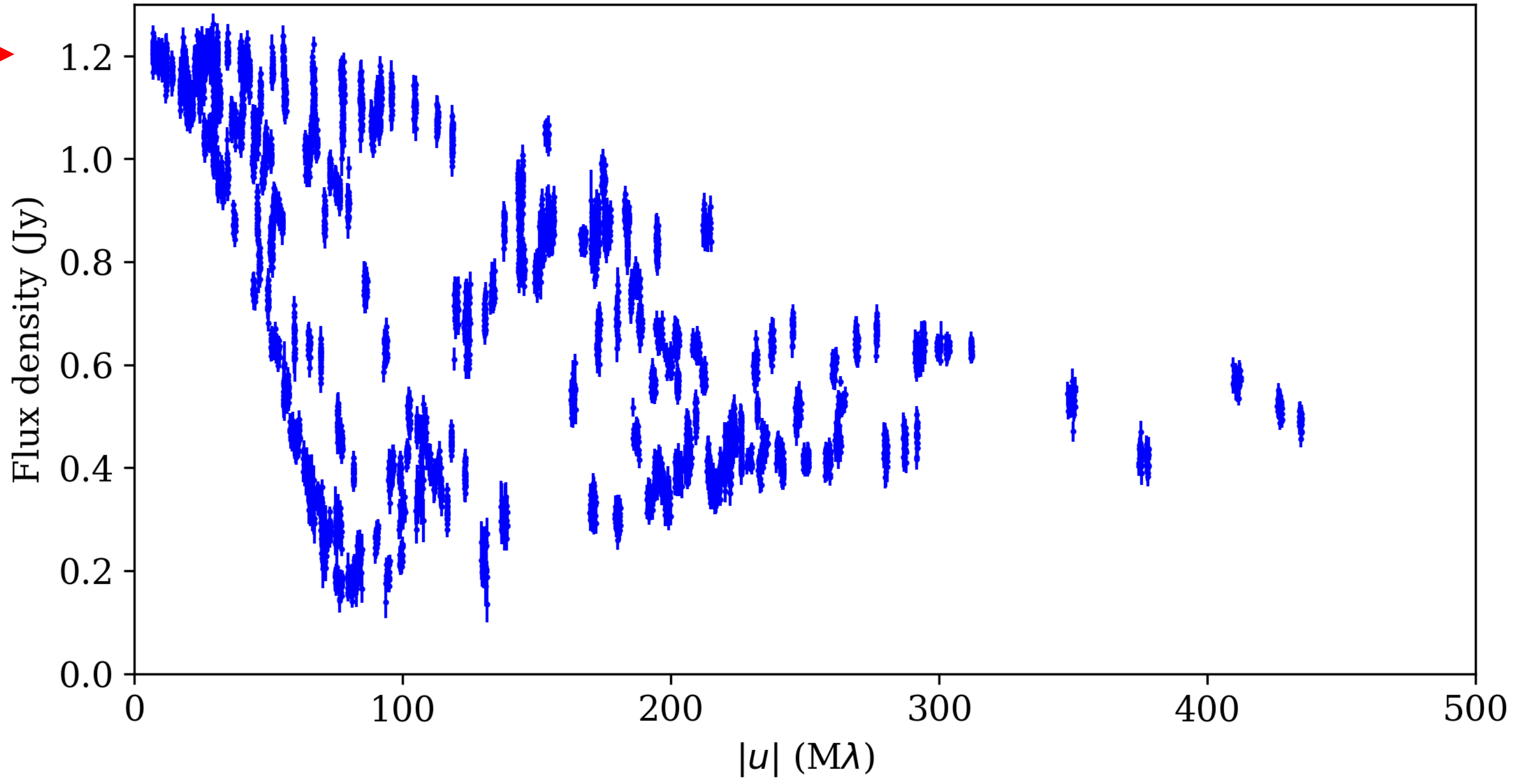

Data credit: MOJAVE team (Lister et al. 2018)

# Data inspection example

Info gathered:

- the total (i.e., spatially-integrated) flux density in the image should be ~1.2 Jy

The envelope of visibility amplitudes is roughly bounded by Gaussians having σ values of 0.75 and 0.1 mas

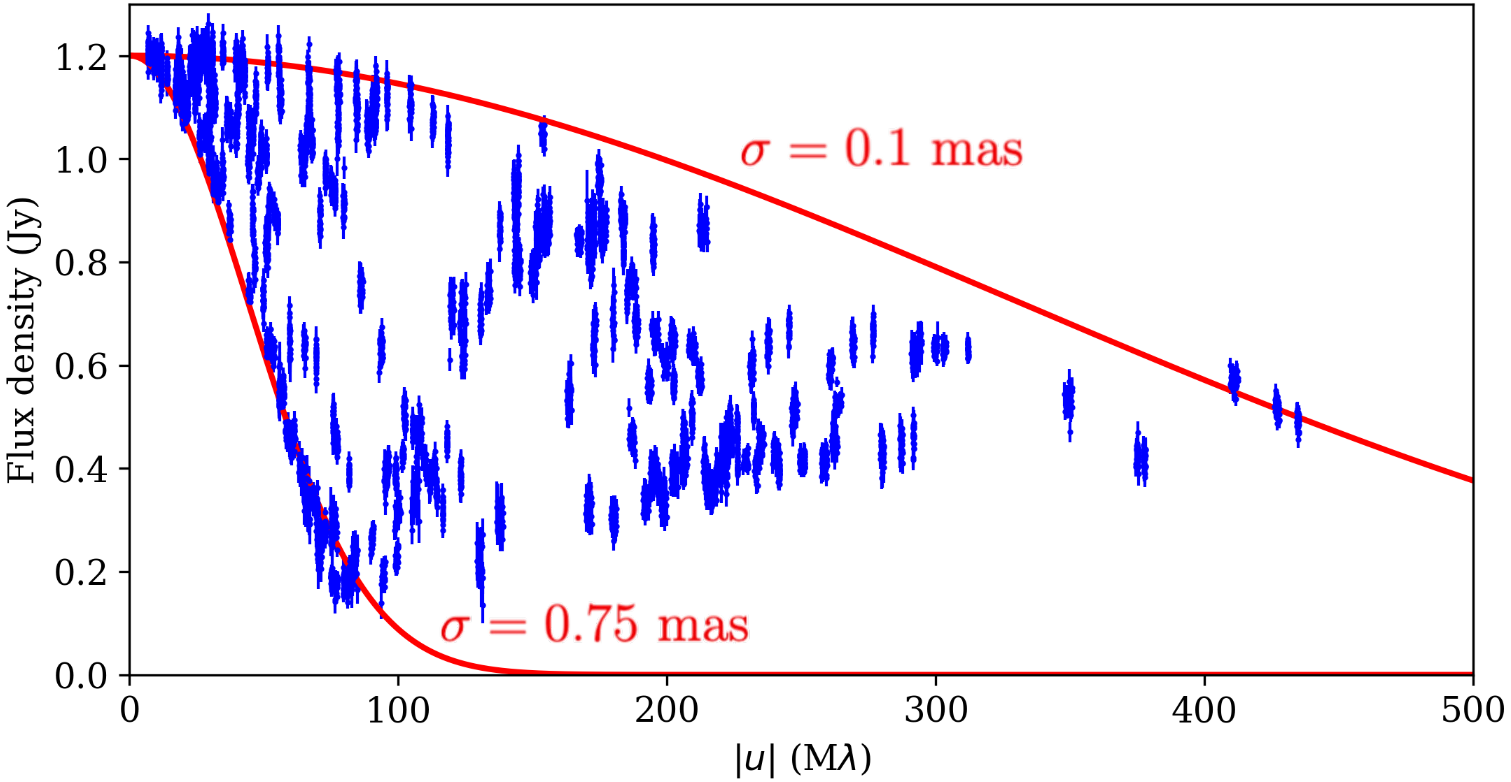

Data credit: MOJAVE team (Lister et al. 2018)

# Data inspection example

Info gathered:

- the total (i.e., spatially-integrated) flux density in the image should be ~1.2 Jy

The envelope of visibility amplitudes is roughly bounded by Gaussians having σ values of 0.75 and 0.1 mas

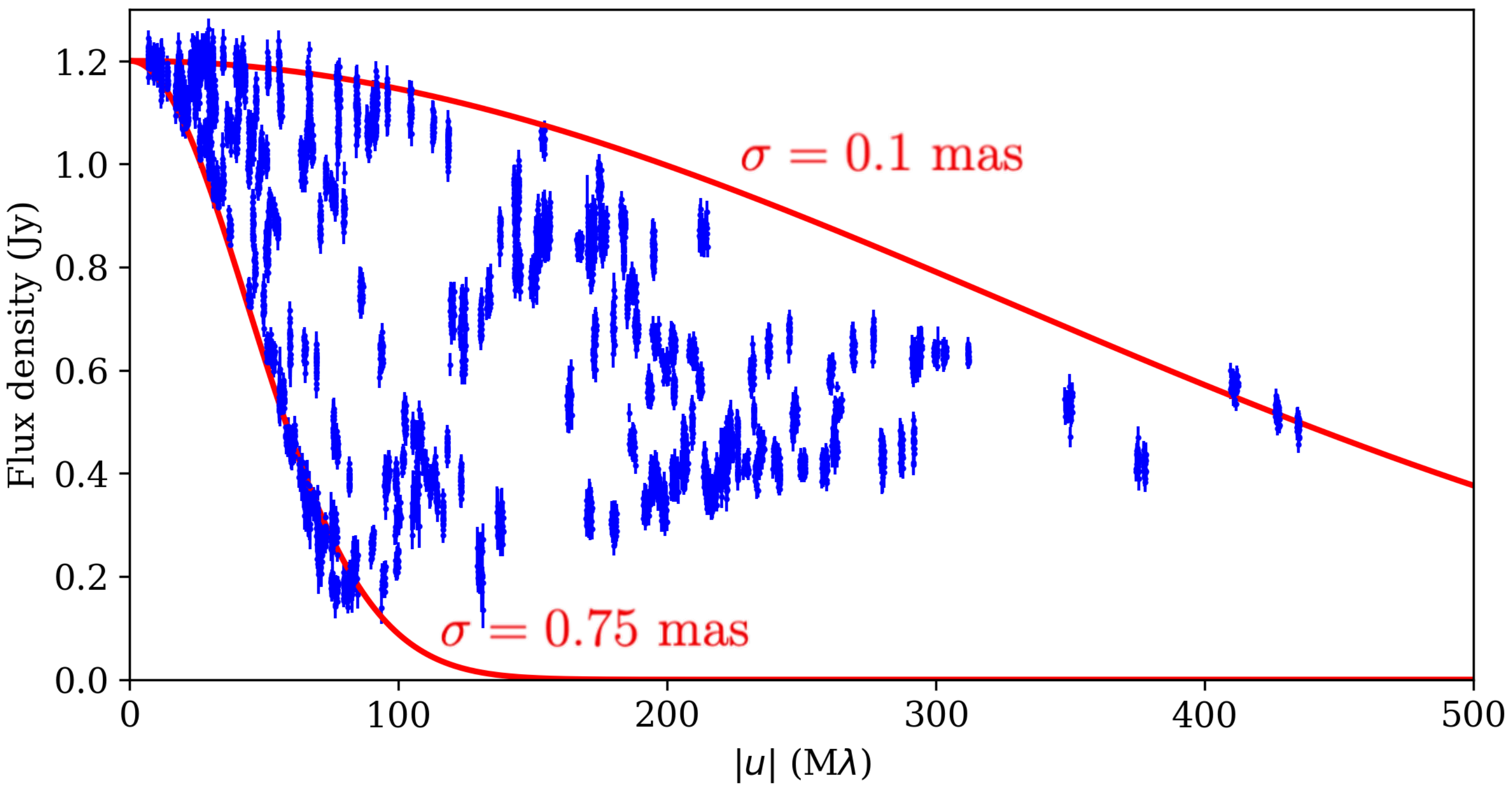


Recall:

$$V(u) \approx V(0) + \frac{1}{2}u^2 V''(0)$$
$$= V(0)\left[1 - \pi^2 u^2 m_2\right]$$

For a Gaussian:

$$m_2 = \sigma^2$$

Data credit: MOJAVE team (Lister et al. 2018)

# Data inspection example

Info gathered:

- the total (i.e., spatially-integrated) flux density in the image should be ~1.2 Jy
- the source has a FWHM extent that is between ~0.24 mas and ~1.8 mas

The envelope of visibility amplitudes is roughly bounded by Gaussians having σ values of 0.75 and 0.1 mas

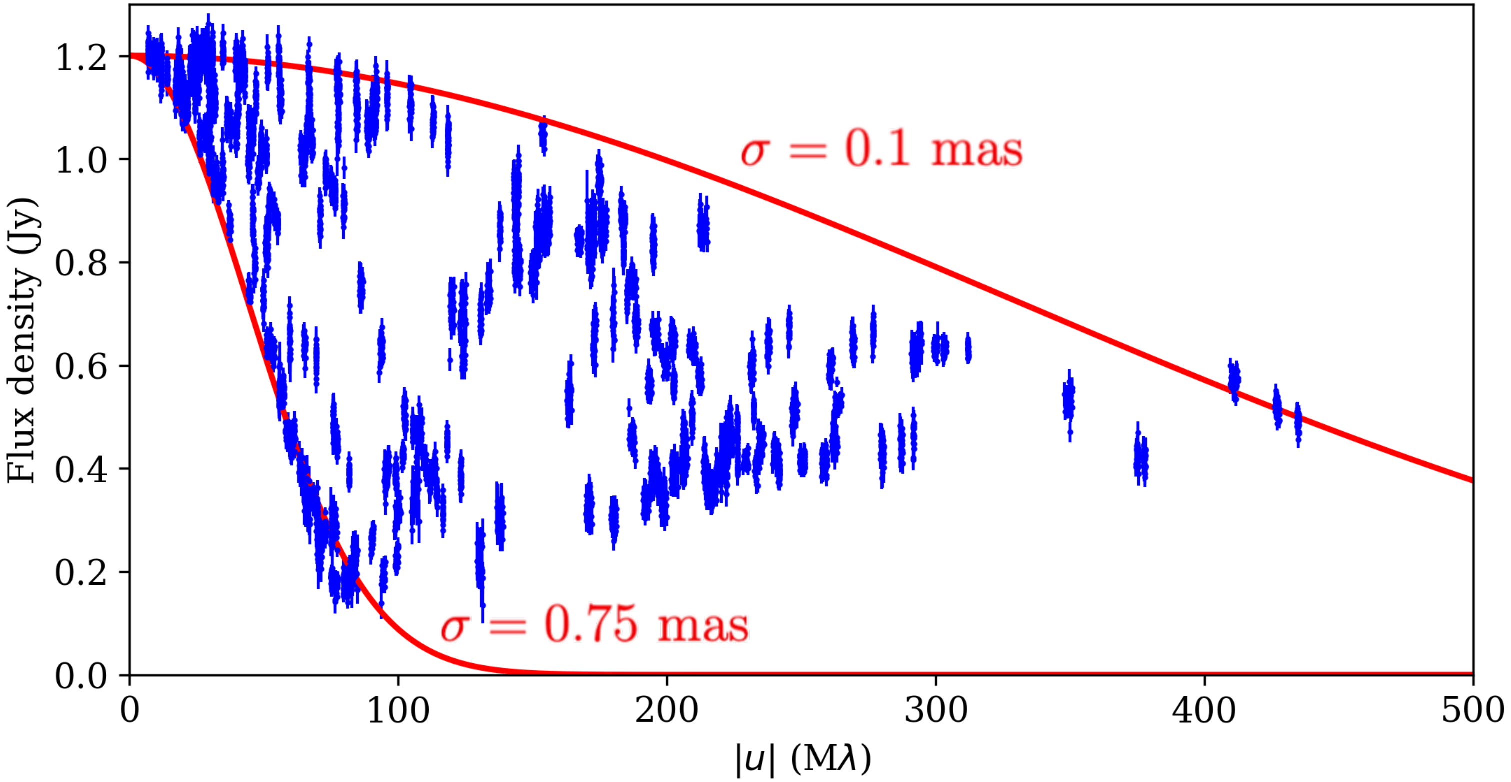


Recall:

$$
\begin{aligned}
V(u) &\approx V(0) + \frac{1}{2}u^2 V''(0) \\
&= V(0)\left[1 - \pi^2 u^2 m_2\right]
\end{aligned}
$$

For a Gaussian:

$$m_2 = \sigma^2$$

# Data inspection example

Info gathered:

- the total (i.e., spatially-integrated) flux density in the image should be ~1.2 Jy
- the source has a FWHM extent that is between ~0.24 mas and ~1.8 mas

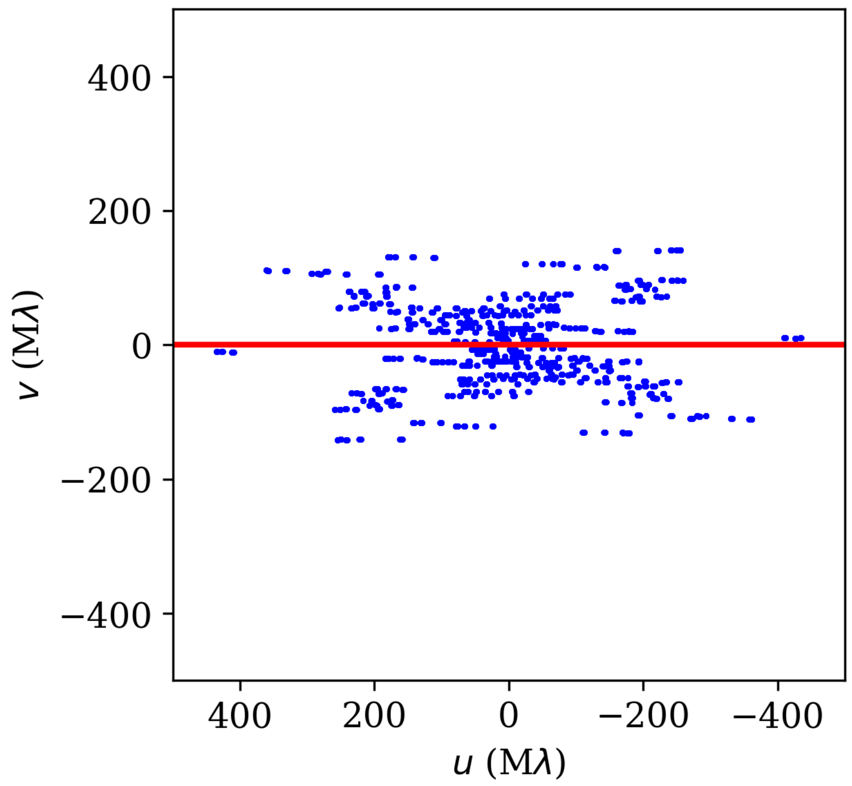


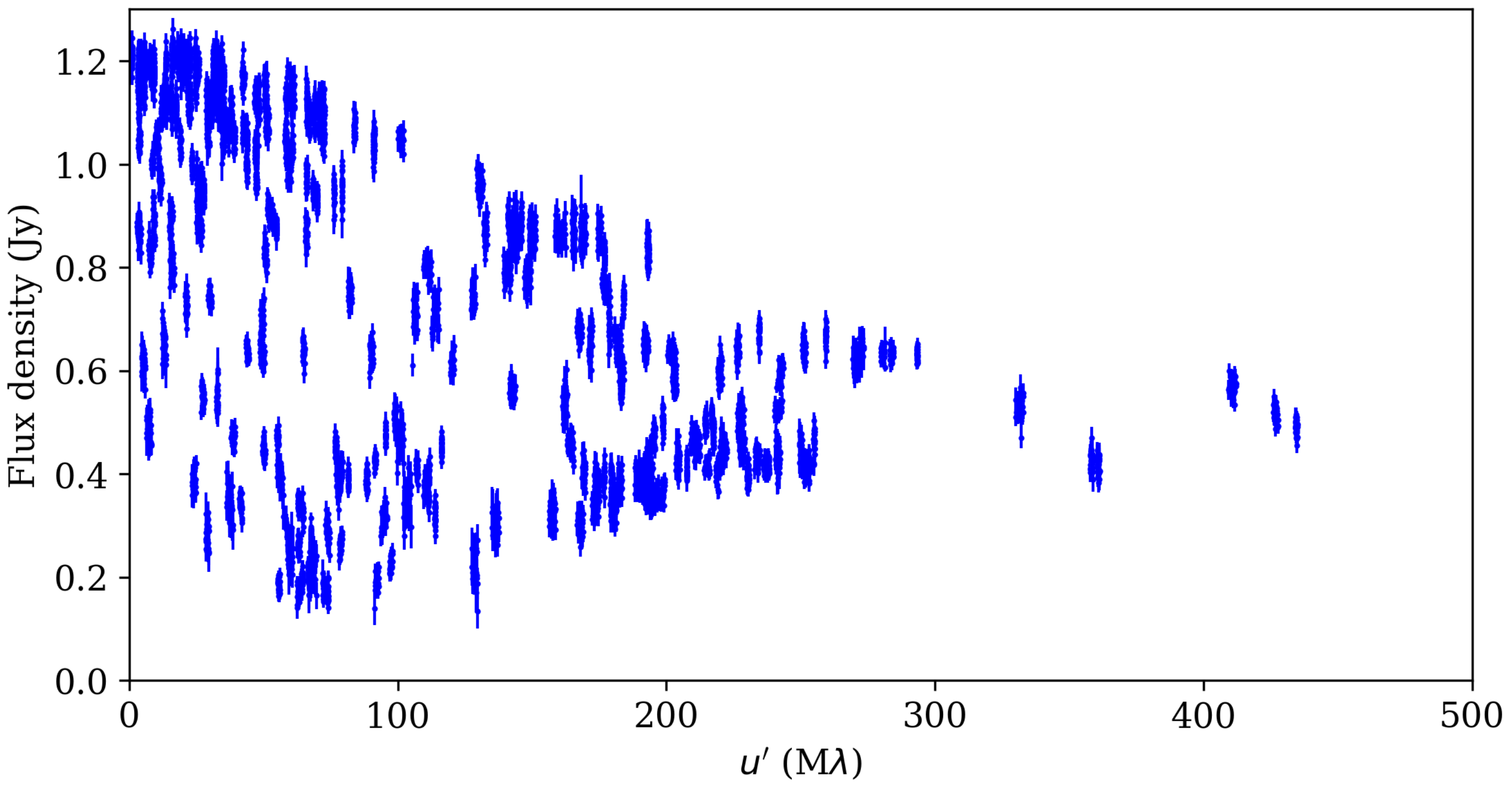

Data credit: MOJAVE team (Lister et al. 2018)

# Data inspection example

Info gathered:

- the total (i.e., spatially-integrated) flux density in the image should be ~1.2 Jy
- the source has a FWHM extent that is between ~0.24 mas and ~1.8 mas

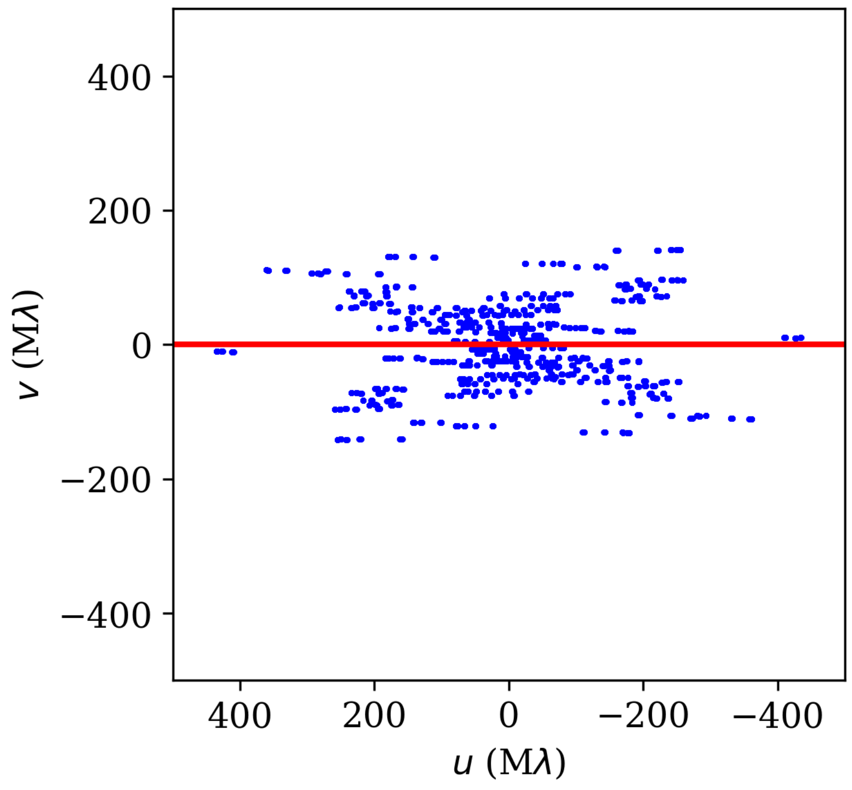


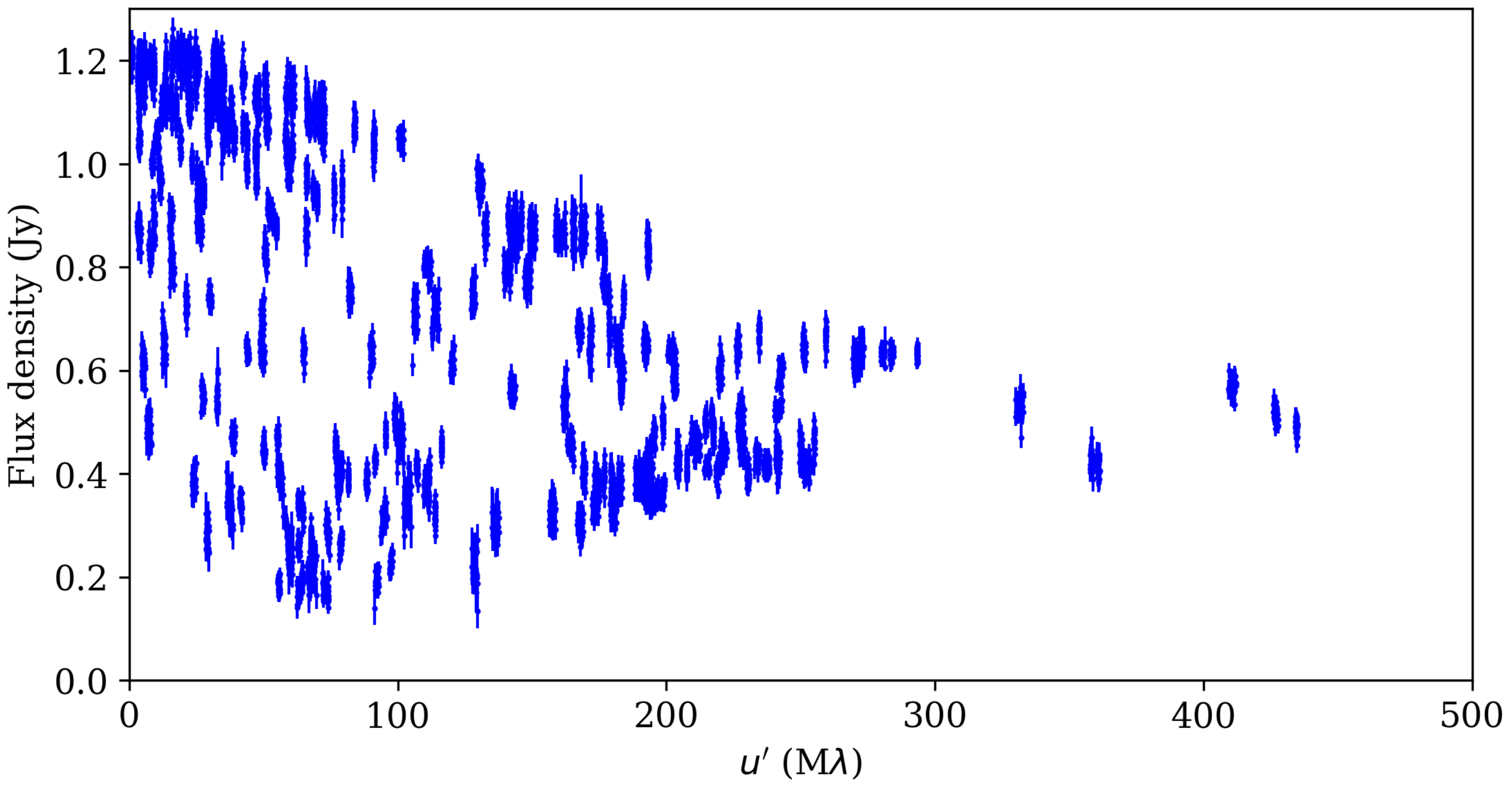

Data credit: MOJAVE team (Lister et al. 2018)

# Data inspection example

Info gathered:

- the total (i.e., spatially-integrated) flux density in the image should be ~1.2 Jy
- the source has a FWHM extent that is between ~0.24 mas and ~1.8 mas
- there's a special orientation at a position angle of ~50 degrees

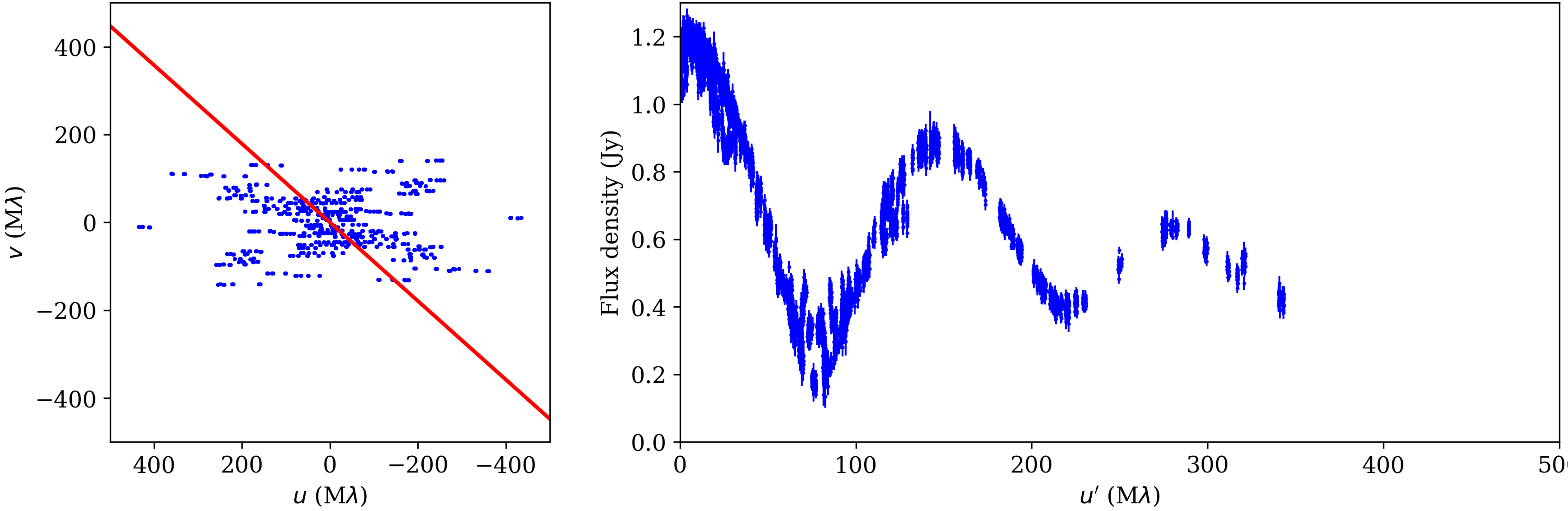

Data credit: MOJAVE team (Lister et al. 2018)

# Data inspection example

Info gathered:

- the total (i.e., spatially-integrated) flux density in the image should be ~1.2 Jy
- the source has a FWHM extent that is between ~0.24 mas and ~1.8 mas
- there's a special orientation at a position angle of ~50 degrees
    - that special orientation has a characteristic length scale of 1/150Mλ ≈ 1.4 mas

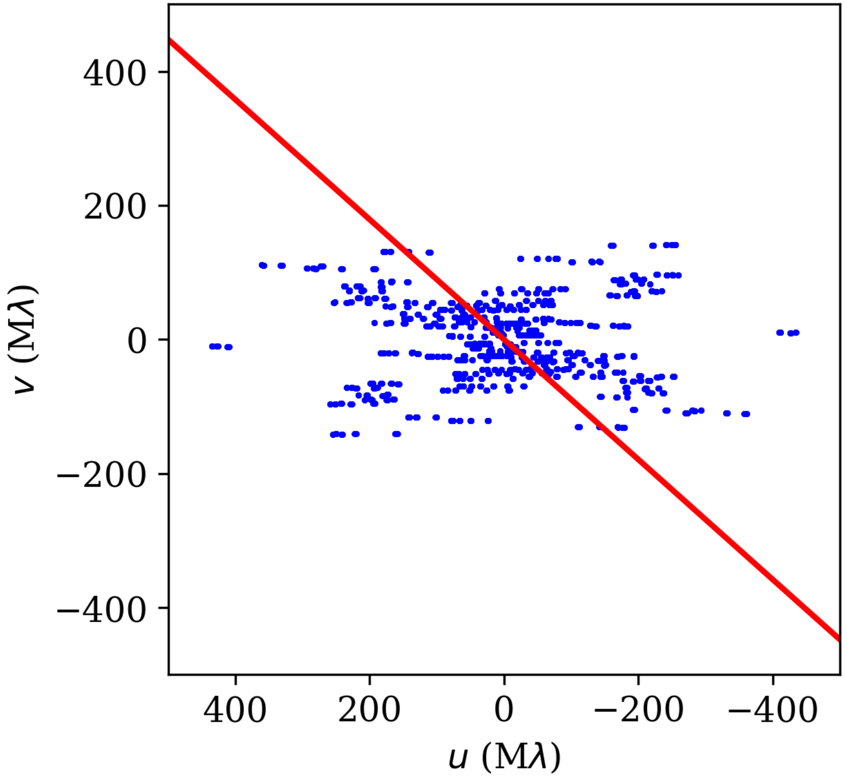


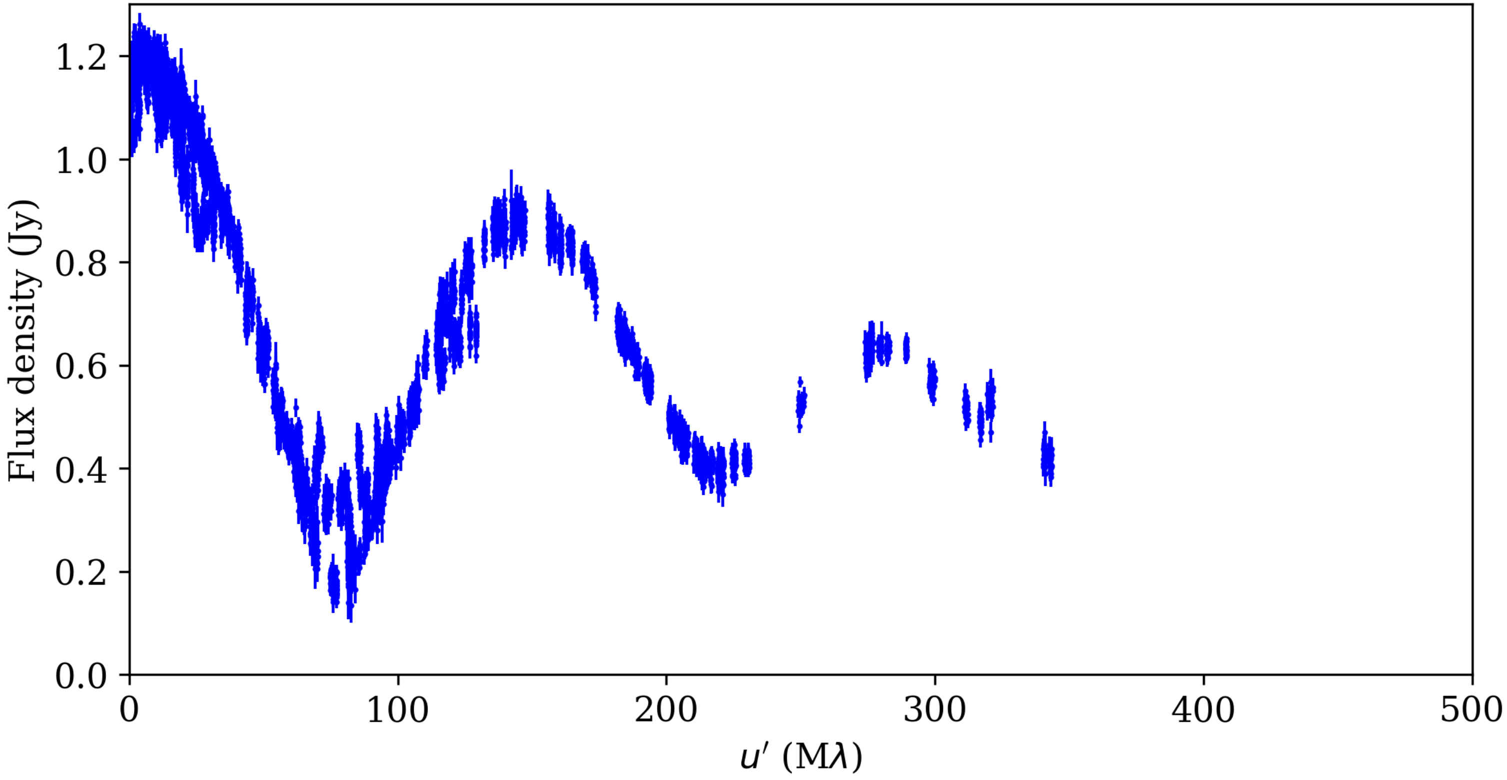

Data credit: MOJAVE team (Lister et al. 2018)

# Data inspection example

Info gathered:

- the total (i.e., spatially-integrated) flux density in the image should be ~1.2 Jy
- the source has a FWHM extent that is between ~0.24 mas and ~1.8 mas
- there's a special orientation at a position angle of ~50 degrees
    - that special orientation has a characteristic length scale of 1/150Mλ ≈ 1.4 mas

How does these expectations compare to the actual image reconstruction?

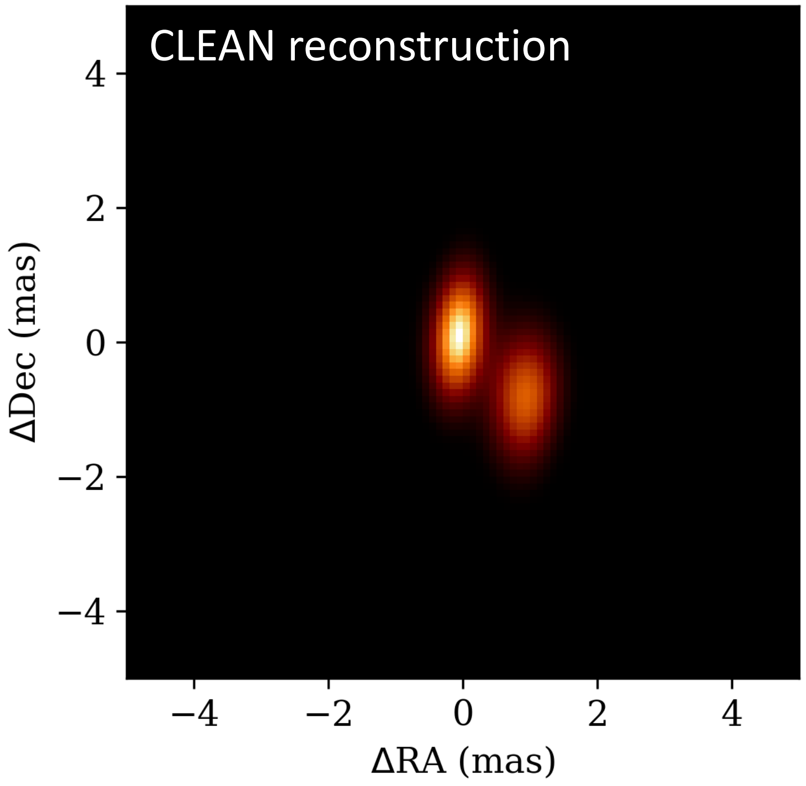

# Data inspection example

Info gathered:

- the total (i.e., spatially-integrated) flux density in the image should be ~1.2 Jy
- the source has a FWHM extent that is between ~0.24 mas and ~1.8 mas
- there's a special orientation at a position angle of ~50 degrees
  - that special orientation has a characteristic length scale of 1/150Mλ ≈ 1.4 mas

How does these expectations compare to the actual image reconstruction?

Total flux density = 1.21 Jy

Second moment principal axes are ~1.35 mas and ~1.5 mas

- beam itself is 0.55 x 1.32 mas

Clear binary structure with a PA of ~50 degrees and a separation of ~1.4 mas

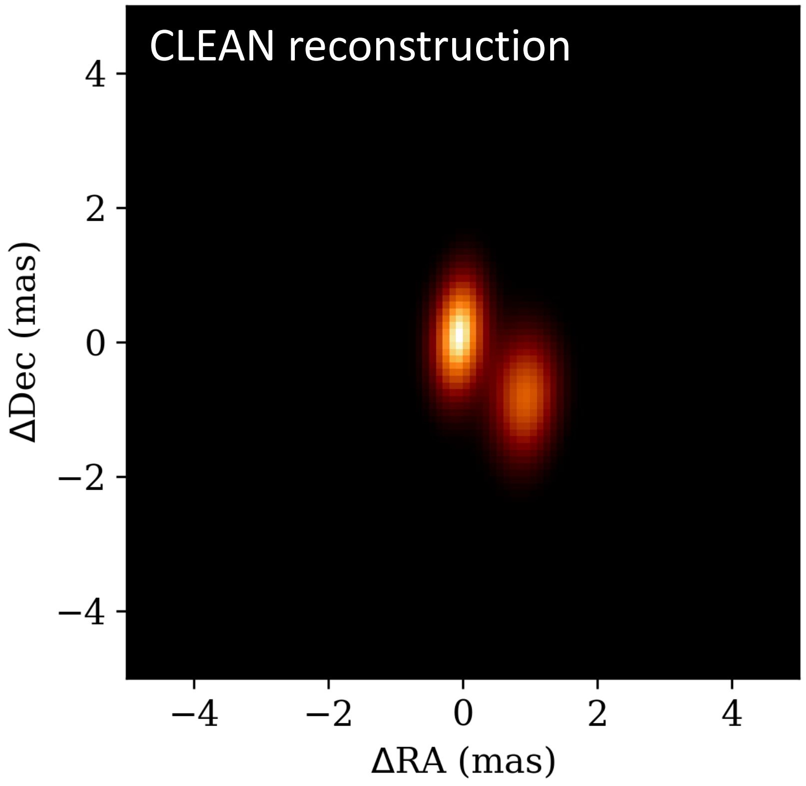

# Additional data products: closure quantities

# Additional data products: closure quantities

Recall: the basic interferometric data products are "visibilities," which are derived from the complex cross-correlation between the electric fields incident at pairs of antennas

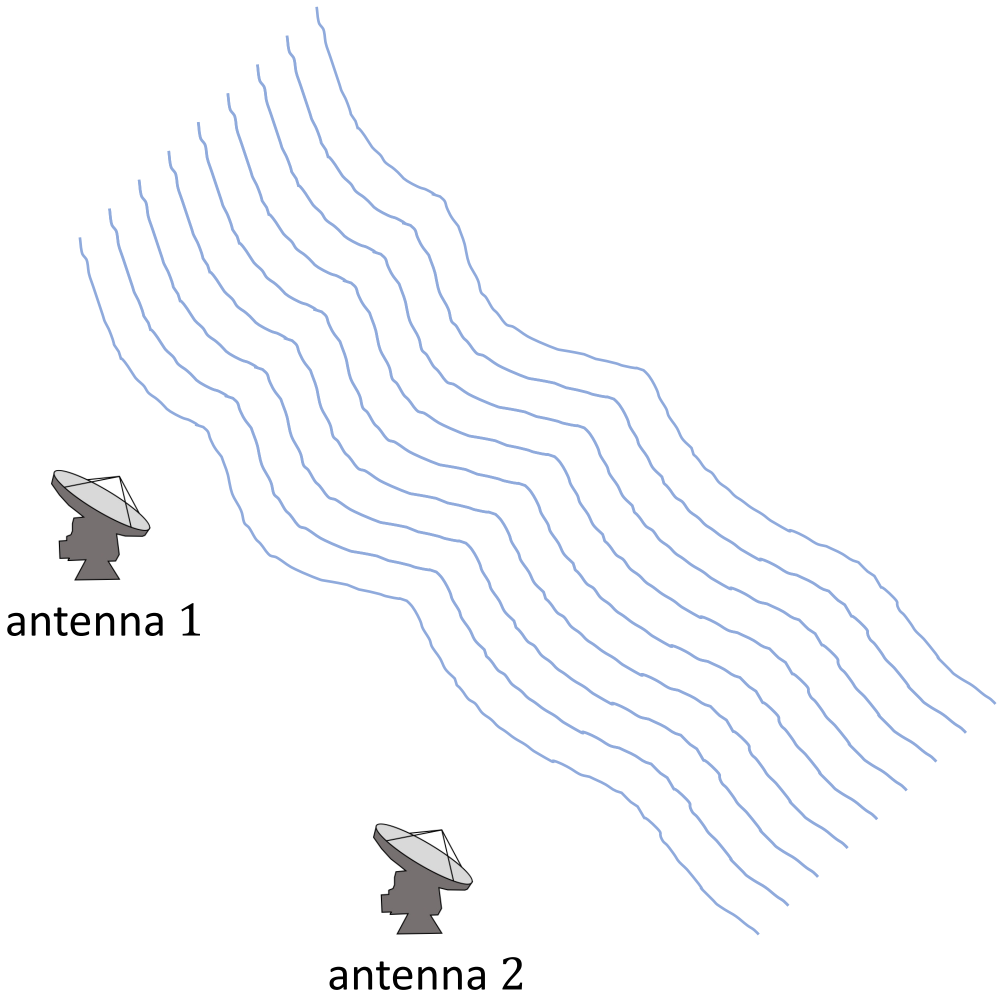


$$V_{12} = \langle E_1 E_2^* \rangle = A_{12} e^{i\phi_{12}}$$

# Additional data products: closure quantities

Recall: the basic interferometric data products are "visibilities," which are derived from the complex cross-correlation between the electric fields incident at pairs of antennas

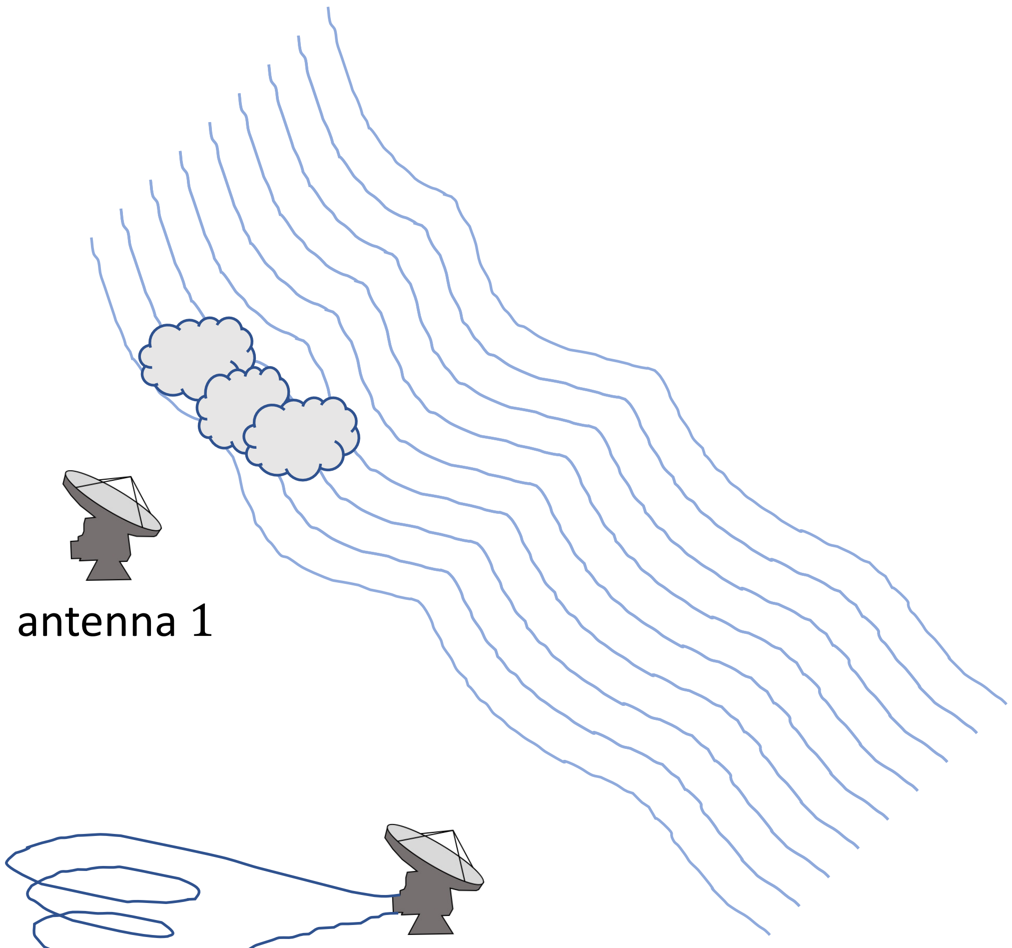


$$V_{12} = \langle E_1 E_2^* \rangle = A_{12} e^{i\phi_{12}}$$

$$\begin{aligned} \hat{V}_{12} &= \langle (G_1 E_1)(G_2 E_2)^* \rangle \\ &= G_1 \langle E_1 E_2^* \rangle G_2^* \\ &= G_1 V_{12} G_2^* \end{aligned}$$

Multiplicative complex "gain" effects at each antenna typically constitute the primary systematic corruption of the measured visibilities

- the gains can be difficult to calibrate, particularly at high observing frequencies or for VLBI observations

# Additional data products: closure quantities

The classic “closure” quantity is the closure phase (Jennison 1958), which is the argument of the product of visibilities around a triangle of baselines

$$\hat{V}_{12}\hat{V}_{23}\hat{V}_{31} = (G_1 V_{12} G_2^*)\,(G_2 V_{23} G_3^*)\,(G_3 V_{31} G_1^*)$$

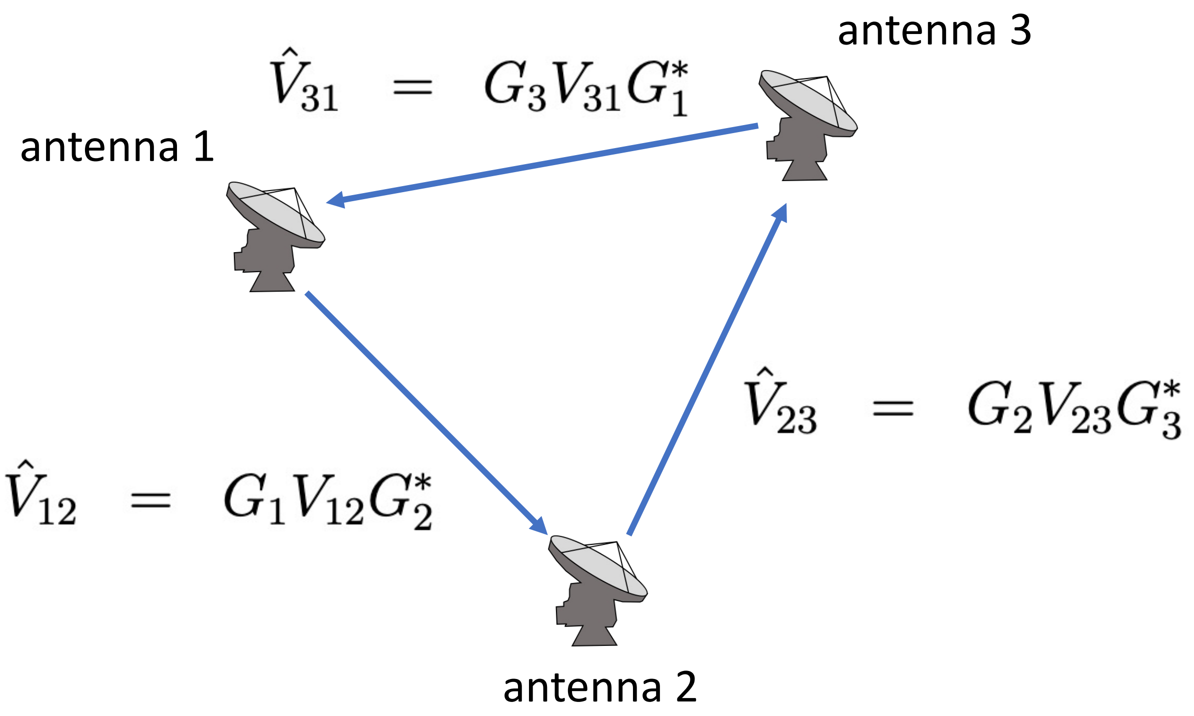

# Additional data products: closure quantities

The classic "closure" quantity is the closure phase (Jennison 1958), which is the argument of the product of visibilities around a triangle of baselines

$$
\begin{aligned}
\hat{V}_{12}\hat{V}_{23}\hat{V}_{31} &= \left(G_1 V_{12} G_2^*\right)\left(G_2 V_{23} G_3^*\right)\left(G_3 V_{31} G_1^*\right) \\
&= \left(G_1 G_1^*\right)\left(G_2 G_2^*\right)\left(G_3 G_3^*\right) V_{12} V_{23} V_{31}
\end{aligned}
$$

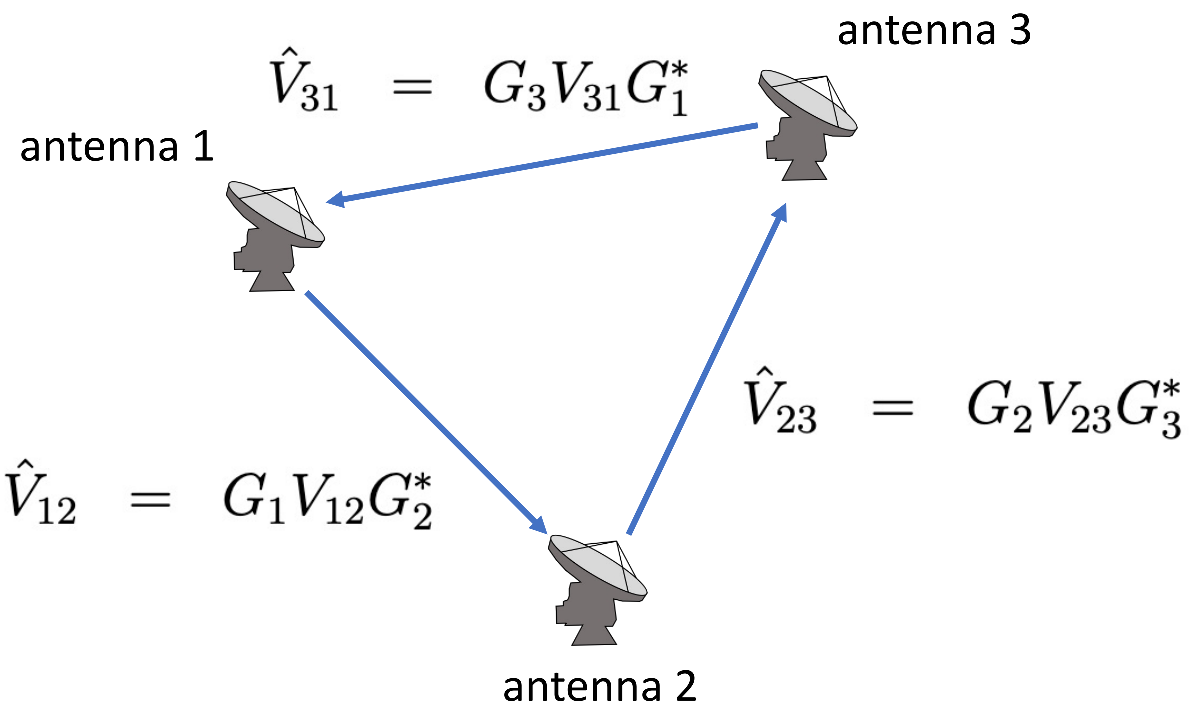

# Additional data products: closure quantities

The classic "closure" quantity is the closure phase (Jennison 1958), which is the argument of the product of visibilities around a triangle of baselines

$$\hat{V}_{12}\hat{V}_{23}\hat{V}_{31} = (G_1 V_{12} G_2^*)(G_2 V_{23} G_3^*)(G_3 V_{31} G_1^*)$$

$$= (G_1 G_1^*)(G_2 G_2^*)(G_3 G_3^*) V_{12} V_{23} V_{31}$$

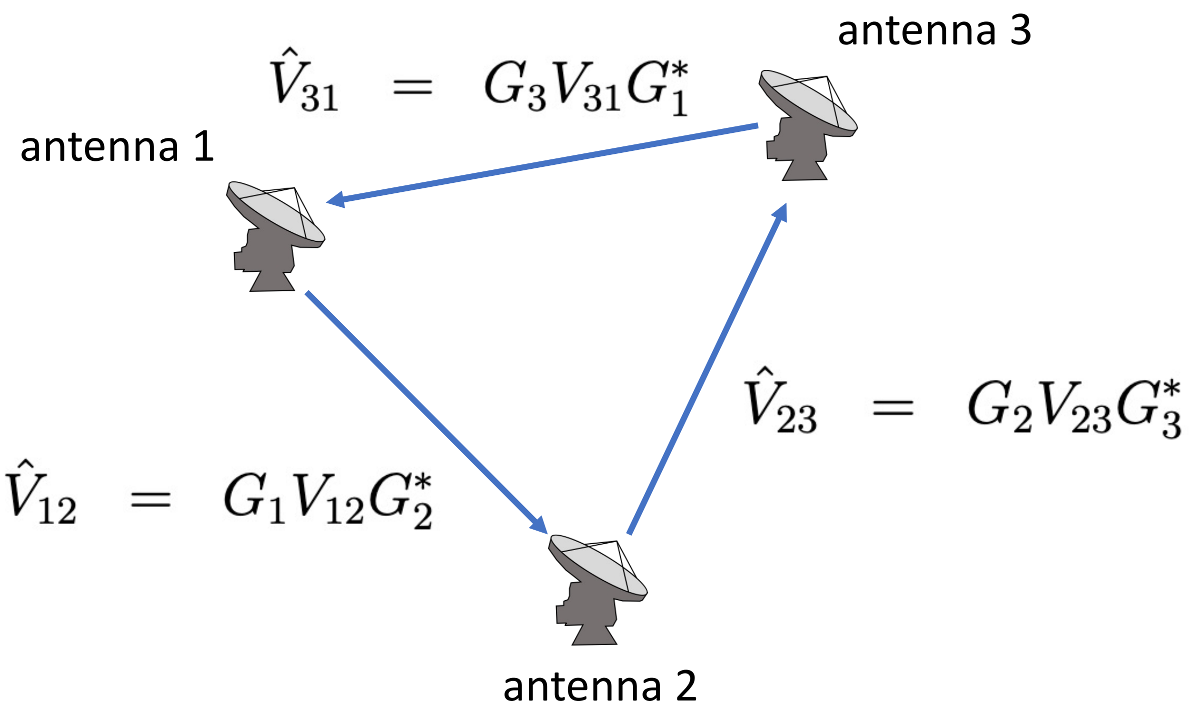


$$\arg\left(\hat{V}_{12}\hat{V}_{23}\hat{V}_{31}\right) = \arg\left(V_{12} V_{23} V_{31}\right)$$

$$\hat{\phi}_{12} + \hat{\phi}_{23} + \hat{\phi}_{31} = \phi_{12} + \phi_{23} + \phi_{31}$$

A key property of the closure phase is that it is invariant to station-based phase corruptions, making it a "robust" observable

# Additional data products: closure quantities

The classic “closure” quantity is the closure phase (Jennison 1958), which is the argument of the product of visibilities around a triangle of baselines

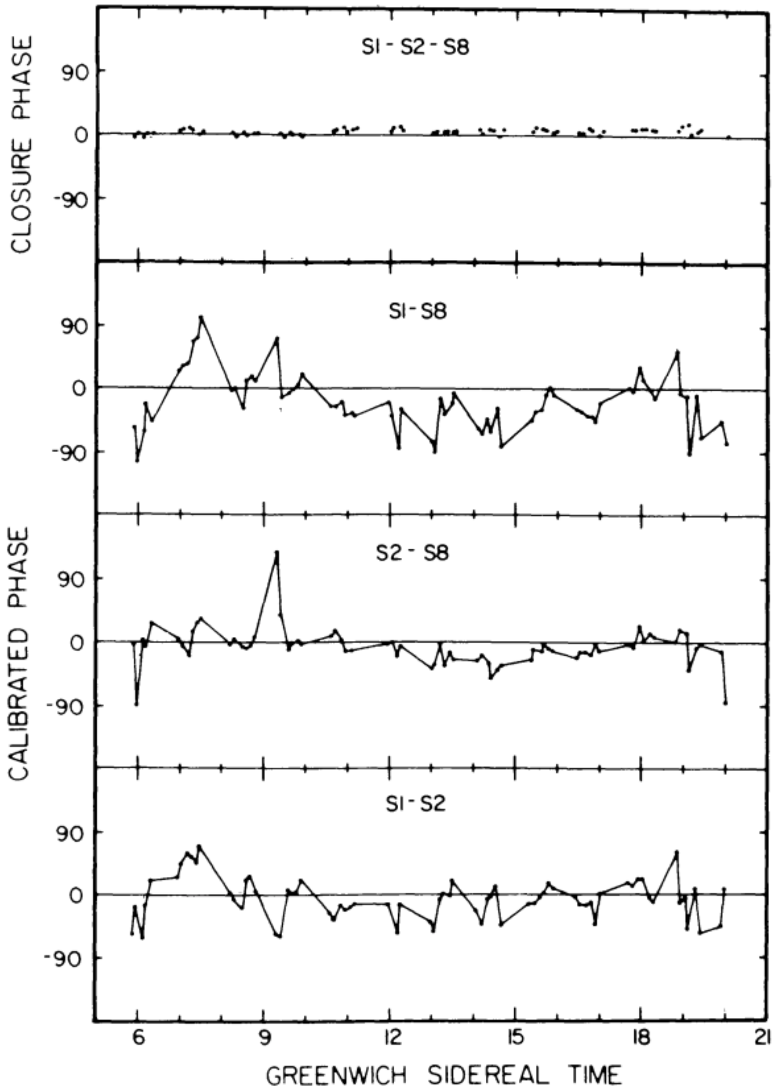


Readhead, Napier, & Bignell (1980)

# Additional data products: closure quantities

The classic "closure" quantity is the closure phase (Jennison 1958), which is the argument of the product of visibilities around a triangle of baselines

Closure phases are difficult to interpret directly, but encode a measure of the "asymmetry" of a source

- any point-symmetric source will have zero-valued closure phases
- nonzero values indicate a departure from point symmetry

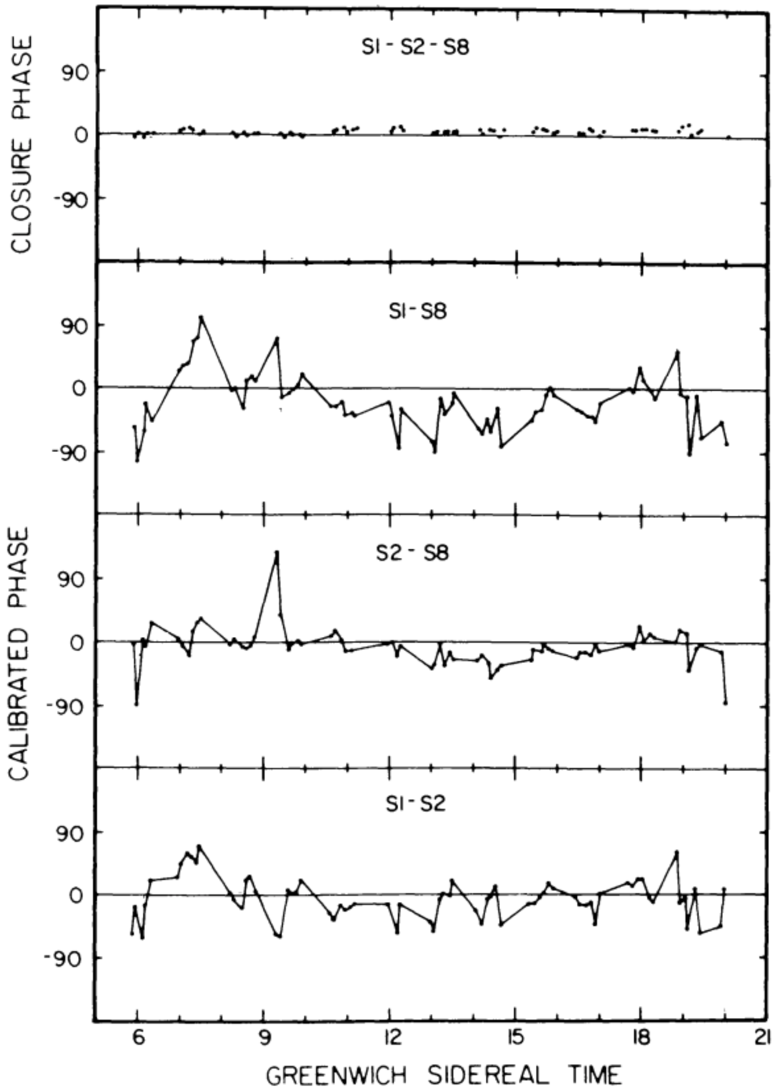


Readhead, Napier, & Bignell (1980)

# Additional data products: closure quantities

The classic "closure" quantity is the closure phase (Jennison 1958), which is the argument of the product of visibilities around a triangle of baselines

Closure phases are difficult to interpret directly, but encode a measure of the "asymmetry" of a source

- any point-symmetric source will have zero-valued closure phases
- nonzero values indicate a departure from point symmetry

However, closure phases are also insensitive to an overall phase gradient

- equivalently, closure phases are insensitive to the absolute position of the source because $\boldsymbol{u}_{12} + \boldsymbol{u}_{23} + \boldsymbol{u}_{31} = 0$

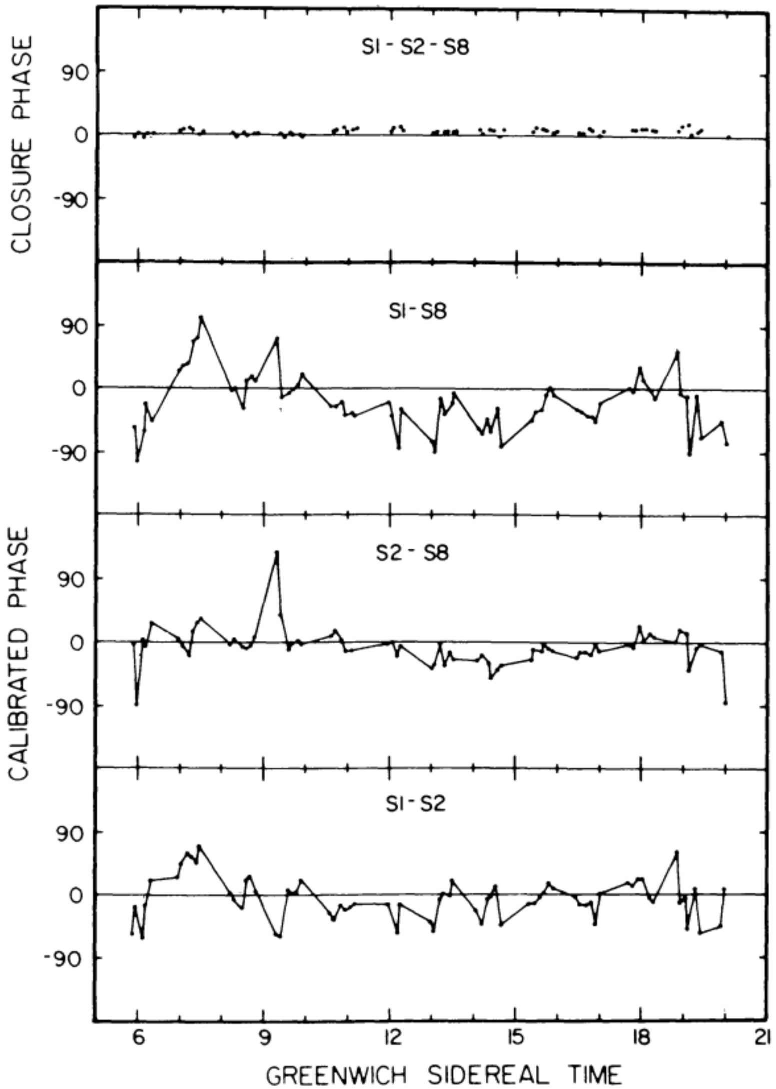


Readhead, Napier, & Bignell (1980)

# Additional data products: closure quantities

The classic "closure" quantity is the closure phase (Jennison 1958), which is the argument of the product of visibilities around a triangle of baselines

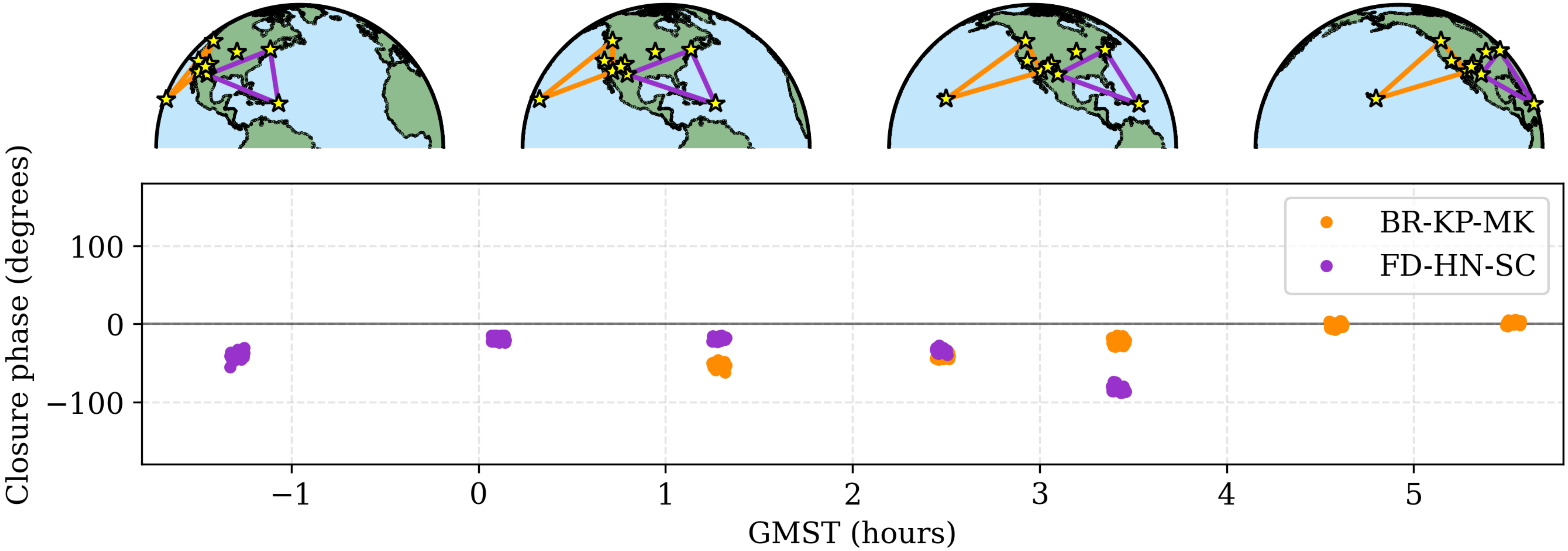


Data credit: MOJAVE team (Lister et al. 2018)

# Additional data products: closure quantities

In addition to the closure phase, an amplitude quantity – called a “closure amplitude” – can be formed from a closed loop of four stations (Twiss, Carter, & Little 1960)

$$\frac{\hat{V}_{12}\hat{V}_{34}}{\hat{V}_{23}\hat{V}_{41}} = \frac{(G_1 V_{12} G_2^*)\,(G_3 V_{34} G_4^*)}{(G_2 V_{23} G_3^*)\,(G_4 V_{41} G_1^*)}$$

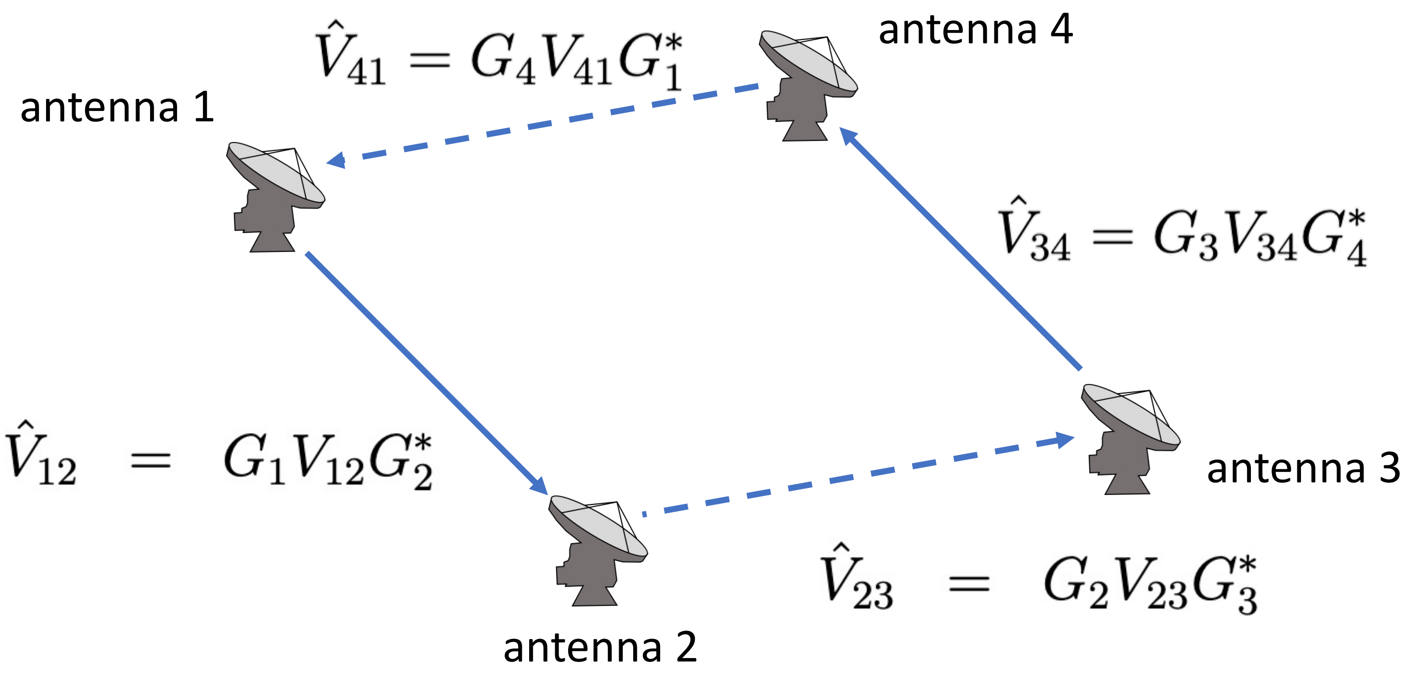

# Additional data products: closure quantities

In addition to the closure phase, an amplitude quantity – called a "closure amplitude" – can be formed from a closed loop of four stations (Twiss, Carter, & Little 1960)

$$\frac{\hat{V}_{12}\hat{V}_{34}}{\hat{V}_{23}\hat{V}_{41}} = \frac{(G_1 V_{12} G_2^*)\,(G_3 V_{34} G_4^*)}{(G_2 V_{23} G_3^*)\,(G_4 V_{41} G_1^*)}$$

$$= \left(\frac{G_1}{G_1^*}\right)\left(\frac{G_2^*}{G_2}\right)\left(\frac{G_3}{G_3^*}\right)\left(\frac{G_4^*}{G_4}\right)\frac{V_{12}V_{34}}{V_{23}V_{41}}$$

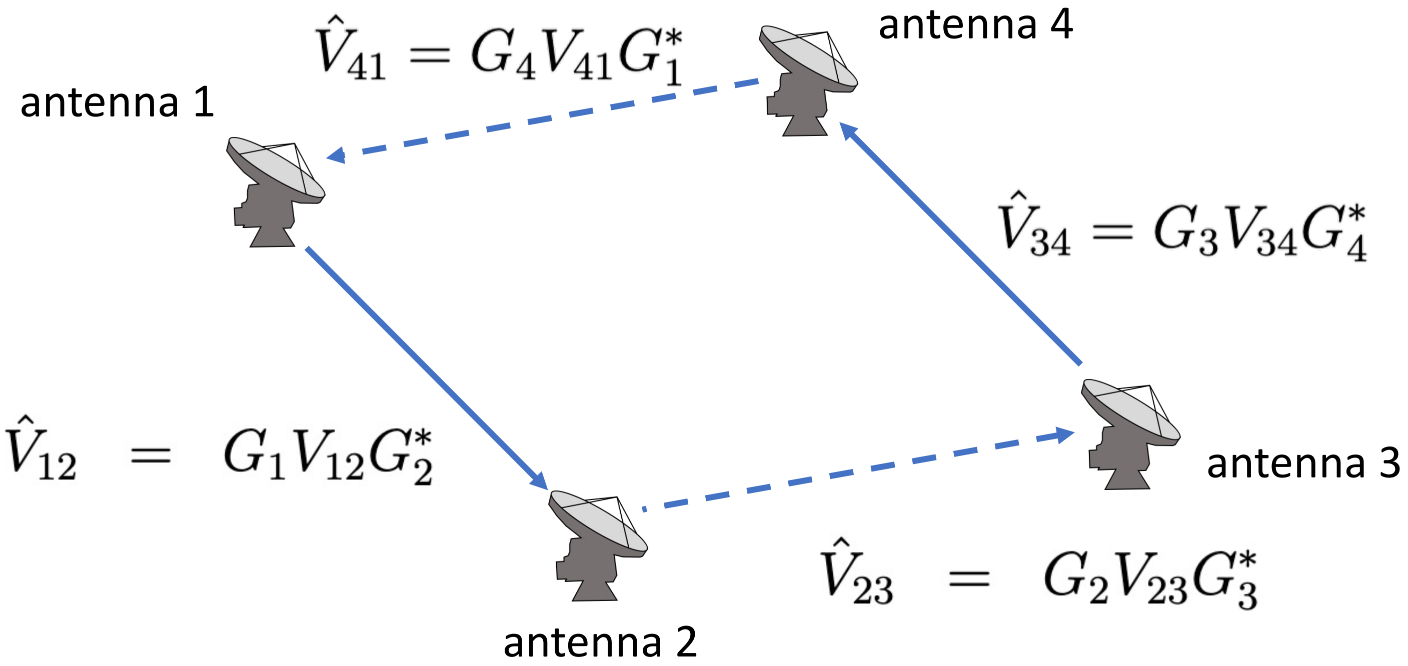

# Additional data products: closure quantities

In addition to the closure phase, an amplitude quantity – called a “closure amplitude” – can be formed from a closed loop of four stations (Twiss, Carter, & Little 1960)

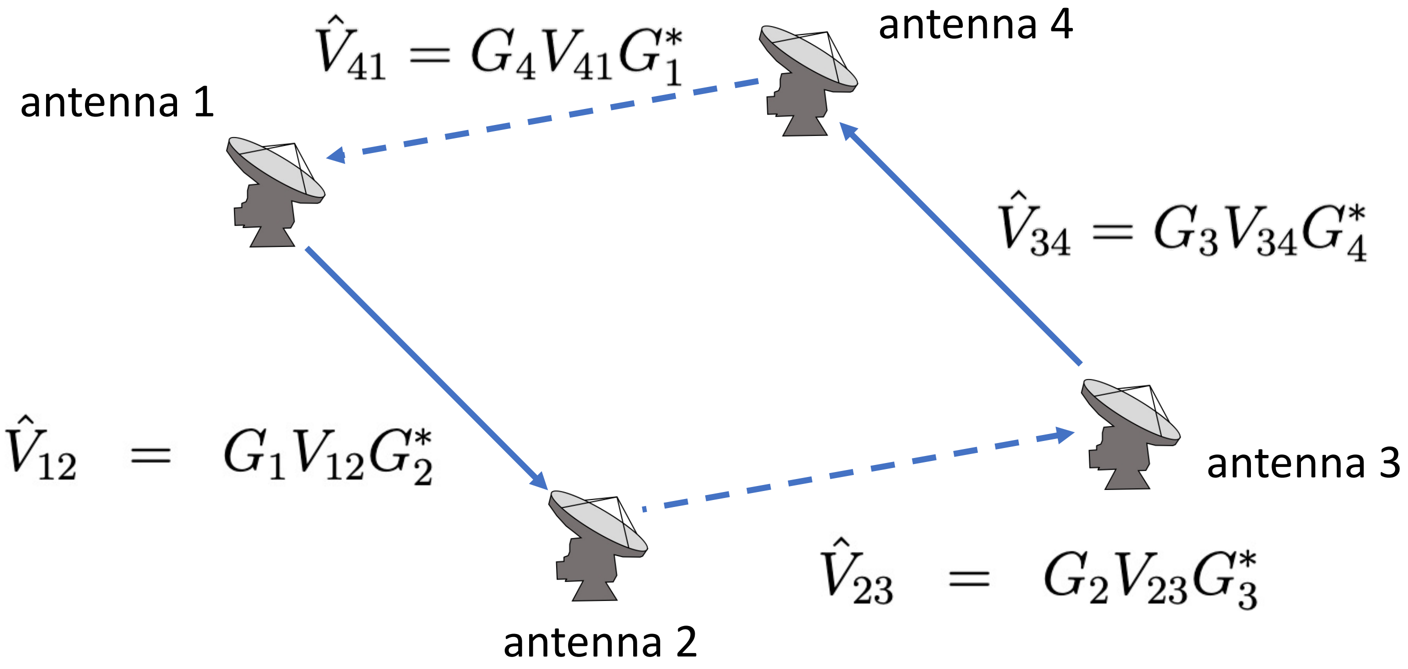


$$\frac{\hat{V}_{12}\hat{V}_{34}}{\hat{V}_{23}\hat{V}_{41}} = \frac{(G_1 V_{12} G_2^*)\,(G_3 V_{34} G_4^*)}{(G_2 V_{23} G_3^*)\,(G_4 V_{41} G_1^*)}$$

$$= \left(\frac{G_1}{G_1^*}\right)\left(\frac{G_2^*}{G_2}\right)\left(\frac{G_3}{G_3^*}\right)\left(\frac{G_4^*}{G_4}\right)\frac{V_{12}V_{34}}{V_{23}V_{41}}$$

$$\left|\frac{\hat{V}_{12}\hat{V}_{34}}{\hat{V}_{23}\hat{V}_{41}}\right| = \left|\frac{V_{12}V_{34}}{V_{23}V_{41}}\right|$$

Closure amplitudes are insensitive to station-based amplitude corruptions

# Additional data products: closure quantities

Between them, the closure phases and amplitudes represent a “complete” set of observables

- i.e., all station gain-independent information in the complex visibilities is retained in the closure phases and amplitudes (Blackburn et al. 2019)

# Additional data products: closure quantities

Between them, the closure phases and amplitudes represent a "complete" set of observables

- i.e., all station gain-independent information in the complex visibilities is retained in the closure phases and amplitudes (Blackburn et al. 2019)

For full-Stokes observations, additional station-based corruptions in the form of polarization leakage become important

- more heavily composite quantities such as "closure traces" (Broderick & Pesce 2020) and "closure invariants" (Samuel, Nityananda, & Thyagarajan 2022) can be constructed that are insensitive to *all* station-based corruptions, including gains and leakage (both phase and amplitude)
- can be used to determine the presence of polarized flux in the source

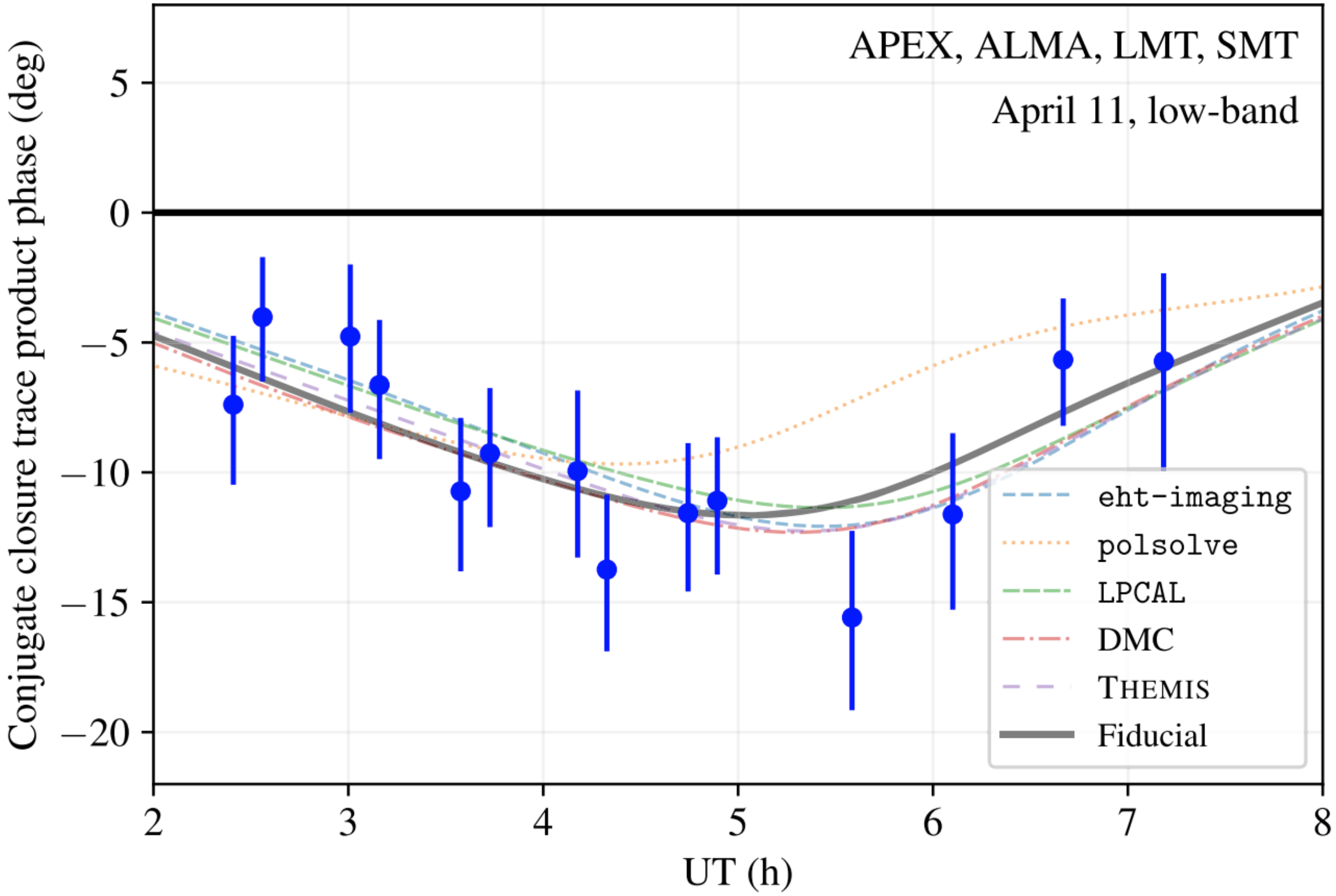


Event Horizon Telescope Collaboration (2021)

# Forward modeling

“Forward” modeling techniques – as contrasted with “inverse” modeling techniques – permit fitting a parameterized model to any desired data product(s)

- inverse modeling directly manipulates the data to produce an estimate of the desired quantity/quantities (e.g., CLEAN)
- forward modeling instead uses a “guess and check” approach

# Forward modeling

"Forward" modeling techniques – as contrasted with "inverse" modeling techniques – permit fitting a parameterized model to any desired data product(s)

- inverse modeling directly manipulates the data to produce an estimate of the desired quantity/quantities (e.g., CLEAN)
- forward modeling instead uses a "guess and check" approach

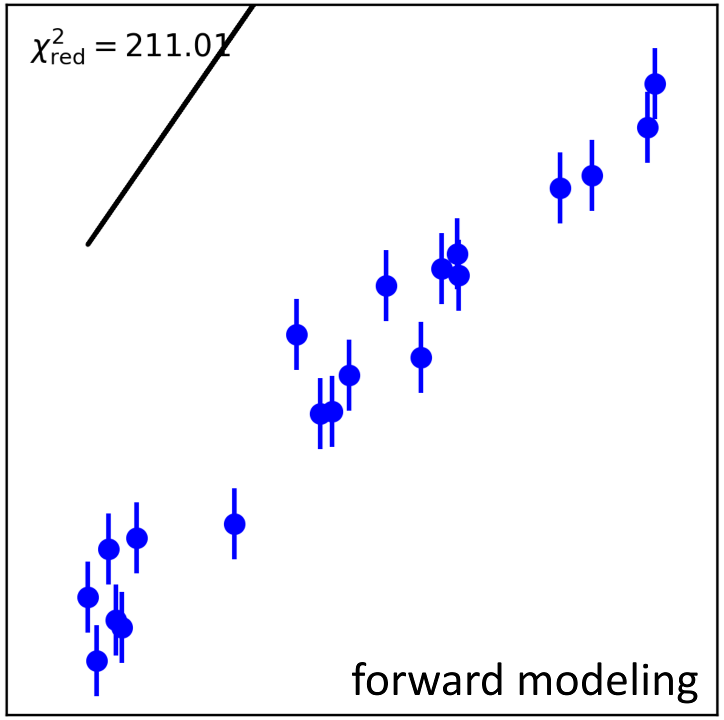

# Forward modeling

"Forward" modeling techniques – as contrasted with "inverse" modeling techniques – permit fitting a parameterized model to any desired data product(s)

- inverse modeling directly manipulates the data to produce an estimate of the desired quantity/quantities (e.g., CLEAN)
- forward modeling instead uses a "guess and check" approach

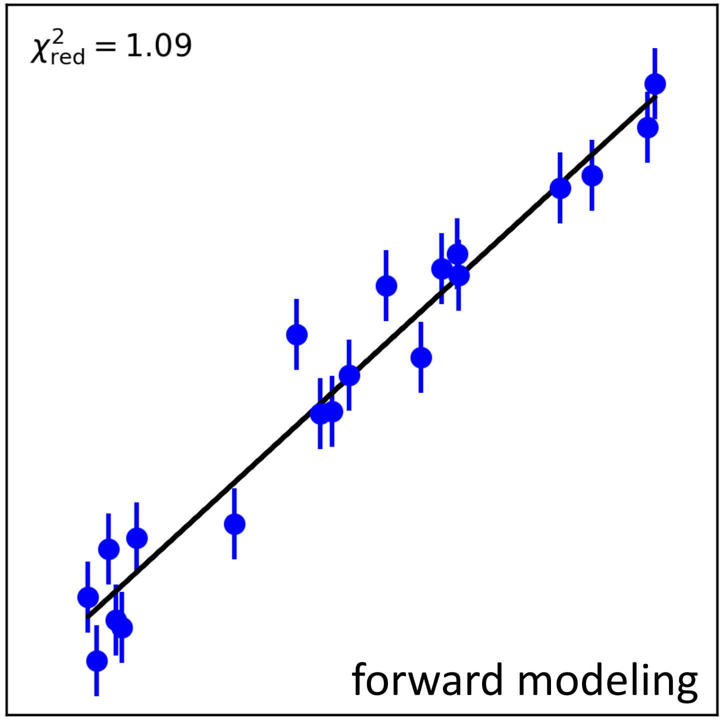


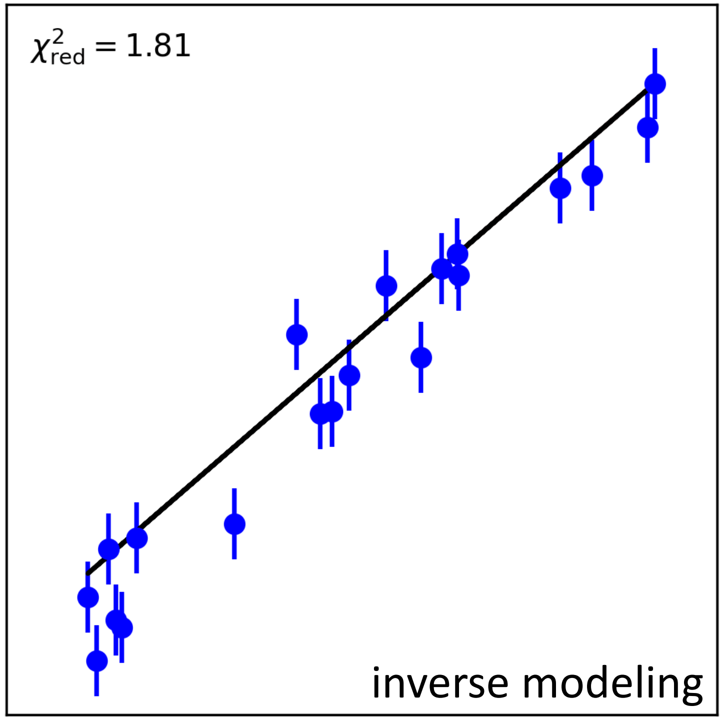

# Forward modeling

“Forward” modeling techniques – as contrasted with “inverse” modeling techniques – permit fitting a parameterized model to any desired data product(s)

- inverse modeling directly manipulates the data to produce an estimate of the desired quantity/quantities (e.g., CLEAN)
- forward modeling instead uses a “guess and check” approach

The increased power + flexibility of forward modeling typically comes at the cost of increased computational expense

- for simple models and modest data volumes, a forward modeling strategy can often be viable

# Forward modeling

"Forward" modeling techniques – as contrasted with "inverse" modeling techniques – permit fitting a parameterized model to any desired data product(s)

- inverse modeling directly manipulates the data to produce an estimate of the desired quantity/quantities (e.g., CLEAN)
- forward modeling instead uses a "guess and check" approach

The increased power + flexibility of forward modeling typically comes at the cost of increased computational expense

- for simple models and modest data volumes, a forward modeling strategy can often be viable

Forward modeling techniques typically seek to either optimize some sort of objective function (e.g., minimize a $\chi^2$, maximize a likelihood) or else to explore the posterior distribution over some set of model parameters

- data uncertainties naturally map to uncertainties on derived parameters
- complex visibilities typically have independent Gaussian uncertainties (!)
  - see, e.g., Thompson, Moran, & Swenson and Blackburn et al. (2019) for other data products

# Simple analytic models: point source

The simplest image structure is a point source:

- flux density $S_0$
- location $(x_0, y_0)$

$$V(u,v) = S_0 e^{-2\pi i (u x_0 + v y_0)}$$

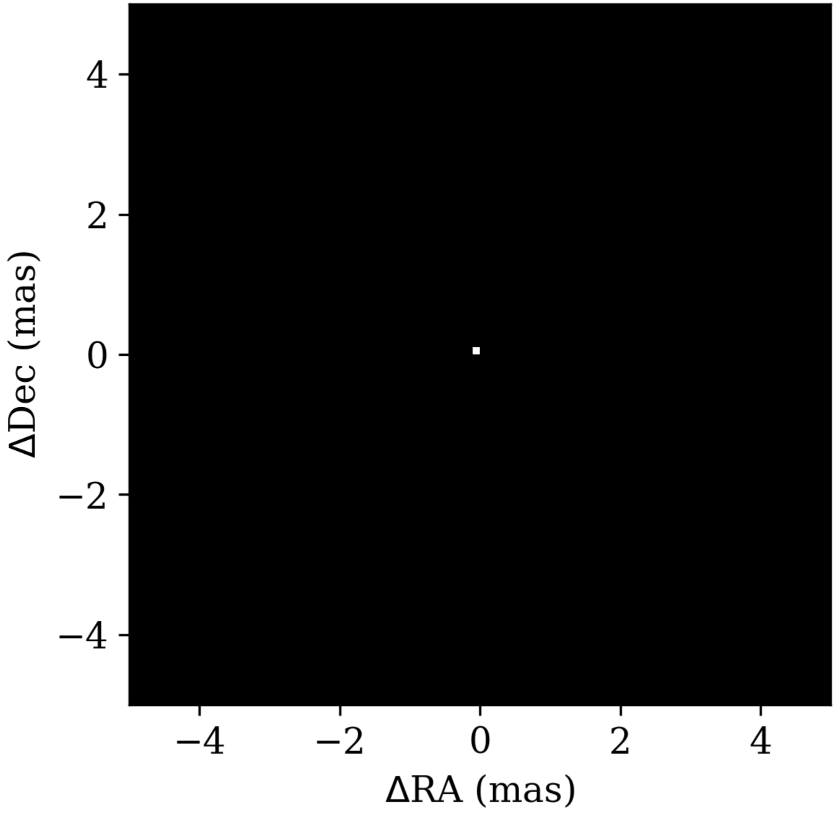


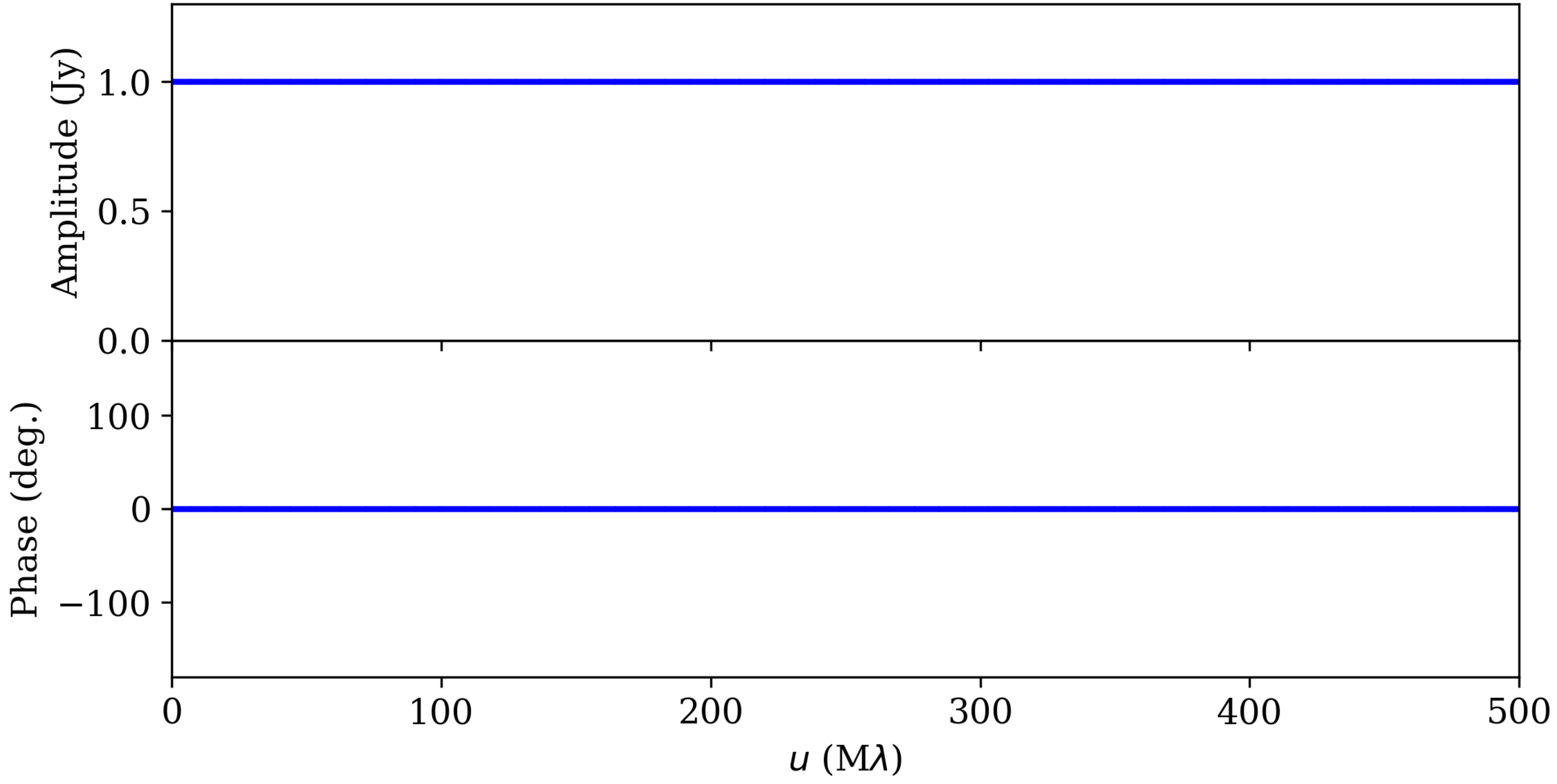

# Simple analytic models: point source

The simplest image structure is a point source:

- flux density $S_0$
- location ($x_0$, $y_0$)

$$V(u, v) = S_0 e^{-2\pi i(ux_0 + vy_0)}$$

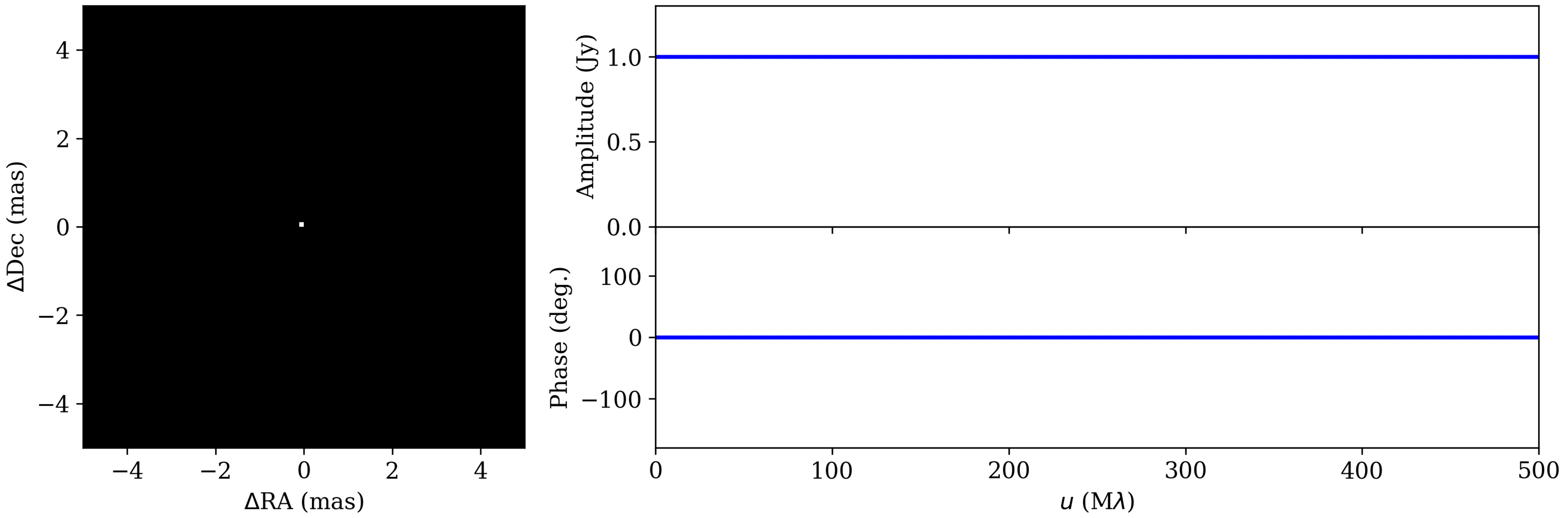

# Simple analytic models: point source

The simplest image structure is a point source:

- flux density $S_0$
- location $(x_0, y_0)$

$$V(u,v) = S_0 e^{-2\pi i (u x_0 + v y_0)}$$

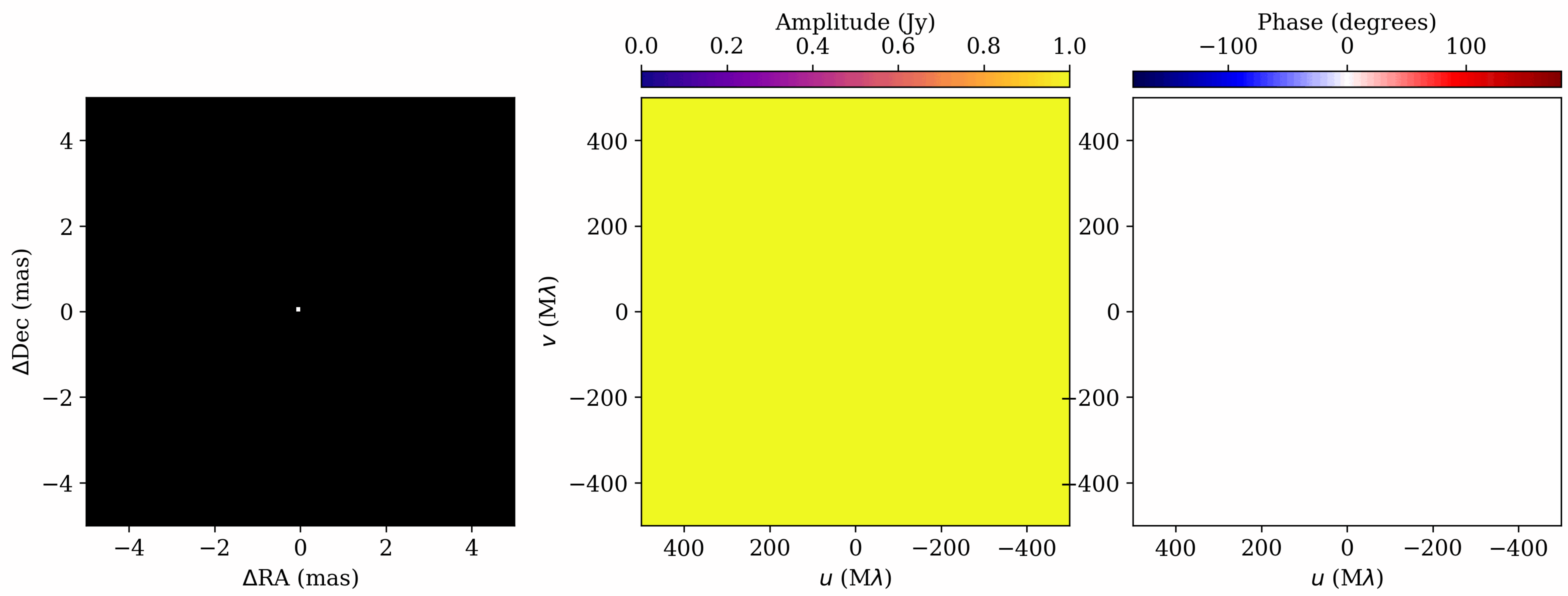

# Simple analytic models: Gaussian

Gaussians are very popular components to use in interferometric data analysis:

- flux density $S_0$
- location ($x_0$, $y_0$)
- width σ

$$V(u,v) = S_0 e^{-2\pi i(ux_0+vy_0)} e^{-2\pi^2\sigma^2(u^2+v^2)}$$

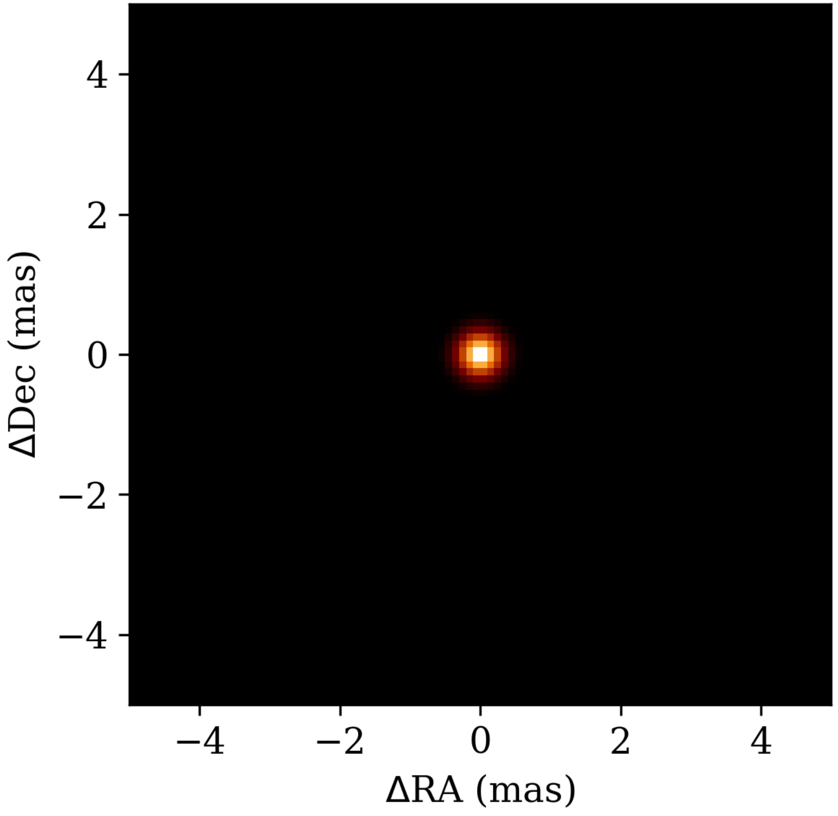


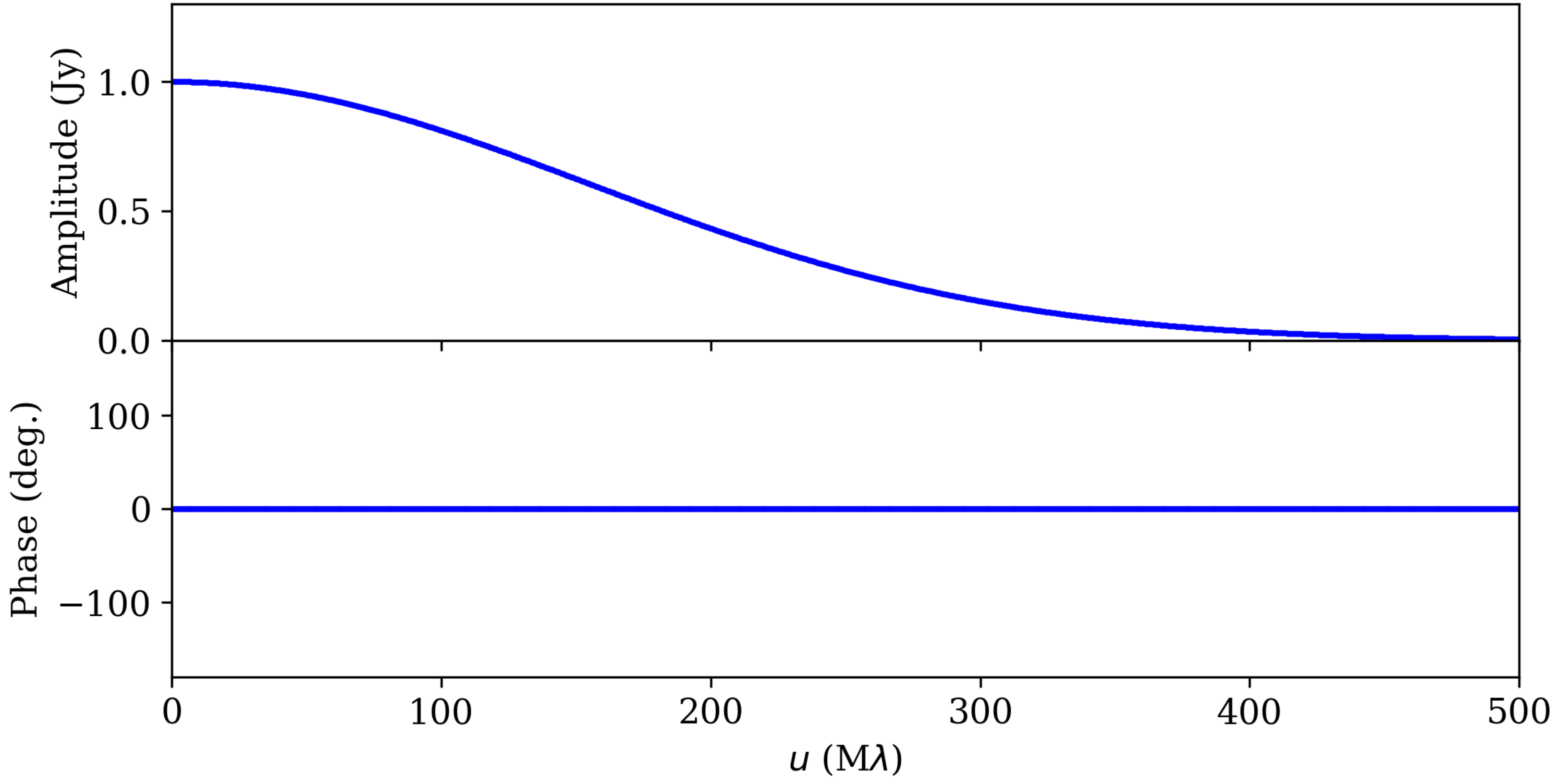

# Simple analytic models: Gaussian

Gaussians are very popular components to use in interferometric data analysis:

- flux density $S_0$
- location ($x_0$, $y_0$)
- width σ

$$V(u,v) = S_0 e^{-2\pi i(ux_0+vy_0)} e^{-2\pi^2\sigma^2(u^2+v^2)}$$

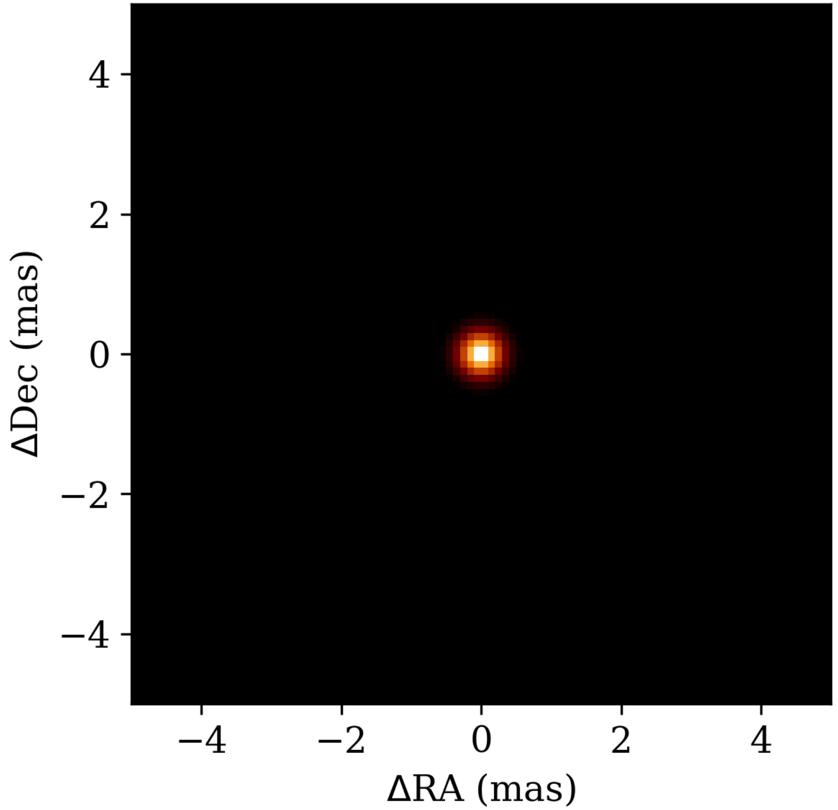


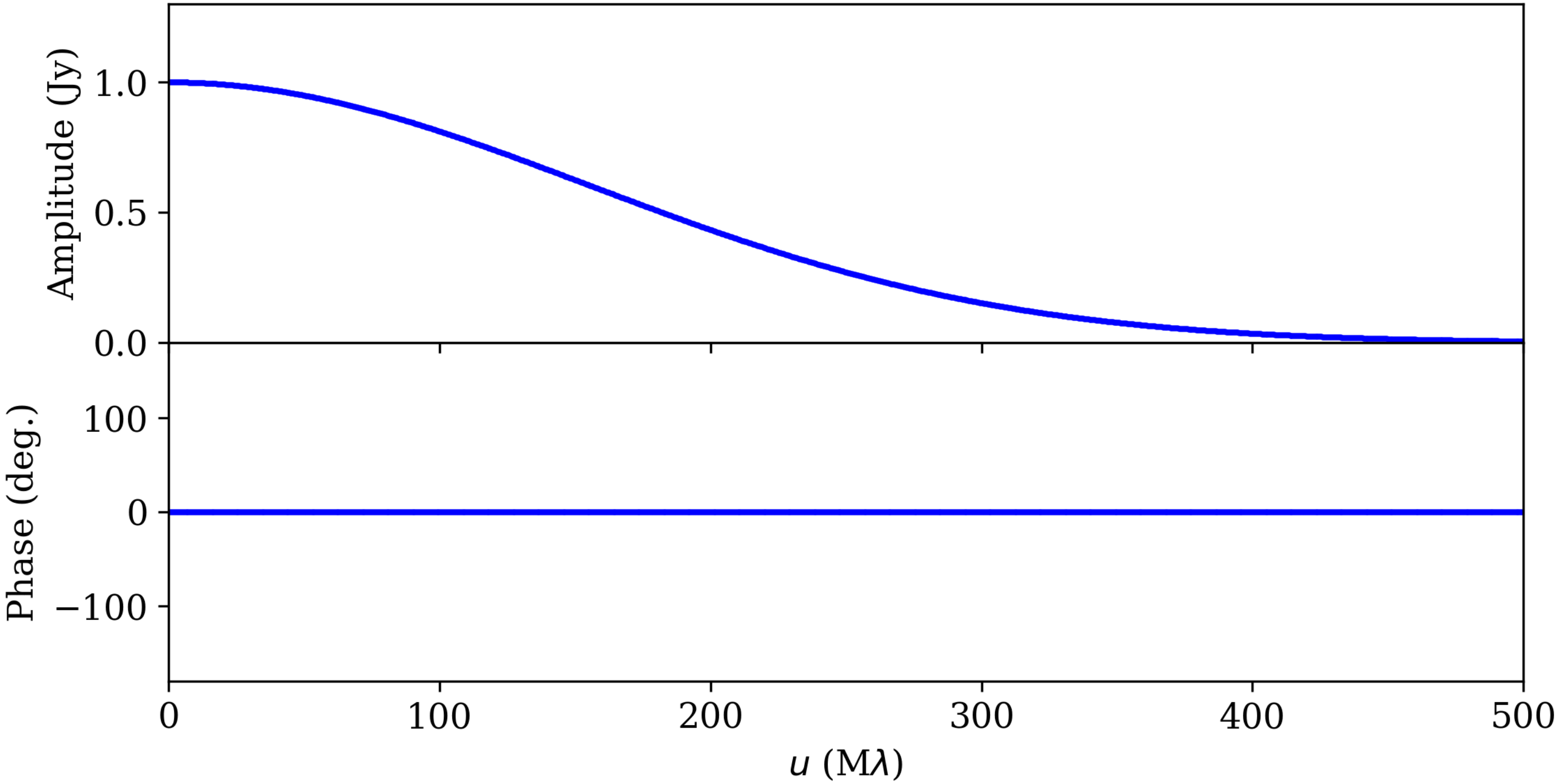

# Simple analytic models: Gaussian

Gaussians are very popular components to use in interferometric data analysis:

- flux density $S_0$
- location $(x_0, y_0)$
- width σ

$$V(u,v) = S_0 e^{-2\pi i(ux_0+vy_0)} e^{-2\pi^2\sigma^2(u^2+v^2)}$$

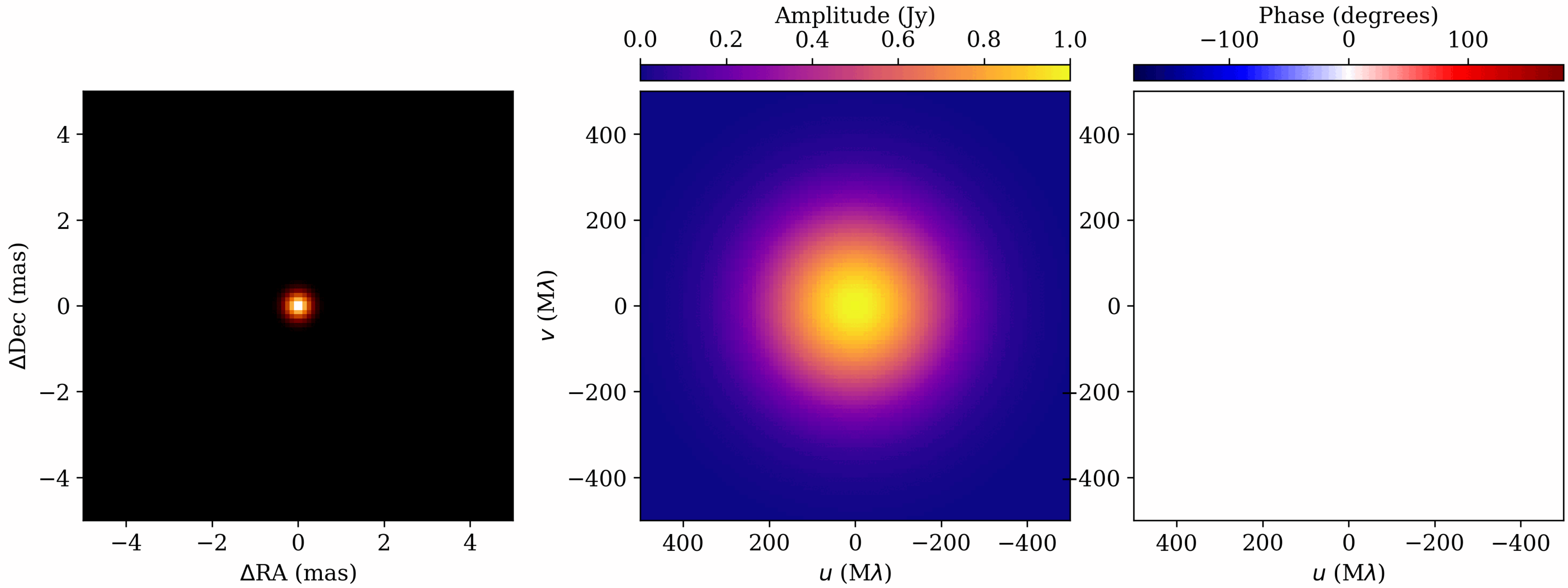

# Simple analytic models: Gaussian

Gaussians are very popular components to use in interferometric data analysis:

- flux density $S_0$
- location $(x_0, y_0)$
- width σ

$$V(u,v) = S_0 e^{-2\pi i(ux_0+vy_0)} e^{-2\pi^2\sigma^2(u^2+v^2)}$$

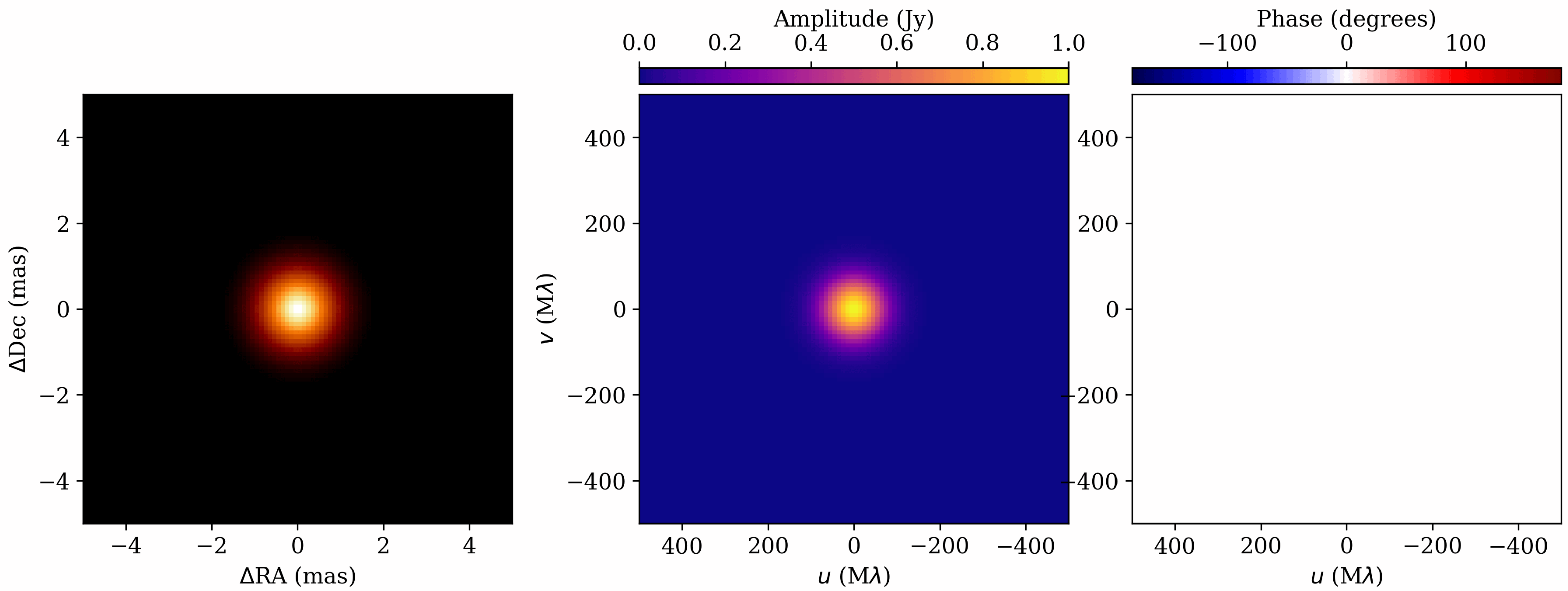

# Simple analytic models

There are other analytic models that get used with some frequency as well:

**ring**

$$V(u) = S_0 J_0(2\pi R u)$$

**disk**

$$V(u) = \frac{S_0}{\pi R u} J_1(2\pi R u)$$

**sphere**

$$V(u) = \frac{3 S_0}{4\pi (R u)^{3/2}} J_{3/2}(2\pi R u)$$

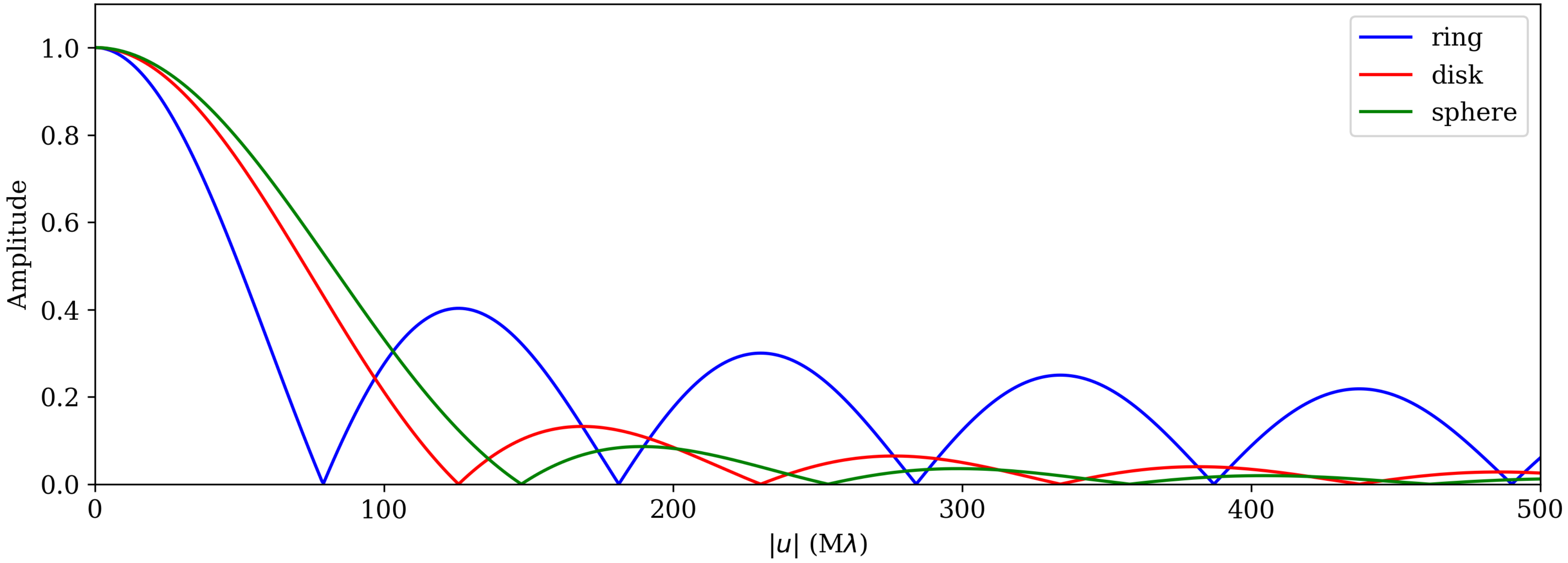

# Simple analytic models

There are other analytic models that get used with some frequency as well:

| ring | disk | sphere |
|---|---|---|
| $V(u) = S_0 J_0(2\pi R u)$ | $V(u) = \frac{S_0}{\pi R u} J_1(2\pi R u)$ | $V(u) = \frac{3S_0}{4\pi (Ru)^{3/2}} J_{3/2}(2\pi R u)$ |
| $R \longrightarrow 1.1R$ | $R \longrightarrow 1.6R$ | $R \longrightarrow 1.8R$ |

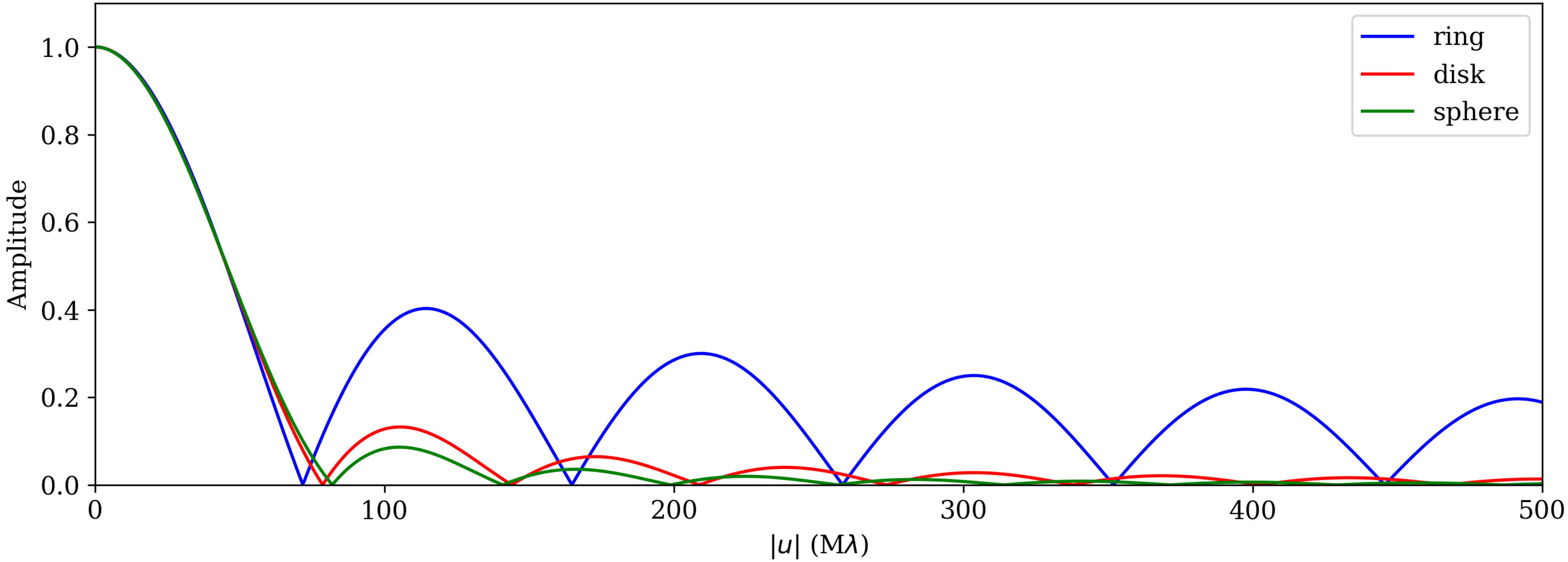

# Some other useful Fourier transform properties

There are a number of useful mappings between manipulations of the image and visibility domains, of which some of the simplest are:

linearity: $aI(x,y) + b \quad \longrightarrow \quad aV(u,v) + b$

scaling: $I(ax,by) \quad \longrightarrow \quad \frac{1}{ab} V\left(\frac{u}{a}, \frac{v}{b}\right)$

convolution theorem: $I_1(x,y) \times I_2(x,y) \quad \longrightarrow \quad V_1(u,v) * V_2(u,v)$

Details on these and other properties (e.g., translations, derivatives, moments) can be found in Thompson, Moran, & Swenson (Chapter 2) and elsewhere

# Examples of visibility-domain model fitting

The precessing jet in the microquasar V404 Cygni evolves too quickly for Earth rotation aperture synthesis to be appropriate

- Miller-Jones et al. (2019) instead fit short segments of data using point source decomposition

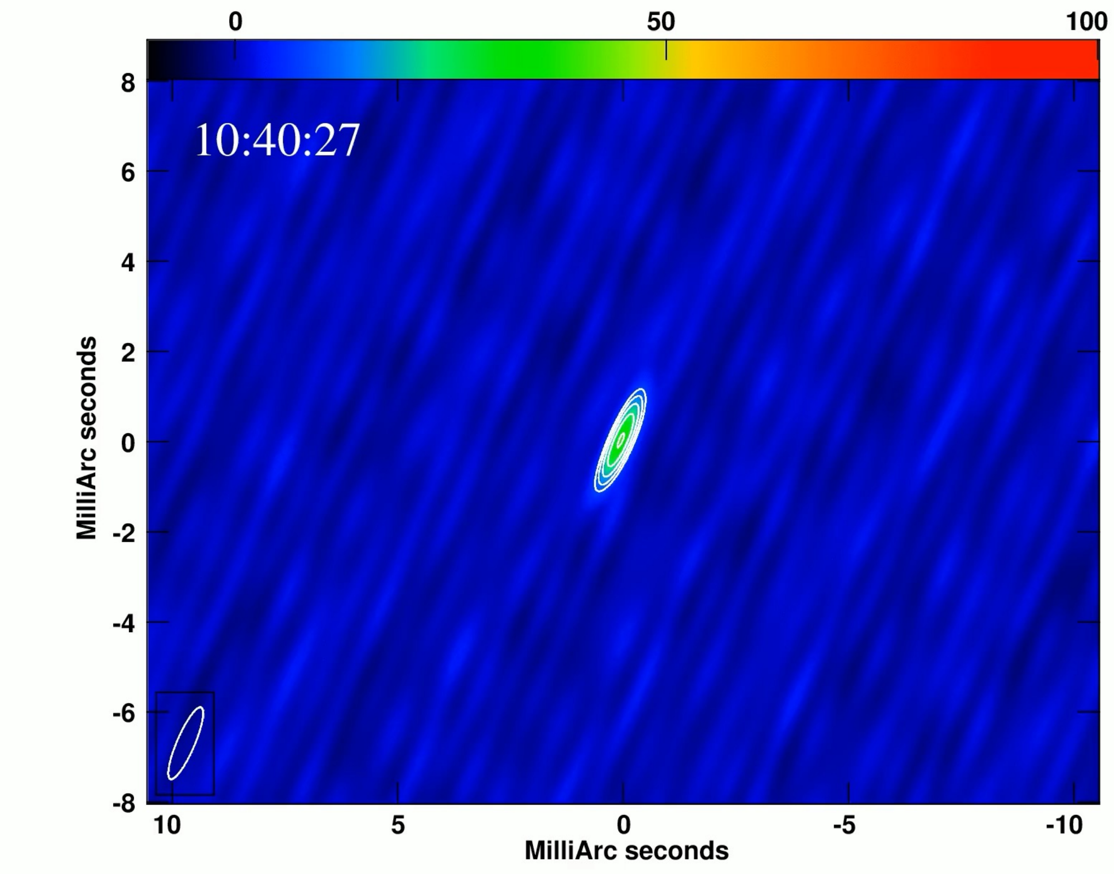


Video credit: Alex Tetarenko

# Examples of visibility-domain model fitting

The precessing jet in the microquasar V404 Cygni evolves too quickly for Earth rotation aperture synthesis to be appropriate

- Miller-Jones et al. (2019) instead fit short segments of data using point source decomposition

The appearance of Sgr A* is heavily blurred-out at radio frequencies by interstellar scattering

- Bower et al. (2014) and Johnson et al. (2021) fit a Gaussian to Sgr A* using closure quantities to measure the scattering kernel

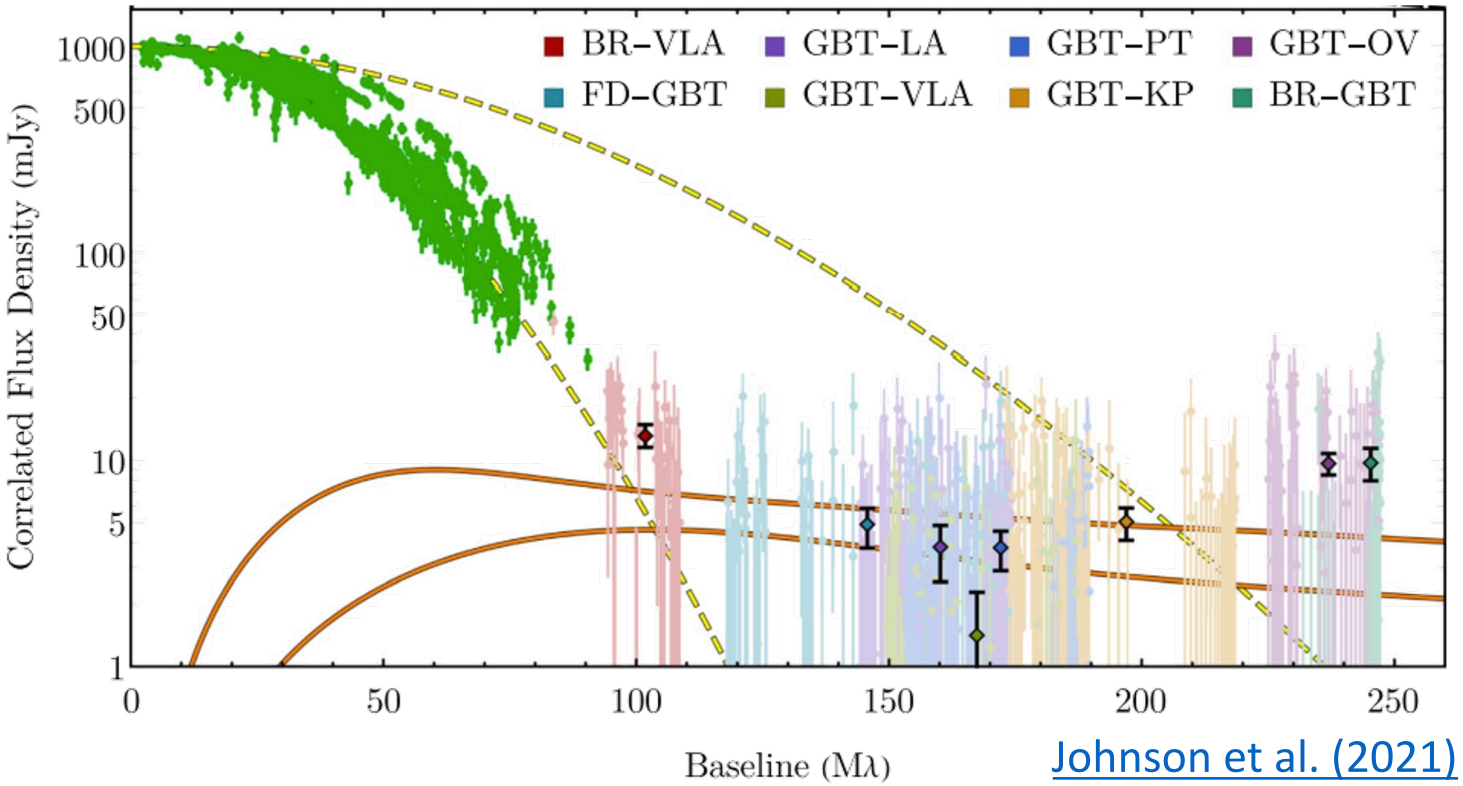


Johnson et al. (2021)

# Examples of visibility-domain model fitting

The precessing jet in the microquasar V404 Cygni evolves too quickly for Earth rotation aperture synthesis to be appropriate

- Miller-Jones et al. (2019) instead fit short segments of data using point source decomposition

The appearance of Sgr A* is heavily blurred-out at radio frequencies by interstellar scattering

- Bower et al. (2014) and Johnson et al. (2021) fit a Gaussian to Sgr A* using closure quantities to measure the scattering kernel

Analysis of the blazar 3C 279 as observed by the EHT revealed a rapid evolution in time over just a few days

- Kim et al. (2020) fit time-variable Gaussian model components to measure brightness changes and speeds of the many different source components

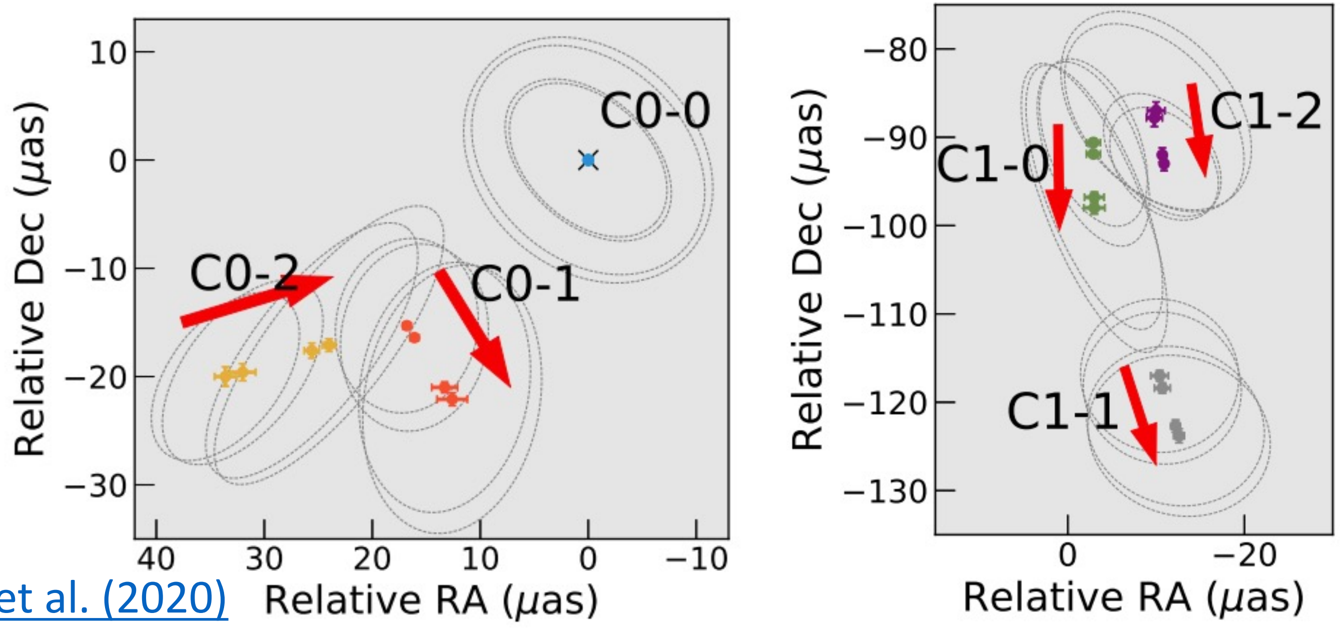


Kim et al. (2020)

# Model-fitting demo: maser spots

Let's return to the example dataset from before, with the ALMA observations of water masers in the Circinus AGN

- calibrated visibility data in a single frequency channel look point-like
- individual data point uncertainties are large and not necessarily well-known

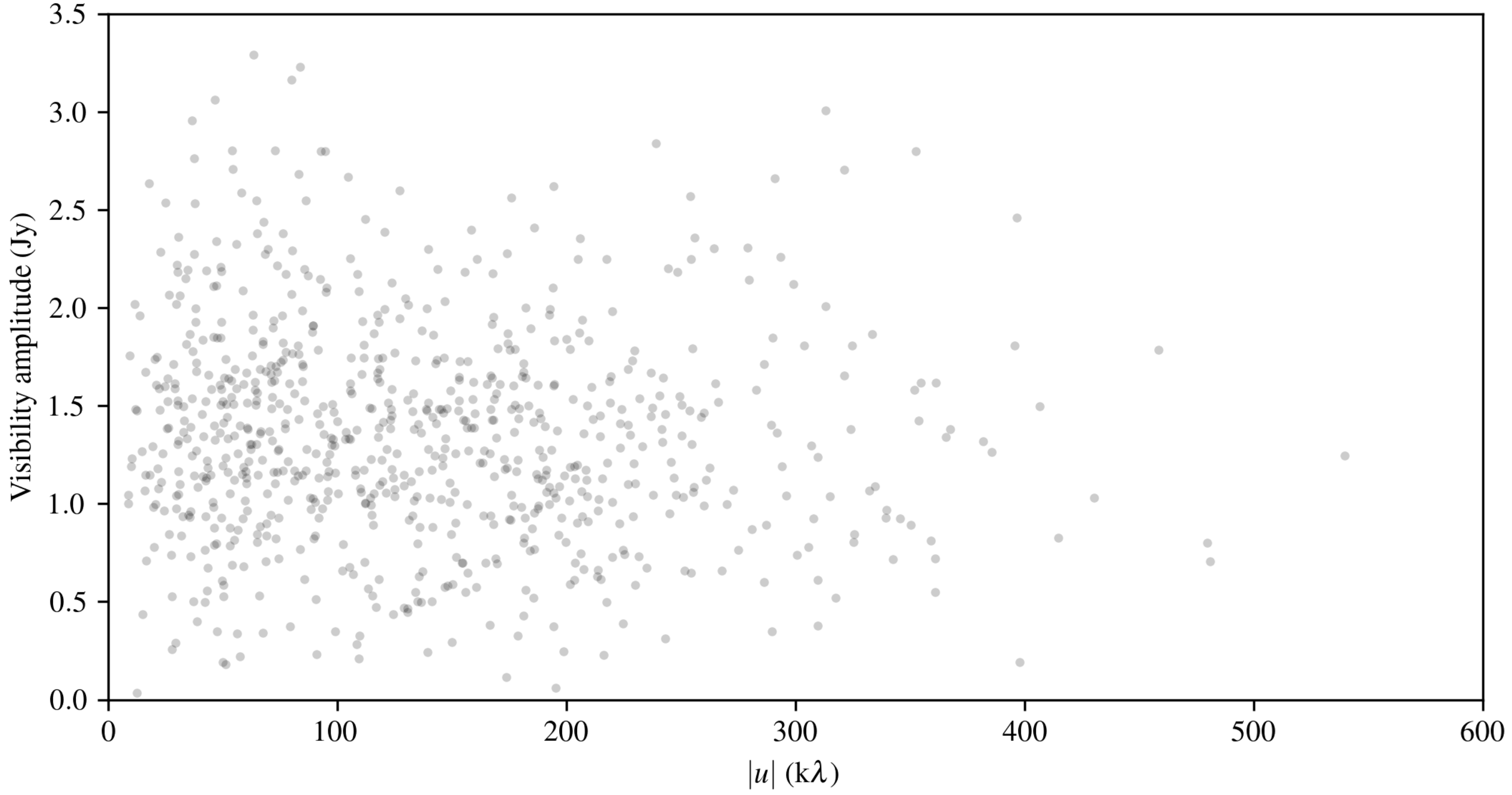


Pesce et al. (*in prep*)

# Model-fitting demo: maser spots

Let's return to the example dataset from before, with the ALMA observations of water masers in the Circinus AGN

- calibrated visibility data in a single frequency channel look point-like
- individual data point uncertainties are large and not necessarily well-known

We can fit a point-source model directly to the visibility data, with free parameters for:

- the total flux density, *S*
- the (*x*,*y*) location
- the visibility uncertainty, *σ*

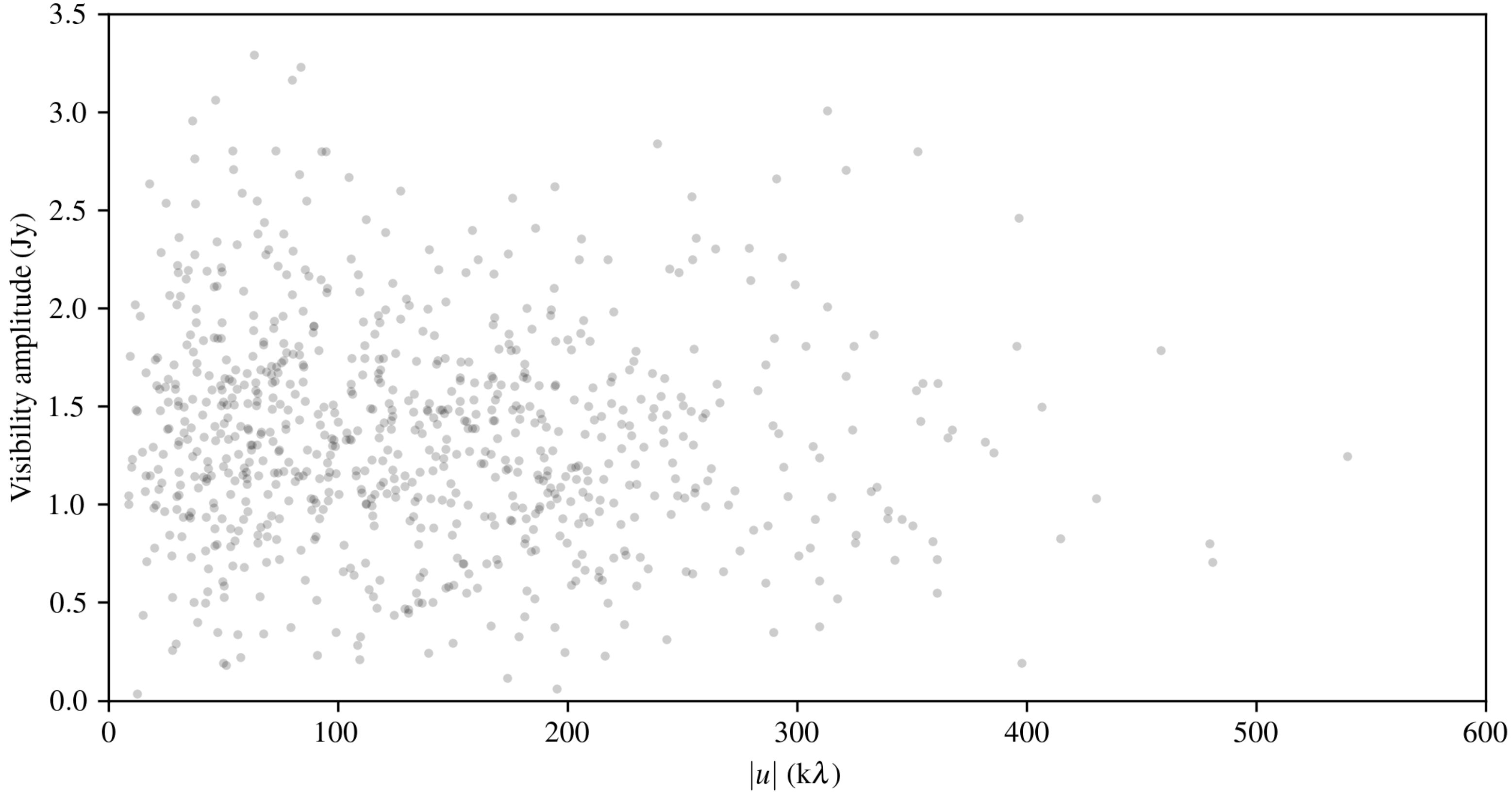


Pesce et al. (*in prep*)

# Model-fitting demo: maser spots

Let's return to the example dataset from before, with the ALMA observations of water masers in the Circinus AGN

- calibrated visibility data in a single frequency channel look point-like
- individual data point uncertainties are large and not necessarily well-known

We can fit a point-source model directly to the visibility data, with free parameters for:

- the total flux density, $S$
- the $(x,y)$ location
- the visibility uncertainty, $\sigma$

Result:

- $S$ = 1.06 Jy
- $x$ = 79 mas
- $y$ = 213 mas
- $\sigma$ = 0.71 Jy

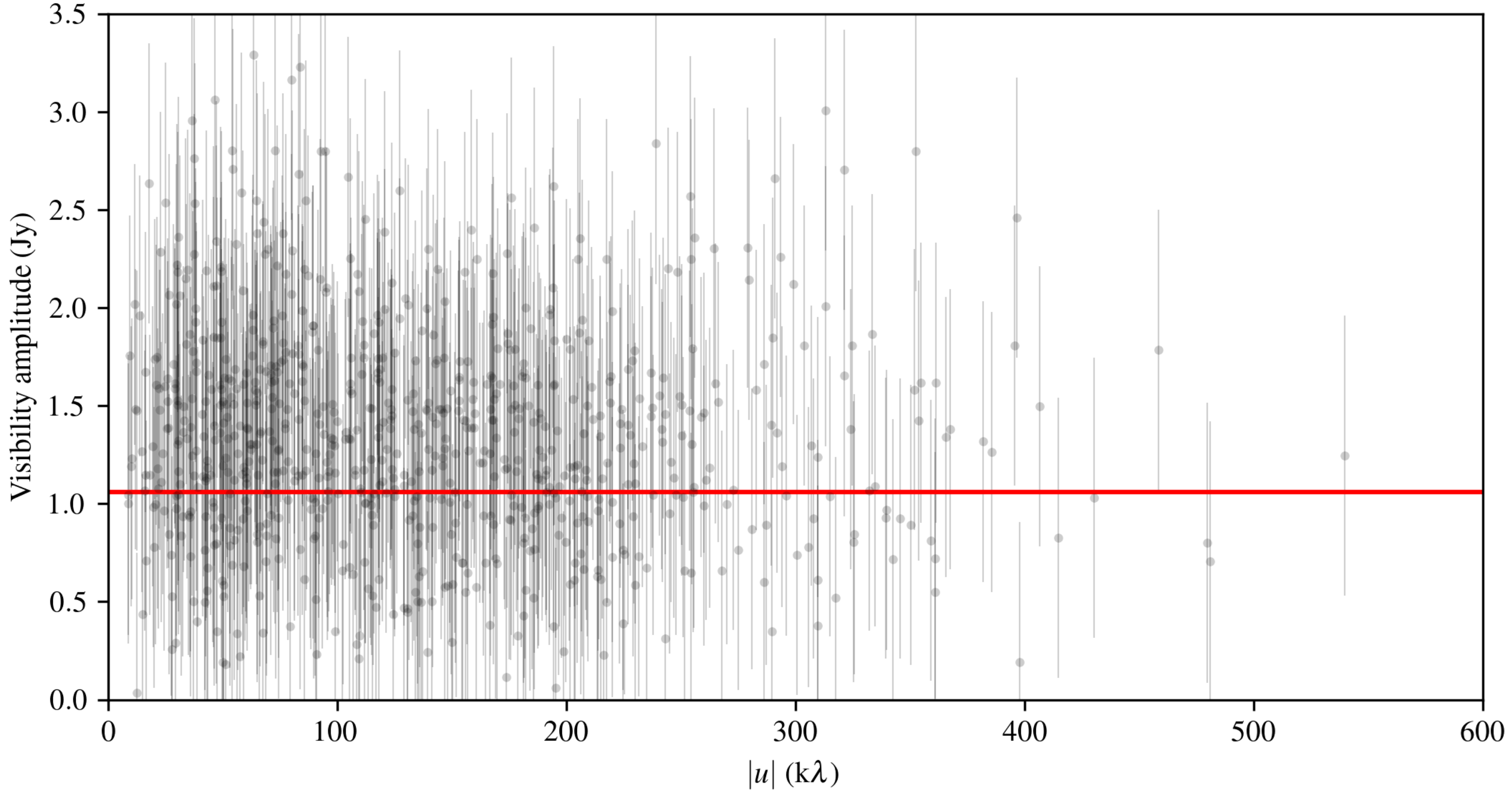


(fit using `dynesty`; Speagle 2020)

Pesce et al. (*in prep*)

# Model-fitting demo: maser spots

Let's return to the example dataset from before, with the ALMA observations of water masers in the Circinus AGN

- calibrated visibility data in a single frequency channel look point-like
- individual data point uncertainties are large and not necessarily well-known

We can fit a point-source model directly to the visibility data, with free parameters for:

- the total flux density, $S$
- the $(x,y)$ location
- the visibility uncertainty, $\sigma$

Result:

- $S$ = 1.06 ± 0.03 Jy
- $x$ = 79 ± 7 mas
- $y$ = 213 ± 8 mas
- $\sigma$ = 0.71 ± 0.01 Jy

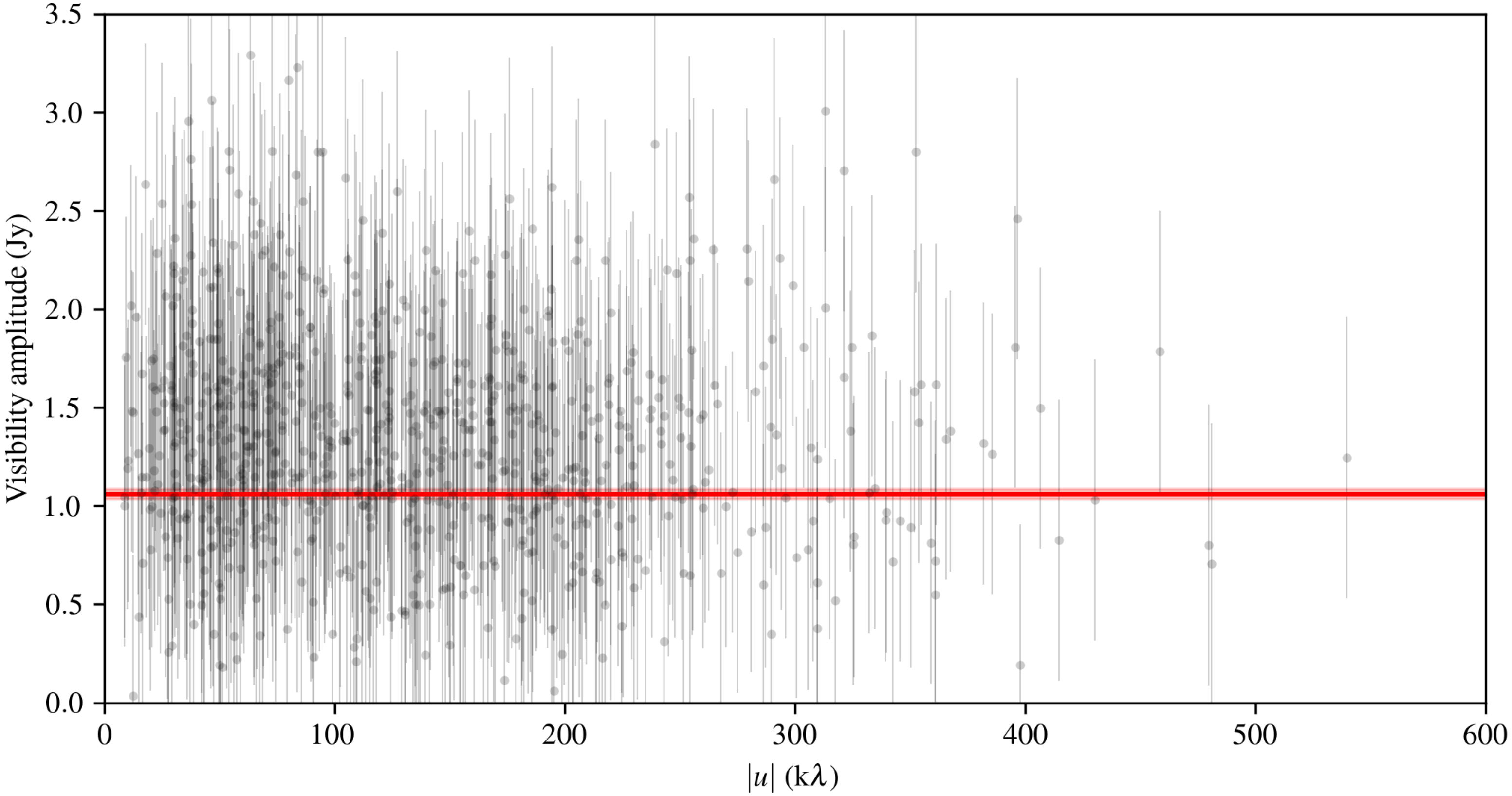


(fit using `dynesty`; Speagle 2020)

Pesce et al. (*in prep*)

# Model-fitting demo: maser spots

Applying the same point-source model to each frequency channel, we can re-generate the map from earlier

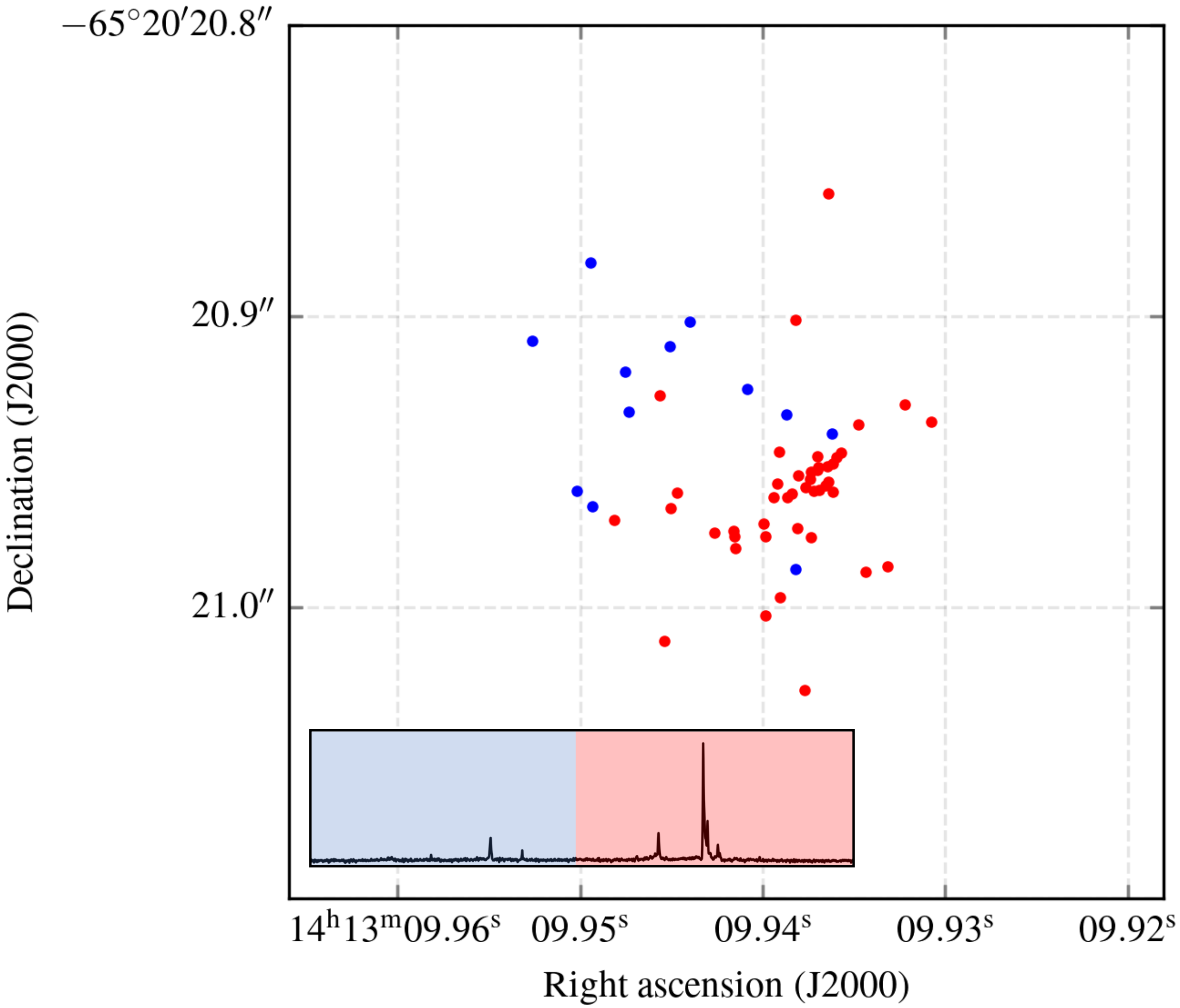


Pesce et al. (*in prep*)

# Model-fitting demo: maser spots

Applying the same point-source model to each frequency channel, we can re-generate the map from earlier

Tracking the same strong maser spots as before, we can see that they have become more concentrated

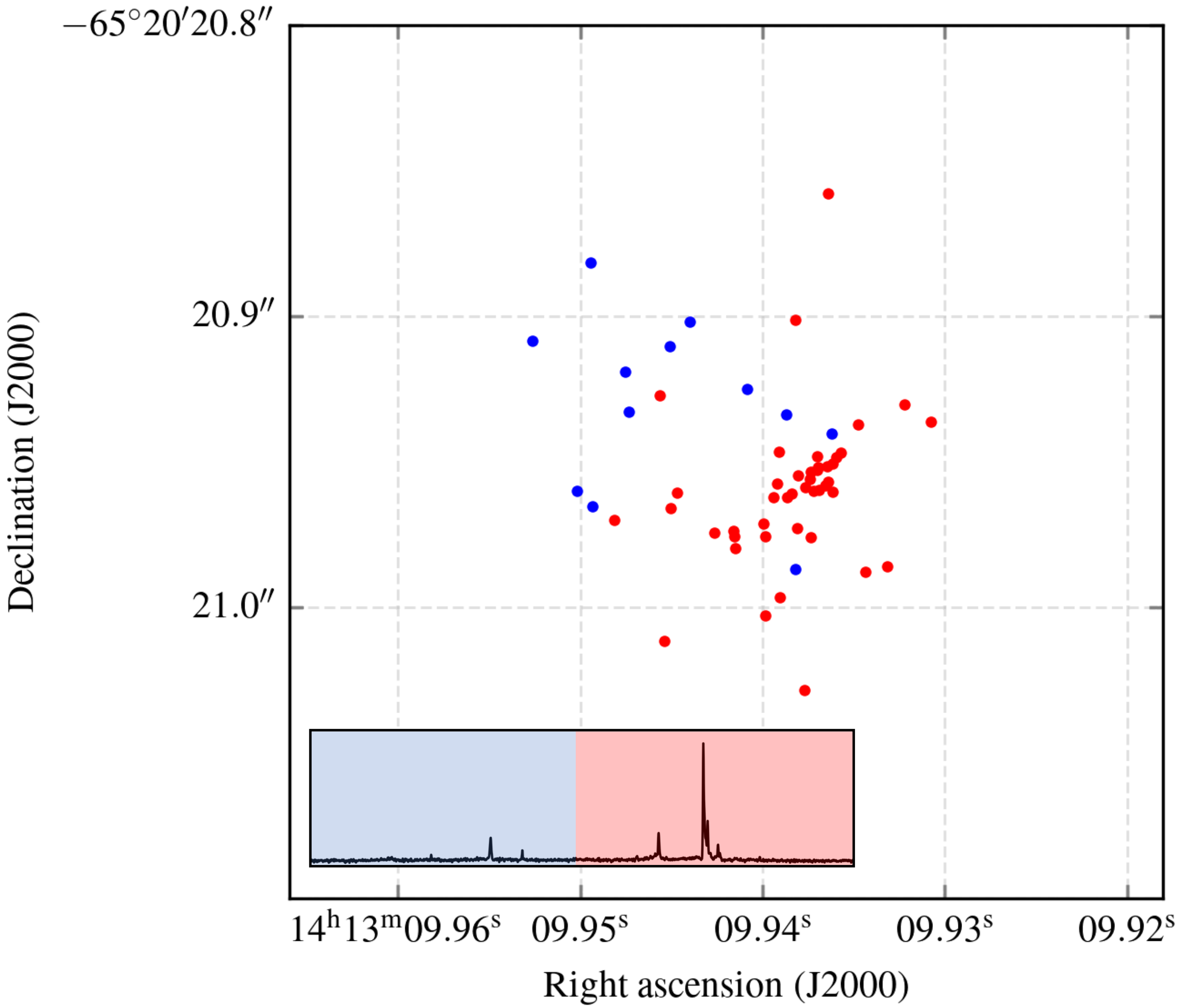


Pesce et al. (*in prep*)

# Model-fitting demo: maser spots

Applying the same point-source model to each frequency channel, we can re-generate the map from earlier

Tracking the same strong maser spots as before, we can see that they have become more concentrated

We now have access to reliable (2D) uncertainty information for each spot, and we can see that indeed the most tightly-constrained positions occur where the spots are most densely concentrated

- i.e., the map exhibits self-consistency
- furthermore, the shapes of the error ellipses closely mirror the beam shape

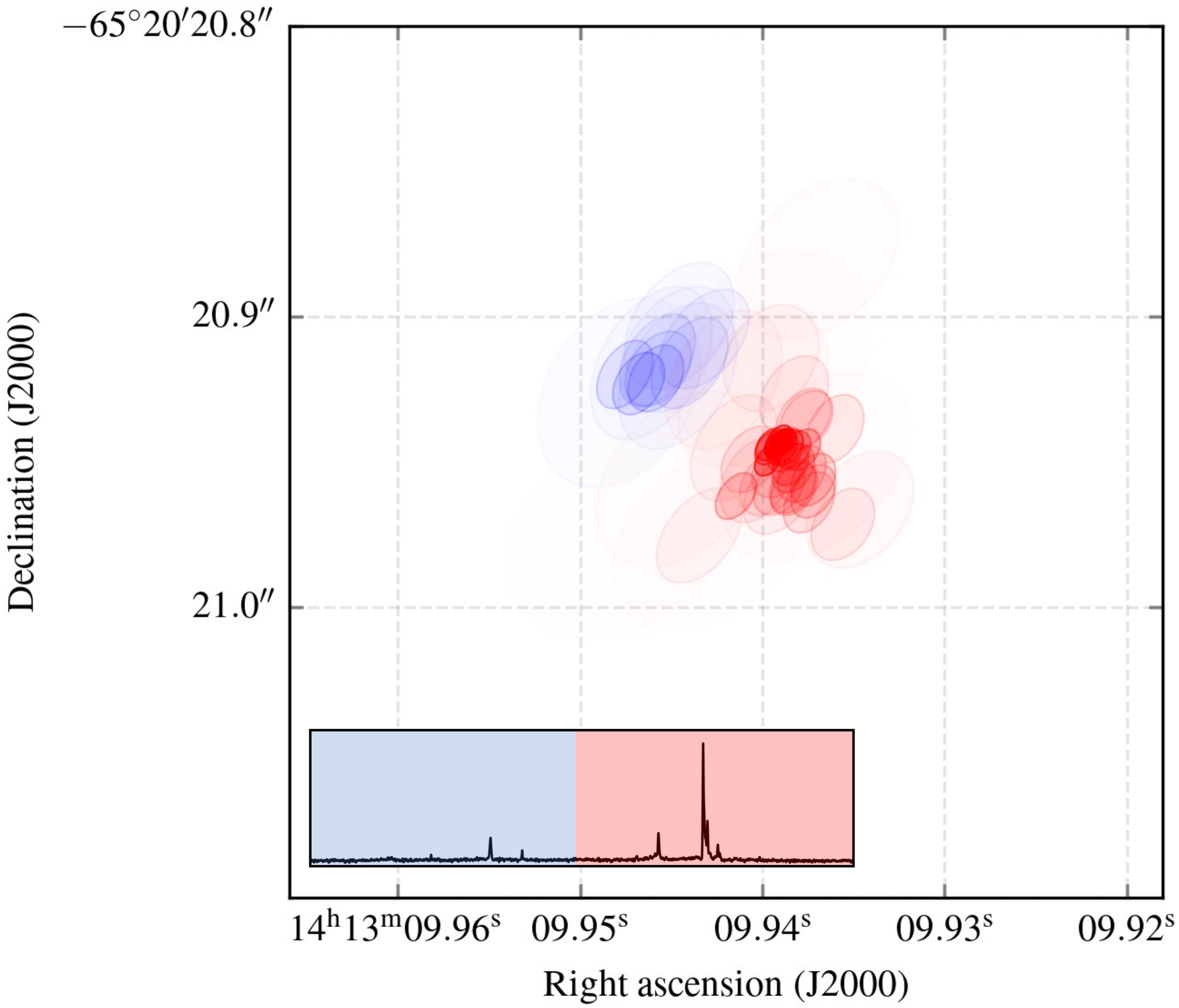


Pesce et al. (*in prep*)

# Model-fitting demo: maser spots

For this system, we happen to know how it behaves from prior VLBI observations

- good agreement despite ~3 orders of magnitude difference in beam size (!)

Greenhill et al. (2003)

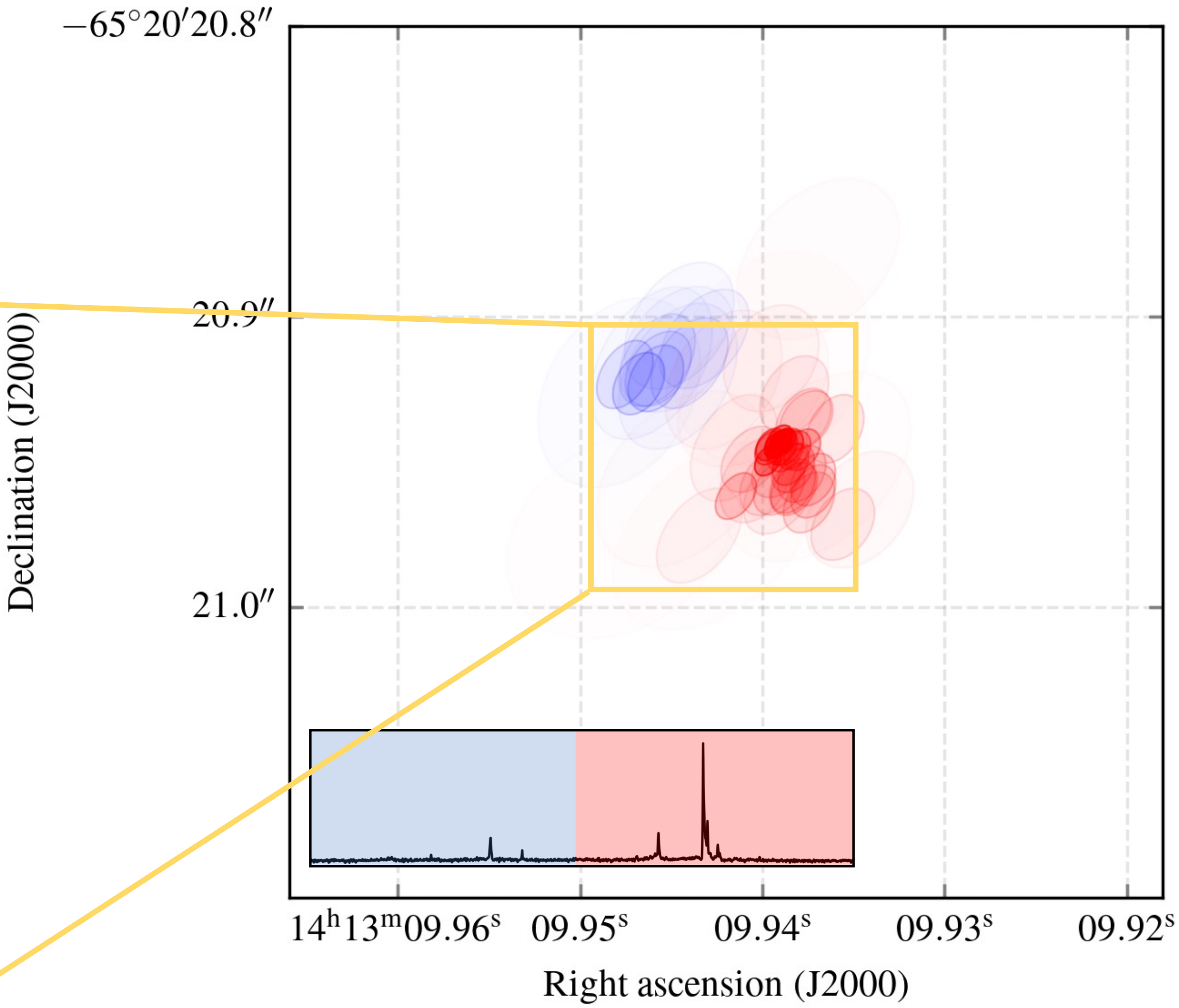


Pesce et al. (*in prep*)

# Summary

Interferometric image reconstructions can be analyzed in any way that other images can be

- common procedures include multi-source or multi-component decomposition, though many other feature extraction analyses have also been employed
- uncertainty estimates on derived quantities are difficult to determine

However, interferometric data do not natively take the form of images, and *non-imaging analyses* are typically both the first (e.g., data inspection) and often the most precise (e.g., uncertainty quantification) means of extracting science

One has many options available during data inspection to understand basic properties of a dataset

- closure quantities (both phases and amplitudes) are immune to various station-based data corruptions and encode information about a source’s (a)symmetry
- closure traces and invariants are further immune to polarimetric leakage and encode information about a source’s polarization state

Forward modeling is a powerful quantitative analysis tool

- any data products can be forward modeled, not just visibilities
- measurement uncertainties on visibilities are typically independent and close to Gaussian, enabling accurate uncertainty estimates for derived / fit quantities